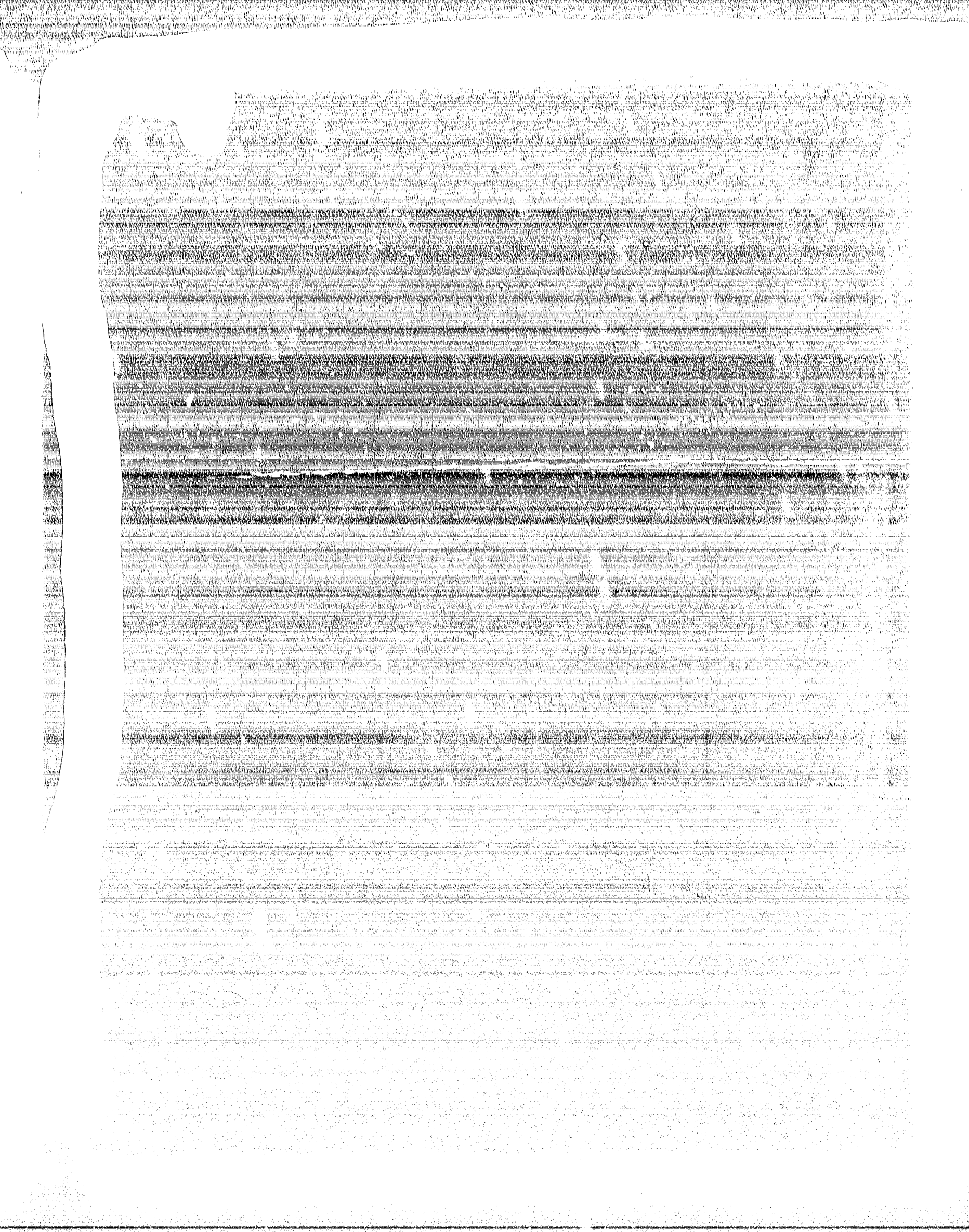


AD A 136947



UNCLASSIFIED

SECURITY CLASSIFICATION OF THIS PAGE (When Data Entered)

(Block 20 continued)

and feedback control on rotor stability were assessed. Results of the investigation indicate that the subject helicopter rotors are unstable in forward flight without feedback control. With feedback, the rotors are stable and controllable. ⚡

UNCLASSIFIED

SECURITY CLASSIFICATION OF THIS PAGE (When Data Entered)

TABLE OF CONTENTS

	Page
LIST OF FIGURES	iv
LIST OF TABLES	iv
NOTATION	v
ABSTRACT	1
ADMINISTRATIVE INFORMATION	1
INTRODUCTION	1
METHODOLOGY	3
ROTOR AERODYNAMIC REPRESENTATION	4
EQUATIONS OF MOTION	5
DISCUSSION	9
ROTOR MODEL	9
HOVER ANALYSIS	10
FORWARD FLIGHT	11
FEEDBACK CONTROL	13
STABILITY	14
RESULTS	14
HOVER ANALYSIS	14
FORWARD FLIGHT	15
FEEDBACK CONTROL	17
STABILITY	20
CONCLUSIONS	21
HOVER	21
FORWARD FLIGHT	21
ACKNOWLEDGMENTS	22
REFERENCES	23

Accession	
NTIS GRA&I	
DTIC TAB	
Unannounced	
Justification	
By	
Distribution/	
Availability Codes	
Avail and/or	
Dist	Special
A1	



LIST OF FIGURES

	Page
1 - Gimballed Rotor Helicopter	24
2 - Rotor Fixed Reference Frame	25
3 - Euler Angles for Rotor Dynamic Calculations	26
4 - Rotor Forces and Moments	27
5 - Euler Angles for Feedback Calculations	28
6 - Rotor Hover Performance Map	29
7 - Rotor Dynamic Equilibrium Boundary in Hover	30
8 - Equilibrium Dynamics in Forward Flight	31
9 - Effect of Principal Axis Location on Rotor Motions for 100-Percent Circulation Control Lift	32
10 - Effect of Principal Axis Location on Rotor Motions for 100-Percent Angle-of-Attack Lift	36
11 - Effect of Principal Axis Location on Rotor Oscillation Frequency	40
12 - Effects of Teeter Feedback	44
13 - Effects of Feather Feedback	53
14 - Effects of Lift Type on Teeter Rate ($k_{\beta} = 400$) Feedback	62
15 - Effect of Lift Type on the Average Equilibrium Rotor Pitch and Roll Angles with Teeter Rate Feedback	66
16 - Effects of Horizontal Gust Disturbances on Open Loop Rotor Dynamics	67
17 - Effects of Horizontal Gust Disturbances on Closed Loop Rotor Dynamics	72

LIST OF TABLES

1 - Rotor Model Characteristics	75
2 - Variation of Rotor Inertias with Principal Axis Location	76

NOTATION

A, A_1	Coefficients of sine cyclic pressure (or pressure ratio)
B, B_1	Coefficients of cosine cyclic pressure (or pressure ratio)
\bar{b}	Vector location of the rotor center of gravity with respect to the gimbal
$d\bar{f}_k^a$	Aerodynamic force vector acting on the k^{th} blade element
$d\bar{M}_k^a$	Aerodynamic moment vector acting on the k^{th} blade element
\bar{F}	Total external force vector acting on the rotor
\bar{G}	Total external moment vector acting on the rotor
$\dot{\bar{h}}$	Rate of change of rotor angular momentum vector
$I, [I]$	Rotor inertia matrix in the rotor fixed frame
	$I = \begin{bmatrix} I_{11} & I_{12} & I_{13} \\ I_{21} & I_{22} & I_{23} \\ I_{31} & I_{32} & I_{33} \end{bmatrix} = \begin{bmatrix} I_{xx} & -I_{xy} & -I_{xz} \\ -I_{yx} & I_{yy} & -I_{yz} \\ -I_{zx} & -I_{zy} & I_{zz} \end{bmatrix}$
\bar{J}_k	Vector location of the k^{th} blade element with respect to the rotor center of gravity
j	Number of aerodynamic elements per blade
$k_\beta, k_\beta^*, k_\beta^{**}$	Teeter angle, rate, acceleration feedback gain constants to rotor duct pressure
$k_\theta, k_\theta^*, k_\theta^{**}$	Feather angle, rate, acceleration feedback gain constants to rotor duct pressure
\bar{M}^a	Total aerodynamic moment vectors about the rotor gimbal
\bar{M}^R	Total of all gimbal related moments about the gimbal (e.g., friction, centering springs)

\bar{M}^{TJ}	Total tip jet thrust moment vector about the rotor gimbal
m	Rotor mass
n	Number of rotor blades or number of tip jets
\bar{P}	Reaction force vector acting at the gimbal
$P_{\text{collective}}$	Rotor pneumatic collective pressure (or pressure ratio)
P_{duct}	Rotor total duct pressure (or pressure ratio)
$\bar{Q}, \dot{\bar{Q}}$	Angular velocity, acceleration of the gimbal with respect to the inertial reference frame rad/s, rad/sec ²
$\bar{r}, \dot{\bar{r}}$	Linear velocity, acceleration vector of the rotor center of gravity with respect to the inertial reference frame
\bar{s}_i	Vector location of the i^{th} tip jet with respect to the rotor center of gravity
T	Rotor thrust - lb (N)
\bar{T}_i	Thrust vector of the i^{th} tip jet
V_{∞}	Forward flight speed fps (m/s)
Δp	Feedback pressure (or pressure ratio) signal
$\Delta\beta^*, \dot{\Delta\beta}^*, \ddot{\Delta\beta}^*$	Teeter angle, rate, acceleration difference
$\Delta\theta^*, \dot{\Delta\theta}^*, \ddot{\Delta\theta}^*$	Feather angle, rate, acceleration difference
θ_c	Rotor collective angle, deg (rad)
ϕ, θ, ψ	Euler angles used for dynamics; roll tilt angle, pitch tilt angle, and azimuth angle, respectively
$\psi^*, \beta^*, \theta^*$	Euler angles used for feedback; azimuth angle, teeter angle, and feather angle, respectively
$\bar{\omega}, \dot{\bar{\omega}}$	Angular velocity acceleration vector of the rotor center of gravity with respect to the inertial frame

- Vector quantity
- { } Column vector
- [] Square matrix
- ~ Cross product operator for converting from vector to matrix operations (notation) eq.,

$$\bar{a} \times \bar{b} = [\tilde{a}] \{b\}$$

where $\bar{a} = a_1 \hat{i} + a_2 \hat{j} + a_3 \hat{k}$

$$\bar{b} = b_1 \hat{i} + b_2 \hat{j} + b_3 \hat{k}$$

$$\bar{a} \times = [\tilde{a}] = \begin{bmatrix} 0 & -a_3 & a_2 \\ a_3 & 0 & -a_1 \\ -a_2 & a_1 & 0 \end{bmatrix}$$

$$\bar{b} = \{b\} = \begin{pmatrix} b_1 \\ b_2 \\ b_3 \end{pmatrix}$$

ABSTRACT

An analytic investigation was made to determine the dynamic properties of a two-bladed rigid fully gimballed helicopter rotor incorporating circulation control airfoils and tip jet propulsion. A time domain analysis was developed which provided the capability of using non-linear airfoil aerodynamics and arbitrary rotor physical characteristics. The effects of feather principal axis of inertia location, horizontal gust disturbances, and feedback control on rotor stability were assessed. Results of the investigation indicate that the subject helicopter rotors are unstable in forward flight without feedback control. With feedback, the rotors are stable and controllable.

ADMINISTRATIVE INFORMATION

The research reported herein is part of the Independent Research Program at the David W. Taylor Naval Ship Research and Development Center (DTNSRDC) and during fiscal years 1981 and 1982. This research was conducted under Naval Material Command Program Element 61152N, Task Area ZR0230201, and Work Unit 1605-402.

INTRODUCTION

The Aviation and Surface Effects Department (ASED) at the David W. Taylor Naval Ship Research and Development Center (DTNSRDC), through its efforts to develop advanced rotorcraft, has considered many innovative concepts which showed a potential to advance the rotary wing state-of-the-art. One such concept which is believed to have significant potential is the fully gimballed helicopter rotor.

A gimballed rotor is a rotor which is free to pitch and roll at the end of the rotor shaft while it rotates. It can be likened to a conventional rotor with a ball joint replacing the rigid attachment of the rotor hub to the rotor shaft (Figure 1). For a rotor to be truly fully gimballed, only forces can be transmitted between the rotor and the fuselage. As a result, no limits are placed on fuselage center of gravity shifts other than those set by fuselage attitude considerations. There are also no rotor control power requirements set by center of gravity shifts because, in steady flight, the resultant force on the fuselage always acts through the rotor gimbal. This means that there is a much greater flexibility in load carrying capability for gimballed rotors than for other rotor types. It is the major advantage of the concept and it is particularly important for heavy lift helicopters.

There are several challenges which must be met in order to design a fully gimballed rotor. The first challenge is the mechanical design problem in which powering the rotor and providing collective and cyclic lift control must be accomplished without passing torques between the rotor and the fuselage. Perhaps the most straightforward means of powering and controlling a fully gimballed rotor is with a completely pneumatic system incorporating tip drive propulsion and circulation control. Tip drive systems have been analyzed extensively, but very few tip driven helicopters have been built. Nichols^{1*} gives a good theoretical analysis of the efficiency of the pressure jet tip drive system in comparison with the turbine powered shaft drive, while Bossler and Harris² compare various rotor drive systems primarily from a weight standpoint. Because there are very few actual data points available for tip driven helicopters, it is difficult to draw hard and fast conclusions as to the superiority of drive system types. For example, both Bossler and Harris,² and Head³ give comparative design examples, but arrive at different conclusions as to which drive system is best. It is clear, however, that tip drive becomes attractive for very large helicopters because it is simple and inexpensive to construct.

Circulation control (CC) is a primary area of expertise in ASED. There are three major programs^{4,5,6} using this technology. Circulation control has the fundamental advantage of providing a simple means of modulating the magnitude and distribution of rotor lift from the nonrotating frame of a helicopter. This lift control is accomplished by tangentially blowing air through a slot near the trailing edge of the airfoil. It is a very effective control and can provide very high lift coefficients.

The concept of a two-bladed fully gimballed rotor incorporating CC airfoils evolved from a perceived need for a large simple helicopter with reduced ship board stowage requirements. Tip drive coupled with CC yields a mechanically simple and low cost rotor system. The two-bladed rotor configuration enhances the design simplicity by eliminating the rotor folding requirement to meet stowage requirements. In a subsequent design study, Head³ demonstrated the additional benefit of reduced gross weight for the two-bladed configuration as compared to higher numbers of blades. For these reasons, the concept of a two-bladed fully gimballed rotor is addressed in this report.

*A complete listing of references is given on page 23.

The second challenge which must be met in order to design a fully gimballed rotor is to ensure that the rotor concept is statically and dynamically well behaved. The best way to meet this challenge is to strive to gain a fundamental understanding of the properties of this type of rotor. Two-bladed gimballed rotors have very high inertias about the rotational and flapwise axes, but very low inertia about the feathering axis. Thus the rotor has a potential for instability especially if the characteristically large pitching moments of CC airfoils are considered. Chaplin⁷ addressed this configuration using a simplified analysis which assumed linearized aerodynamics, constant rotor speed, and zero or low forward speed. He concluded that a rigid two-bladed fully gimballed rotor "can be rendered dynamically stable by appropriate mass balancing."

This report describes the methodology and results of an effort to analyze the dynamic properties of a rigid two-bladed gimballed rotor with circulation control using a comprehensive time domain simulation. No consideration is given to fuselage coupling effects, and results should be considered as equivalent to those obtainable in a wind tunnel.

METHODOLOGY

Considerable expertise has been gained in time domain simulation as part of the CC rotor program. By using time rather than frequency domain analysis, it is possible to incorporate more complete aerodynamic and more flexible geometric representations in the simulation.

A comprehensive computer program (HELSTAB), which simulates the blade and vehicle dynamics of articulated and hingeless (A/H) rotor helicopters, was previously developed by ASED in support of the CC rotor project. The general features of HELSTAB* are

1. Time history analysis--to provide fully coupled degrees of freedom, to avoid the restrictions inherent in linearized eigenvalue solutions, and to allow for a more general vehicle and aerodynamic model.
2. Modular programming--to maintain separate and distinct program modules for ease of modification and transportability.

*HELSTAB has not been formally documented. The primary contributors to its development were J.B. Wilkerson, P.S. Montana, and D.W. Poe of DTNSRDC, with contract support from the University of Maryland on specific tasks, and consultative support from Kaman Aerospace in areas related to the XH-2/CCR demonstrator aircraft.

3. Balanced approach--to provide the necessary balance between rotor and vehicle aerodynamic, dynamic, and geometric descriptions.

The gimballed rotor is fundamentally different from A/H rotors. This difference stems from an assumption, commonly made in the study of A/H rotors, that the rotor shaft angular velocity with respect to the fuselage is constant. Since the rotor hub is rigidly attached to the rotor shaft, the rotor blades may be treated independently of each other in solving for their motions. For a gimballed rotor, the rotor shaft velocity is not constant in either magnitude or direction. In fact, the dynamics of gimballed rotors are best characterized by shaft tilt angles rather than by the flap, lag, and feather of individual blades. While it may initially appear that the study of a rigid gimballed rotor (i.e., no blade motion with respect to the rotor hub) is less general than the study of A/H rotors with first mode blade motion (i.e., rigid blade flap, lag, and feather), the studies are equivalent. Both result in first order tip path plane motion, and both model the n-blade per revolution vibrations which affect the fuselage.

The architecture of the HELSTAB program allowed modifications for the analysis of gimballed rotors to be incorporated. The main modifications to HELSTAB consisted of the replacement of program modules containing equations for computing: rotor angular accelerations, rotor forces, and blade element velocities. Changes were made to input and output modules, and several new modules were added to the program to account for blade element angle-of-attack variation due to blade collective angle change and for feedback of rotor angles, angular rates, and accelerations to the rotor control system. The modified computer program (GIMSTAB) was exercised for a variety of cases in hover and forward flight.

ROTOR AERODYNAMIC REPRESENTATION

The HELSTAB simulation program was designed to allow the selection of the levels of sophistication of rotor and vehicle analyses via the insertion of different program modules. Considerable effort has been devoted in ASED to the development of circulation control rotor (CCR) aerodynamic performance capability. The best methodology available was incorporated in GIMSTAB when it was developed. Wilkerson et al.⁴ discuss the correlation of the rotor aerodynamic performance methodology with full-scale wind tunnel data obtained as part of the CCR flight demonstrator test program. In brief, the aerodynamic model is based on strip theory

with Glauert inflow. All CC airfoil characteristics (e.g., chord, thickness, slot height) could be varied radially. The basic airfoil characteristics were input as a series of data tables for the specific airfoils used. Corrections were made for tip losses, and compressibility and Reynolds' effects. The model was used for calculating the radial distribution of blowing jet, momentum coefficient, and weight flow in addition to the lift, drag, and pitching moments. The blade lift, drag, and pitching moments were provided as inputs to the rotor dynamics portion of the GIMSTAB program.

EQUATIONS OF MOTION

The equations of motion for rigid gimballed rotors were derived in a relatively conventional fashion based on Newton's Second Law and closely following the method and notation of Etkin.⁸ The analytic rotor model selected was very general and provided a maximum flexibility in the description of the rotor. Derivations were made with the following limitations placed on the model and program architecture.

1. The rotor was rigid. The motion of the rotor's center of gravity and of each blade is described explicitly by the motion of the gimbal in inertial space plus the kinematics of the rotor about the gimbal.
2. The motion of the gimbal was prescribed by a global vehicle dynamics solution external to the rotor dynamics model.
3. Total aerodynamic forces and moments were computed and supplied to the rotor dynamics model by a separate aerodynamics model.
4. Tip jet thrust was also supplied to the dynamics model.
5. Gimbal reaction forces were computed by the dynamics model.
6. Gimbal restraint moments were accommodated within the dynamics model to provide for frictional losses and the potential need for damping and/or centering springs as rotor motion limiters. These provisions were in the nature of damping and friction coefficients and spring rates coupled to angular rates and deflections to produce torques about the gimbal. The nature of the structural limitations imposed on the model were in keeping with the modular nature of the GIMSTAB program.

The equations of motion of the rotor were derived in a reference frame (Figure 2) attached to the rotor located at its center of gravity (c.g.). In this reference frame, rotor inertias are invariant and rotor weight does not contribute a moment.

A draw back of the c.g. centered frame is the appearance of gimbals reaction forces in the moment equations. However, the kinematic relationship of linear motion to angular motion (i.e., rigid rotor assumption) allows the force equations to be used to determine gimbals reaction rather than rotor c.g. linear motion. Thus, the six fundamental equations of motion were reduced to three moment equations. As a consequence of the time history approach, these three equations were solved explicitly for three Euler angular accelerations. (Euler angles used in the equation of motion are shown in Figure 3.) A complete description of the rotor motion was then available by numerically integrating* the angular accelerations.

The details of the derivation of the equations of motion are as follows. The symbols are defined in the separate notation section; however, the meaning of most symbols can be determined from the equations and from Figure 4.

Newton's Second Law yields six equations

$$\begin{aligned} \left[\begin{array}{l} \text{Rate of Change} \\ \text{of Angular} \\ \text{Momentum} \end{array} \right] &= \left[\begin{array}{l} \text{Sum of the} \\ \text{Applied External} \\ \text{Moments} \end{array} \right] \\ \dot{\vec{h}} &= \vec{G} \\ \dot{I\vec{\omega}} + \vec{\omega} \times I\vec{\omega} &= \vec{G} \end{aligned} \quad (1)$$

$$\left[\begin{array}{l} \text{Rate of Change} \\ \text{of Linear} \\ \text{Momentum} \end{array} \right] = \left[\begin{array}{l} \text{Sum of the} \\ \text{Applied External} \\ \text{Forces} \end{array} \right]$$

$$\frac{d}{dt} (m\vec{r}) = \vec{F}$$

which reduces to

$$m\ddot{\vec{r}} = \vec{F} \quad (2)$$

for constant rotor mass. The total external moment applied to the rotor consists of

*The integrations were carried out using a four-step Runge-Kutta (R-K) formulation.⁹ This technique was compared to a six-step R-K and variable time step methods and was found to have adequate numerical accuracy and the highest time efficiency.

$$\bar{G} = \begin{bmatrix} \text{Aerodynamic} \\ \text{Moment} \end{bmatrix} + \begin{bmatrix} \text{Reaction Moment} \\ \text{at the Gimbal} \end{bmatrix} + \begin{bmatrix} \text{Tip Jet} \\ \text{Moment} \end{bmatrix}$$

$$\bar{G} = \sum_{k=-j}^j [d\bar{M}_k^a + (\bar{J}_k \times d\bar{f}_k^a)] + [\bar{M}^R - \bar{b} \times \bar{P}] + \sum_{i=1}^n [\bar{S}_i \times \bar{T}_i] \quad (3)$$

The total external force applied to the rotor consists of

$$\bar{F} = \begin{bmatrix} \text{Aerodynamic} \\ \text{Force} \end{bmatrix} + \begin{bmatrix} \text{Tip Jet} \\ \text{Thrust} \end{bmatrix} + \begin{bmatrix} \text{Weight} \end{bmatrix} + \begin{bmatrix} \text{General Reaction} \\ \text{Force} \end{bmatrix}$$

$$\bar{F} = \sum_{k=-j}^j d\bar{f}_k^a + \sum_{i=1}^n \bar{T}_i + m\bar{g} + \bar{P} \quad (4)$$

Solving the force Equations (4) for the gimbal reaction force, \bar{P} , gives

$$\bar{P} = m(\ddot{\bar{r}} - \bar{g}) - \sum_{k=-j}^j d\bar{f}_k^a - \sum_{i=1}^n \bar{T}_i \quad (5)$$

Substituting for \bar{P} in the moment equations yields

$$I\ddot{\bar{\omega}} + \bar{\omega} \times I\bar{\omega} = \sum_{k=-j}^j [d\bar{M}_k^a + (\bar{J}_k + \bar{b}) \times d\bar{f}_k^a] - \bar{b} \times (\ddot{\bar{r}} - \bar{g}) m + \bar{M}^R + \sum_{i=1}^n [(\bar{b} + \bar{s}_i) \times \bar{T}_i]$$

$$I\ddot{\bar{\omega}} + \bar{\omega} \times I\bar{\omega} = \bar{M}^a - \bar{b} \times (\ddot{\bar{r}} - \bar{g}) m + \bar{M}^R + \bar{M}^{TJ} \quad (6)$$

It is this final set of Equations (6) which must be solved for the Euler angle accelerations $(\ddot{\phi}, \ddot{\theta}, \ddot{\psi})$. These angular accelerations appear in only two terms, $\ddot{\bar{\omega}}$ and $\ddot{\bar{r}}$. The solution procedure is shown symbolically in Equations (7)-(10) in which the previous vector notation is replaced with matrix notation and where

$$\bar{I}\dot{\omega} = [A] \begin{Bmatrix} \ddot{\phi} \\ \ddot{\theta} \\ \ddot{\psi} \end{Bmatrix} + \{D\}$$

$$\bar{r} = [a] \begin{Bmatrix} \ddot{\phi} \\ \ddot{\theta} \\ \ddot{\psi} \end{Bmatrix} + \{d\}$$

$$[A] \begin{Bmatrix} \ddot{\phi} \\ \ddot{\theta} \\ \ddot{\psi} \end{Bmatrix} + \{D\} + [\tilde{\omega}] [I] \{\omega\} = \{M^a\} - [\tilde{b}] [a] \begin{Bmatrix} \ddot{\phi} \\ \ddot{\theta} \\ \ddot{\psi} \end{Bmatrix} + \{d\} - \{g\} m + \{M^R\} + \{M^{TJ}\} \quad (7)$$

$$\underbrace{[A] + [\tilde{b}] [a] m}_{[K]} \begin{Bmatrix} \ddot{\phi} \\ \ddot{\theta} \\ \ddot{\psi} \end{Bmatrix} = \underbrace{\{M^a\} - [\tilde{b}] \{d\} - \{g\} m + \{M^R\} - \{D\} - [\tilde{\omega}] [I] \{\omega\} + \{M^{TJ}\}}_{\{C\}} \quad (8)$$

$$\begin{matrix} \cdot \\ \cdot \\ \cdot \\ [K] \end{matrix} \begin{Bmatrix} \ddot{\phi} \\ \ddot{\theta} \\ \ddot{\psi} \end{Bmatrix} = \begin{matrix} \cdot \\ \cdot \\ \cdot \\ [C] \end{matrix} \quad (9)$$

$$\begin{Bmatrix} \ddot{\phi} \\ \ddot{\theta} \\ \ddot{\psi} \end{Bmatrix} = [K]^{-1} \{C\} \quad (10)$$

It is worth noting here that the solution was a complex undertaking. The main difficulty was associated with the intermediate frames of reference between the gimbal and the rotor in which the Euler angles (ϕ, θ, ψ) were defined. This inherent cross coupling introduced a myriad of terms consisting of products of direction cosines. No small angle assumptions were made to simplify the equations. The solution was accomplished with the use of the Project MAC's Symbolic Manipulation

System¹⁰ (MACSYMA) available on the Navy Laboratory Computer Network. The main benefit of MACSYMA in this application was its ability to symbolically manipulate matrices. It was also possible to store results and to automatically convert equations to FORTRAN coding on the system. With intermediate steps, the FORTRAN statements were transmitted to DTNSRDC's computers for incorporation in the GIMSTAB program.

DISCUSSION

The objective of this program was to analyze the dynamic properties of two-bladed rigid gimballed rotors incorporating CC airfoils. Time domain analysis was selected to accomplish the objective to allow the use of nonlinear aerodynamics and to provide a flexible and complete geometric model of the rotor. There were three steps taken to accomplish the objective: (1) selection of a rotor physical model, (2) determination of hover characteristics, and (3) simulation of forward flight characteristics.

ROTOR MODEL

At the time the the gimballed rotor project was executed, the best defined CC rotor was the one employed by the XH-2/CCR flight demonstrator aircraft. The airfoil characteristics were well known and data tables were in existence for use in rotor performance simulations. In addition, the actual physical characteristics of the flight demonstrator's rotor had been measured and were available.* The physical characteristics of the XH-2/CCR rotor blades and hub were modified to reflect the change from four blades to two blades; an emphasis was placed on preserving, as much as possible, the combined hub and blade characteristics. For instance, total hub and blade weight and rotational inertia, and solidity were held constant. Individual blade characteristics were scaled as follows:

1. Radial location of the blade center of gravity was held constant.
2. Blade thickness ratio distribution was held constant.
3. Blade weight was doubled.
4. Blade chord was doubled.
5. Blade inertias were scaled consistent with items 1 through 4.

*These characteristics were provided by Kaman Aerospace Corporation.

6. Blade airfoil selection was held constant.

7. All blade nondimensional CC parameters were held constant.

A description of the rotor model is given in Tables 1 and 2.

HOVER ANALYSIS

The hover analysis established the baseline characteristics of the gimballed rotor model. The central feature of these characteristics was the development of a stability* boundary in regard to the location of the rotor's principal axis of inertia. As noted in the introduction, a two-bladed gimballed rotor has very high inertias about two axes, flap and azimuth, and very low inertia about one axis, feather. Chaplin⁷ identified the feather principal axis of inertia location relative to the blade aerodynamic center as a key parameter affecting rotor dynamic stability for two-bladed gimballed rotors. Feather principal axis location is important whether CC or conventional airfoils are employed; however, the use of CC airfoils complicates the relationship of principal axis of inertia location to stability.

A salient feature of circulation control airfoils is the existence of two aerodynamic centers. Conventional airfoils employed on helicopters have one aerodynamic center (a.c.) located near the quarter chord. Since angle of attack determines lift (for a given velocity and air density), the location of the principal axis (center of gravity for sections) with respect to the a.c. determines whether the response to an angle-of-attack disturbance is stable or unstable. For stability, the principal axis should be ahead (upstream) of the a.c.; thus, a positive lift disturbance would yield a nose down moment tending to reduce angle of attack and lift.

Circulation control airfoils have both angle of attack and CC lift. The CC lift is relatively independent of angle of attack, but is dependent upon the characteristics of the trailing edge blowing. The a.c. for CC lift is located near the half chord. When the complex flow over a rotor in forward flight is considered, it is apparent that the combined lift on the individual airfoil sections along a blade may act at the quarter chord, half chord, or anywhere in between.

*The term "stability" is used in this report in several ways, some of which do not precisely match traditional interpretations. Definitions of "stability" used in this report are given on pages 11 and 14.

In order to classify feather principal axis locations, the 0.7 rotor radius station was selected as a reference for axis location. The location is specified as a fraction of chord length from the leading edge. The 0.7 radius station is a standard aerodynamic reference and is considered to be typical of rotor aerodynamics based on strip theory combined with nominal tip losses.

Part of the definition of rotor characteristics was the generation of a rotor performance map in hover. The map covers a range of parameters representative of the XH-2/CCR aircraft. The parameters include: thrust from 0 to 13,000 lb (57,829 N), blade duct pressure ratios from 1.0 to 1.8, and blade collective feather angles from -6 to +10 deg (-0.10 to 0.017 rad). The map was generated for a principal axis of inertia location at 30-percent chord at the 0.7 radius station. An assumption made during the hover performance analysis was constant average tip speed of 615 ft/sec which was accomplished through the use of constant tip jet thrust. Tip jet thrust depended upon blade collective angle, duct pressure ratio, and rotor thrust.

Stability in hover was defined as the ability to sustain a vertical rotor axis position during time integration without simulated disturbances. While this was an unsophisticated test, it did succeed in establishing a boundary which was later correlated by the method of Chaplin.⁷ Chaplin's method was based on constant instantaneous rotor tip speed. Hence, his stability boundary is not a function of the distribution of lift between angle of attack and circulation control. The present results confirm this assumption by showing only a small sensitivity to angle of attack versus CC lift distribution. There is a need to investigate the possibility of stable precessional modes in hover which is not addressed here.

FORWARD FLIGHT

The analysis of the motions of helicopters differs from that of fixed wing aircraft in the ability to simplify the problem by separating modes. For fixed-wing aircraft, it is possible to consider the lateral and longitudinal motions separately because of the existence of left to right geometric and flow symmetries. Helicopters possess the same type of geometric symmetry in the fuselage and have geometric rotational symmetry of the rotor blades about the rotor hub. However, the flow over a helicopter is not symmetric in either hover or forward flight. Rotational velocity components exist in the rotor downwash which affect the sides of the fuselage

differently. In forward flight, the velocity of each blade element is composed mainly of forward speed and rotational speed; hence it is a function of the azimuth position of the rotor blade. The blades of most rotors are treated individually. In steady state forward flight, they experience a once per revolution cyclic aerodynamic perturbation. The blades of a rigid gimballed rotor are treated collectively because their motions are kinematically related. As a result, the whole rotor, including each blade, responds to a cyclic aerodynamic perturbation occurring at the rotor's rotational speed times the number of blades, n , per revolution. Hence, in steady state forward flight, the dynamics of a gimballed rotor can be expected to repeat every $1/n$ revolution (i.e., at the same frequency as the forcing function).

The normal means of determining whether or not an articulated rotor has reached blade dynamic equilibrium in the time domain is to integrate the rotor motions for one complete revolution and compare the starting and ending blade angles of flap, lag, and feather. If the angles repeat within specified tolerances, the dynamics are defined as being in equilibrium. This method is possible because of the tacit assumption of constant rotor speed. This assumption makes time and rotor azimuth angle equivalent. The individual rotor blades also experience a very strong centrifugal force which tends to quickly stabilize the motions.

For gimballed rotors, the dynamic angles are rotor roll, pitch, and azimuth. Since rotor speed (i.e., azimuth angle rate) is not constant, the normal means for determining dynamic equilibrium is not possible with a constant time step integration technique. The practical alternative to a sophisticated variable time step integration was an average rotor speed controller. This approach is also realistic because of the aerodynamic and structural design optimization of all rotors for a given rotor speed.

A twofold approach was used to achieve constant average rotor speed. The azimuth position at the end of the integration interval (time for one-half revolution of a two-bladed rotor at the desired average rotor speed) was compared to the starting position. If the rotor had not completed or had exceeded a half revolution, the average tip jet thrust was adjusted to correct the error. During the time integration, the rotor azimuthal acceleration was monitored; and the average tip jet thrust was corrected (with a maximum of 50% authority) to attempt to achieve zero acceleration. This unsophisticated method proved to be fairly successful when the rotor was stable or mildly unstable (i.e., near equilibrium).

In spite of the use of rotor speed control, it took lengthy simulations and many iterations of cyclic blowing to reach equilibrium for a specified rotor collective angle and thrust value. The strong stabilizing influence of centrifugal force is not present for gimballed rotors. By nature, gimballed rotors are different from articulated rotors. Rotor dynamic equilibrium is a much more restrictive condition for the gimballed rotor, because it requires that the net moments acting on the rotor be zero in addition to the other common requirements.

FEEDBACK CONTROL

As a result of experience using the simulation program, it was obvious that a means of reaching dynamic equilibrium in forward flight was needed. After several unsuccessful trials using rotor tilt angle (pitch and roll) feedback, it was found that feeding back of rotor teeter rate was a highly effective means of quickly reaching dynamic equilibrium.[†] The algorithm developed for this type of feedback was very general in nature and was capable of generating feedback signals to blade duct pressure for teeter and feather angles^{††} and their first and second derivatives. The relationship used to generate a control pressure^{†††} signal was

$$\Delta p = k_{\beta} \Delta \beta^* + k_{\dot{\beta}} \Delta \dot{\beta}^* + k_{\ddot{\beta}} \Delta \ddot{\beta}^* + k_{\theta} \Delta \theta^* + k_{\dot{\theta}} \Delta \dot{\theta}^* + k_{\ddot{\theta}} \Delta \ddot{\theta}^*$$

where each of the Δ -quantities (with the exception of pressure) was the difference between actual (simulated) and commanded angles, rates, or accelerations. The k -quantities were simple gain constants. Feedback was implemented by modifying the normal blade duct pressure relation.

$$P_{\text{duct}} = P_{\text{collective}} + A \sin \psi + B \cos \psi$$

[†]The use of teeter rate feedback was an extension of a suggestion made by H.R. Chaplin, in informal communications, that the use of teeter angle feedback might be effective in stabilizing the rotor.

^{††}The teeter and feather angles are Euler angles which are indicated in Figure 5.

^{†††}Because the control pressure signal is a function of feather and teeter angles, which are harmonic functions of azimuth angle, the control pressure signal is also a harmonic function of azimuth angle.

using the new cyclic pressure coefficient definitions

$$A = A_1 + \Delta p \sin \psi^*$$

$$B = B_1 + \Delta p \cos \psi^*$$

where A_1 and B_1 were the previous (commanded) values. Substituting the new definition results in

$$P_{\text{duct}} = P_{\text{collective}} + A_1 \sin \psi + B_1 \cos \psi + \Delta p (\sin \psi^* \sin \psi + \cos \psi^* \cos \psi)$$

or

$$P_{\text{duct}} \approx P_{\text{collective}} + A_1 \sin \psi + B_1 \cos \psi + \Delta p$$

(for small values of β and Θ).

STABILITY

Several tests were used to establish rotor stability characteristics. The first test was whether or not rotor dynamic equilibrium could be reached without feedback. This was a very cumbersome process since the required cyclic pressure and rotor collective angle combination for a desired rotor tilt angle was not known, and the rotor had to be very close to the equilibrium dynamics to begin to stabilize. The second test was to disturb the rotor from equilibrium with a pulsed horizontal gust of one-half revolution duration. The pulse test was used to determine if the rotor possessed any inherent damping. The third test was to disturb the rotor from equilibrium with a step horizontal gust. The intent of this test was to determine if the rotor's response was predictable and if the rotor would transit to a new equilibrium position. All tests were performed both with and without feedback.

RESULTS

HOVER ANALYSIS

The hover analysis yielded two products, a rotor performance map and a principal axis stability boundary. The rotor performance map (Figure 6) was generated for a

range of parameters representative of the XH-2/CCR aircraft: thrust from 0 to 13,000 lb (57,824 N), blade duct pressure ratios from 1.0 to 1.8, and blade collective angles from -6 to +10 deg (-0.105 to 0.175 rad). The rotor feather principal axis was located at 30% chord at the 0.7 radius station. The map shows that a desired rotor thrust can be achieved with a variety of combinations of blade duct pressure ratio and blade collective angle. It also shows that tip jet thrust can be minimized by selecting the proper combination of the same variables for a given rotor thrust setting.

The rotor principal axis stability boundary, as discussed previously, is a boundary describing conditions for which rotor dynamic equilibrium in hover at a thrust of 11,000 lb (48,928 N) was possible. The boundary (Figure 7) proved to be insensitive to the distribution of lift between angle of attack and CC until a blade duct pressure ratio of about 1.7 was exceeded. This value of duct pressure ratio corresponds approximately with the region for which angle-of-attack lift changes from positive to negative. It is not unreasonable to expect a change in stability characteristics near this condition.

FORWARD FLIGHT

Forward flight analysis proved to be more complicated than originally envisioned. Achieving dynamic equilibrium, with the attendant requirement of constant average rotor speed, was the most significant problem. Once the difficulty reaching dynamic equilibrium was fully appreciated the other areas of investigation were developed as logical extensions of the effort.

The forward flight analysis was limited to a forward speed of 50 ft/sec (15.24 m/s) and a thrust level of 12,000 lb (53,376 N).

Open Loop Dynamic Equilibrium

The conditions for which rotor dynamic equilibrium was desired were -5 deg (-0.087 rad) rotor forward tilt and 0.0 deg (0 rad) lateral tilt with the feather principal axis located at $x/c = 0.2$. This feather principal axis location was selected because of stability considerations which indicated that the center of lift on the rotor blade should always be located aft of the principal axis. Blade duct pressure was selected as 1.8 to allow for the potential of maximum cyclic blowing. Equilibrium dynamics were achieved using an exhaustive trial and error method.

The required cyclic blowing pressure ratios were $(A,B) = (-0.0327, 0.0384)$ which were very nominal values; the required collective pitch angle was -4.6 deg (-0.080 rad). Figure 8 shows about 14 consecutive rotor revolutions. A small amount of drift was still present in the two per revolution rotor "wobble"*; however, the conditions were sufficiently stable for equilibrium to be assumed.

Effect of Principal Axis Location

The effect of principal axis location was evaluated for two cases: 100% angle-of-attack lift and about 100% CC lift. In both cases, the feather principal axis location was varied from 20% to 40% of the chord at the 0.7 radius station. Non-equilibrium initial conditions were selected to amplify the dynamic tendencies of the rotor. The initial conditions were: rotor tilt angles equal to zero; rotor azimuth rate, 27.9545 rad/s; all other rates and accelerations equal to zero. No cyclic blowing was used. For the 100% angle-of-attack lift cases, the collective angle was 7.5 deg (0.131 rad) and the collective pressure ratio was 1.0; and for the 100% CC lift cases, they were -4.6 deg (-0.080 rad) and 1.8, respectively.

The results are shown in Figures 9 and 10 as plots of rotor tilt angles, ϕ versus θ . These plots show that the rate of departure of the rotor from the non-equilibrium starting condition and the frequency and amplitude of the rotor motions are functions of the feather principal axis location and distribution of lift between CC and angle of attack, specifically:

1. The 100% CC lift cases depart from the initial condition at less than one-half the rate of the equivalent 100% angle-of-attack lift cases. This result reflects the postulate that CC lift is insensitive to angle of attack. (Angle of attack and local velocity vary with azimuth position in forward flight.)
2. The minimum departure rates for both the CC and angle-of-attack lift cases occur for a feather principal axis location of 30% chord. This result indicates that there is an optimum principal axis location for each CC rotor design and that, contrary to the original belief, a too far forward principal axis location can reduce rather than enhance stability.

*"Wobble" refers to the conical motion that the R_3 axis (Figure 2) attached to the rotor hub would scribe. Refer also to Figure 11a which shows rotor angular motions in the more traditional form as plots versus azimuth angle.

3. The minimum amplitude of the tilt angle oscillations occur for a feather principal axis location of 30% chord.

4. The frequency of the tilt angle oscillations changes from two to one per revolution as the principal axis location moves from 25% to 40% chord. The effect is shown in Figure 11.

FEEDBACK CONTROL

All six types of feedback provided in the duct pressure feedback relationship were evaluated individually. Initially, the purpose of feedback was to accelerate the convergence of rotor motion to dynamic equilibrium. The test used to evaluate the effect of feedback was to start the rotor in an unstable condition and monitor its progress toward equilibrium. All tests were performed using the same starting conditions--zero rotor pitch and roll angles, 27.9545 rad/s azimuth rate, 50 ft/sec (15.24 m/s) flight velocity, zero cyclic and 1.8 collective pressure ratios, -4.6 deg (-0.0803 rad) collective angle, and 20% chord feather principal axis location. The feedback control signals were generated by comparing the rotor's computed angles, rates, or accelerations with those equivalent to the average open loop equilibrium condition of -5 deg (-0.0873 rad) pitch and 0 deg (0 rad) roll. The results of the feedback trials (Figures 12 and 13) were compared with the open loop results for the same starting conditions (Figure 9a) to obtain a qualitative assessment of the value of feedback.

Teeter (Flap) Feedback

The effects of the various types of teeter feedback are shown in Figure 12. Both positive and negative gain constants, k_β , k'_β , or k''_β , were used. The results are summarized as follows:

1. Negative teeter angle feedback is slightly stabilizing in that the resulting complex dynamics appear to be centered near the desired rotor tilt angles. The dynamics contain a two per revolution oscillation with variable amplitude superimposed on a longer period oscillation whose frequency is a function of gain constant, k_β .

2. Positive teeter angle feedback is destabilizing.

3. Positive teeter rate feedback is very stabilizing. For $k'_\beta = 400$, the rotor reached a near equilibrium dynamic condition within about 1.5 seconds. The rotor oscillations were two per revolution with constant amplitude.

4. Negative teeter rate feedback is destabilizing.

5. Negative teeter acceleration feedback is slightly stabilizing in the sense that the departure rate from the starting condition is reduced from the open loop case. The character of the oscillations is two per revolution with near constant amplitude. Large values of teeter acceleration feedback gain, k_{β}'' , change the character of the oscillations to one per revolution with increasing amplitude and hence, have a destabilizing influence.

6. Positive teeter acceleration feedback is destabilizing.

Feather Feedback

The effects of various types of feather feedback are shown in Figure 13. The results are summarized as follows:

1. Negative feather angle feedback is slightly stabilizing in that it reduces the rate of departure from starting conditions as compared to the open loop case.

2. Positive feather angle feedback is destabilizing.

3. Negative feather rate feedback is stabilizing; there appears to be an optimum gain value near, $k_{\dot{\theta}} = -100$. Larger gain values seem to excite lower frequency oscillation. Characteristics for $k_{\dot{\theta}} = -100$ include the expected two per revolution oscillations and relatively steady dynamics.

4. Positive feather rate feedback is destabilizing.

5. Negative feather acceleration feedback did not appear to be stabilizing for the length of the simulation.

6. Positive feather acceleration feedback is destabilizing.

Effect of Lift Type

Several trials were made to assess the effect of the type of lift, angle of attack, or CC on rotor dynamic characteristics with teeter rate feedback, $k_{\dot{\theta}} = 400$. The results of these trials, which had the same initial conditions as above, are shown in Figure 14. In general, the distribution of lift between types did not affect the ability of the rotor to reach dynamic equilibrium or the speed at which equilibrium was approached. The type of lift distribution did influence the location of equilibrium dynamics slightly. This is shown graphically in Figure 15 as plots of mean rotor equilibrium pitch and roll tilt angles versus blade collective pressure ratio. There is a previously unmentioned feature of the simulations

pneumatic algorithm which should be noted. The pneumatic algorithm was designed to prevent the evaluation of rotor aerodynamics for duct pressure ratios less than 1.0, a condition which corresponds to suction rather than blowing at the CC slot. While suction can be a very powerful boundary layer control, it is not the phenomena which CC airfoils were designed to exploit. No data are available for CC airfoils with suction instead of blowing. And, in reality, it would be difficult to design a pneumatic system to accommodate mass flow in either direction. For these reasons, whenever a duct pressure ratio less than 1.0 was calculated, the duct pressure ratio was assigned a value of 1.0.

For the trials under consideration, when the collective pressure ratio was 1.0 (i.e., the rotor only had angle-of-attack lift), the feedback control algorithm was only allowed to generate a pressure signal when the change in pressure was positive. This is the probable cause for the shift in mean rotor roll tilt angle as the pressure ratio approached 1.0 which was evident in Figure 15. The ability of the rotor to stabilize with a partial pressure wave form is another indication of the versatility of the CC rotor concept.

The success of feedback, particularly teeter rate feedback, has implications beyond the achievement of dynamic equilibrium for simulation purposes. The dynamic equilibrium which was reached with feedback was not the same as the dynamic equilibrium reached through trial and error without feedback; hence, its utility is limited for the purpose of accelerating convergence to an open loop condition. However, teeter rate feedback was so successful that it should be considered as the primary means of controlling this type of rotor. For example, rather than connect a pilot's control stick mechanically to a pneumatic valving system to generate the cyclic pressure variation needed to control the rotor's thrust vector orientation (mean tip path plane), the pilot's control stick orientation could be used as the commanded rotor tilt angle with the feedback control system generating the appropriate pressure variation to achieve the desired mean rotor tilt angles. This method would eliminate the need for a mechanical linkage between the pilot's control stick and the rotor or control system without introducing additional complexity into the helicopters stability augmentation system (SAS). (The SAS must modify mechanical control inputs to account for changes in rotor phase relationships which are functions of speed, thrust, etc.) The one complexity which would be introduced

is the need for stick position, rotor position, and rate sensors. This method of controlling a rigid gimballed rotor is very promising and may have some application for articulated CC rotors.

STABILITY

As previously discussed, the tests, applied to determine stability characteristics once dynamic equilibrium was reached, consisted of monitoring the rotor's response to pulse and step gusts. The gusts applied were in the direction of the forward flight velocity and added either 10% or 50% to the magnitude of the flight velocity. The initial conditions for all cases were those of open loop dynamic equilibrium shown in Figure 8. These were 50 ft/sec (15.24 m/s) forward flight speed, -4.6 deg (-0.0803 rad) blade collective angle, 1.8 blade duct pressure ratio, and 20% chord principal axis location. For the open loop cases, the sine cyclic pressure ratio was -0.0327 and cosine cyclic pressure ratio was 0.0384. One set of flap rate feedback cases was run with a gain of $k_{\beta} = 400$ and with zero sine and cosine cyclic pressure ratios.

Time history rotor dynamics were simulated for 14 rotor revolutions, or about 3.15 seconds. The gusts were initiated at the beginning of the second half revolution. The pulsed gust had a duration of one-half revolution.

Open Loop Stability

The results of the open loop stability simulation are shown in Figure 16 for no disturbance, 10% and 50% pulsed gusts, and 10% and 50% step gusts. The responses to the pulsed gusts were relatively stable in the sense that the excursions damped out fairly quickly; however, the rotor did not immediately return to its initial conditions. When the rotor was disturbed with step gusts, it departed aft and to the left of the equilibrium condition. The departure angle was approximately constant at 33 deg (0.58 rad), measured from the gust axis, and the departure rate was proportional to the magnitude of the gust. Another feature of the open loop step gust response shown in the figure is the increasing spacing of the circular oscillations which indicates that the rate of departure is increasing. From these results, it is evident that the two-bladed rigid gimballed rotors are unstable in forward flight without feedback.

Closed Loop Stability

The results of the closed loop simulations with teeter rate feedback, $k_{\beta} = 400$, are shown in Figure 17 for no disturbances, a 50% pulse gust, and a 50% step gust. A significant difference between the open loop and closed loop simulations was the presence of transitional dynamics which may be seen by comparing Figures 16a and 17a. These dynamics are present in the closed loop cases because of the selection of open loop dynamics as initial conditions. The transitional dynamics damped very quickly as the closed loop equilibrium conditions were approached.

The response to the 50% pulse gust was a brief set of well damped two per revolution oscillations followed by a rapid convergence to the closed loop equilibrium dynamics. The response to the 50% step gust was well controlled, also. It consisted of brief oscillatory excursions followed by convergence to a new equilibrium dynamic condition pitched slightly forward (nose down) from the original, no disturbance, feedback equilibrium condition.

The step gust response which was expected was a shift to an equilibrium condition pitched slightly aft from the original feedback equilibrium condition. A slight speed instability is indicated by the nose down pitch which would increase the forward thrust component resulting in a further increase in forward speed. However, the fact that the dynamics damped to a new equilibrium quickly and that the equilibrium was close to the undisturbed feedback case, indicates a high probability of maintaining control of the vehicle's motion.

CONCLUSIONS

HOVER

1. Tip jet thrust may be minimized for a given rotor thrust by selecting the proper combination of rotor collective pressure ratio and collective angle.
2. Rotor dynamic equilibrium was insensitive to the distribution of lift between angle of attack and circulation control.

FORWARD FLIGHT

1. Rotor dynamic equilibrium was attainable through the proper selection of cyclic blowing pressure ratios.

2. The two-bladed rigid gimballed rotor was unstable without feedback control as evidenced by its inability to reach dynamic equilibrium after being disturbed by step gusts.

3. The rotor was less unstable with CC lift than with angle-of-attack lift.

4. There was an optimum feather principal axis of inertia location which minimized the rate of rotor divergence and wobble amplitude.

5. Frequency of the rotor's wobble changed from two to one per revolution when the feather principal axis was located too far aft.

6. Feedback control, especially teeter rate feedback, stabilized the two-bladed rigid gimballed rotor.

7. The teeter rate feedback stabilized the rotor regardless of the distribution of lift between CC and angle of attack.

8. The teeter rate feedback stabilized rotor had predictable response resulting in equilibrium dynamics when disturbed by large gusts.

ACKNOWLEDGMENTS

The author would like to express appreciation to Dr. Harvey R. Chaplin for his support and for many valuable interactions relating to gimbal rotor dynamics, to Mr. Joseph B. Wilkerson for frequent discussions on circulation control and articulated rotor dynamics and control, and to Mr. Daniel W. Poe for assistance in modifying the HELSTAB computer program.

REFERENCES

1. Nichols, J.B., "The Pressure Jet Helicopter Propulsion System," Hughes Tool Company, Aircraft Division Report 70-81 (1970).
2. Bossler, R.B., Jr. and W.R. Harris, Jr., "Power Transfer Systems for Future Helicopters," American Helicopter Society, 29th Annual National Forum, Preprint No. 773, Washington, DC (May 1973).
3. Head, R.E. (Hughes Helicopters, Inc.), "Preliminary Design of a Tip Jet Driven Heavy Lift Helicopter Incorporating Circulation Control," Report DTNSRDC/ASED-81/07 (Mar 1981).
4. Wilkerson, J.B. et al., "The Circulation Control Rotor Flight Demonstrator Test Program," American Helicopter Society, 35th Annual National Forum, Preprint No. 79-51, Washington, DC (May 1979).
5. Reader, K.R. et al., "Status Report on Advanced Development Programs Utilizing Circulation Control Rotor Technology," Fourth European Rotorcraft and Powered Lift Aircraft Forum, Paper No. 44, Stresa, Italy (Sep 1978).
6. Englar, R.J. et al., "Design of the Circulation Control Wing STOL Demonstrator Aircraft," American Institute of Aeronautics and Astronautics Aircraft Systems and Technology Meeting, Paper No. 79-1842, New York, NY (Aug 1979).
7. Chaplin, H.R., "Some Dynamic Properties of a Rigid Two-Bladed Fully Gimballed Tip-Jet Helicopter Rotor with Circulation Control," DTNSRDC/TM-16-80/16 (Aug 1980).
8. Etkin, B., "Dynamics of Atmospheric Flight," John Wiley and Sons, Inc., New York (1972), pp. 112-120, 134-141.
9. Lee, J.A.N., "Numerical Analysis for Computers," Reinhold Publishing Corporation, New York (1966), pp. 199-201.
10. Bogen, R. et al., "MACSYMA Reference Manual," 2nd ed., Massachusetts Institute of Technology, Cambridge, MA (1977).

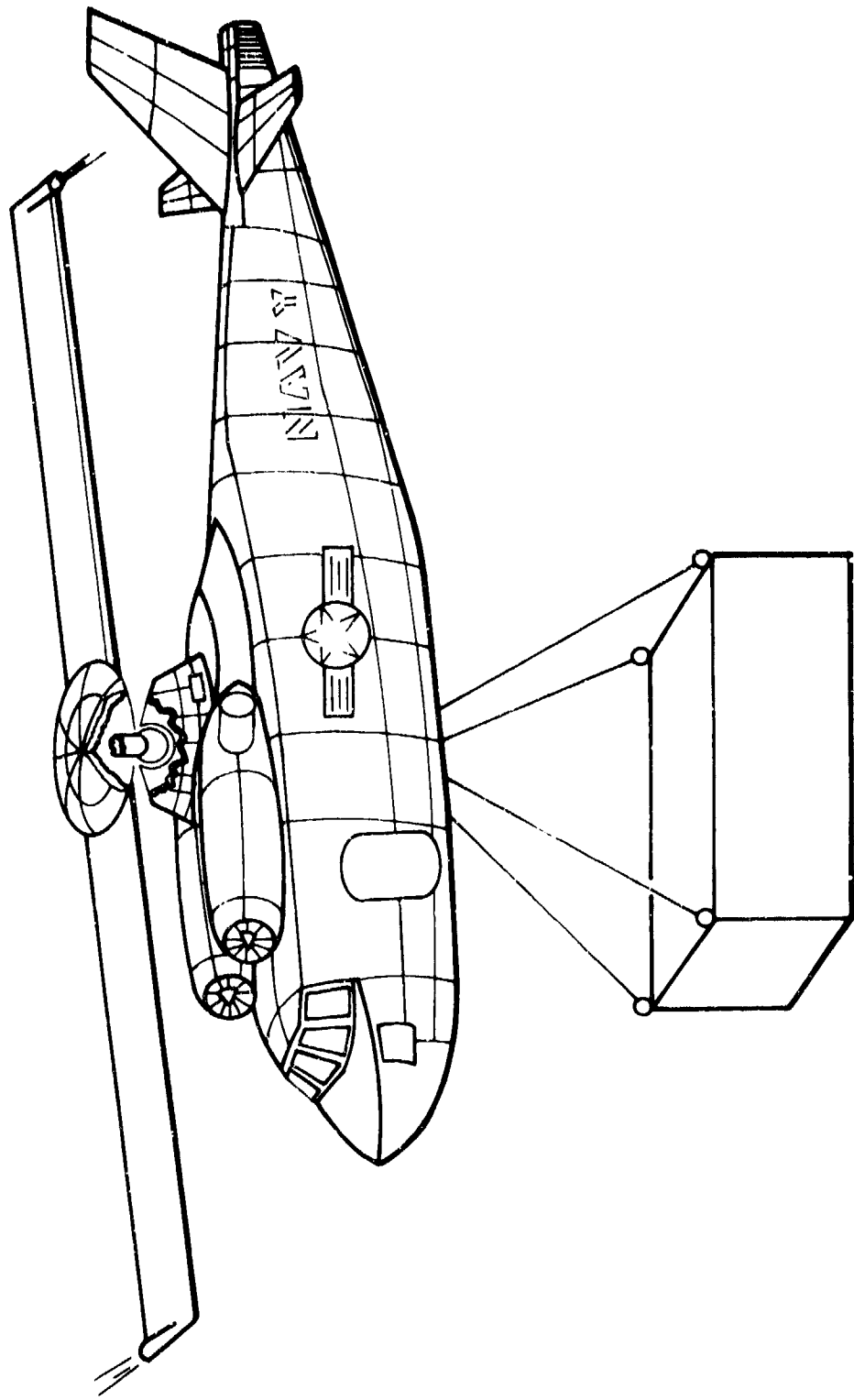


Figure 1 - Gimballed Rotor Helicopter

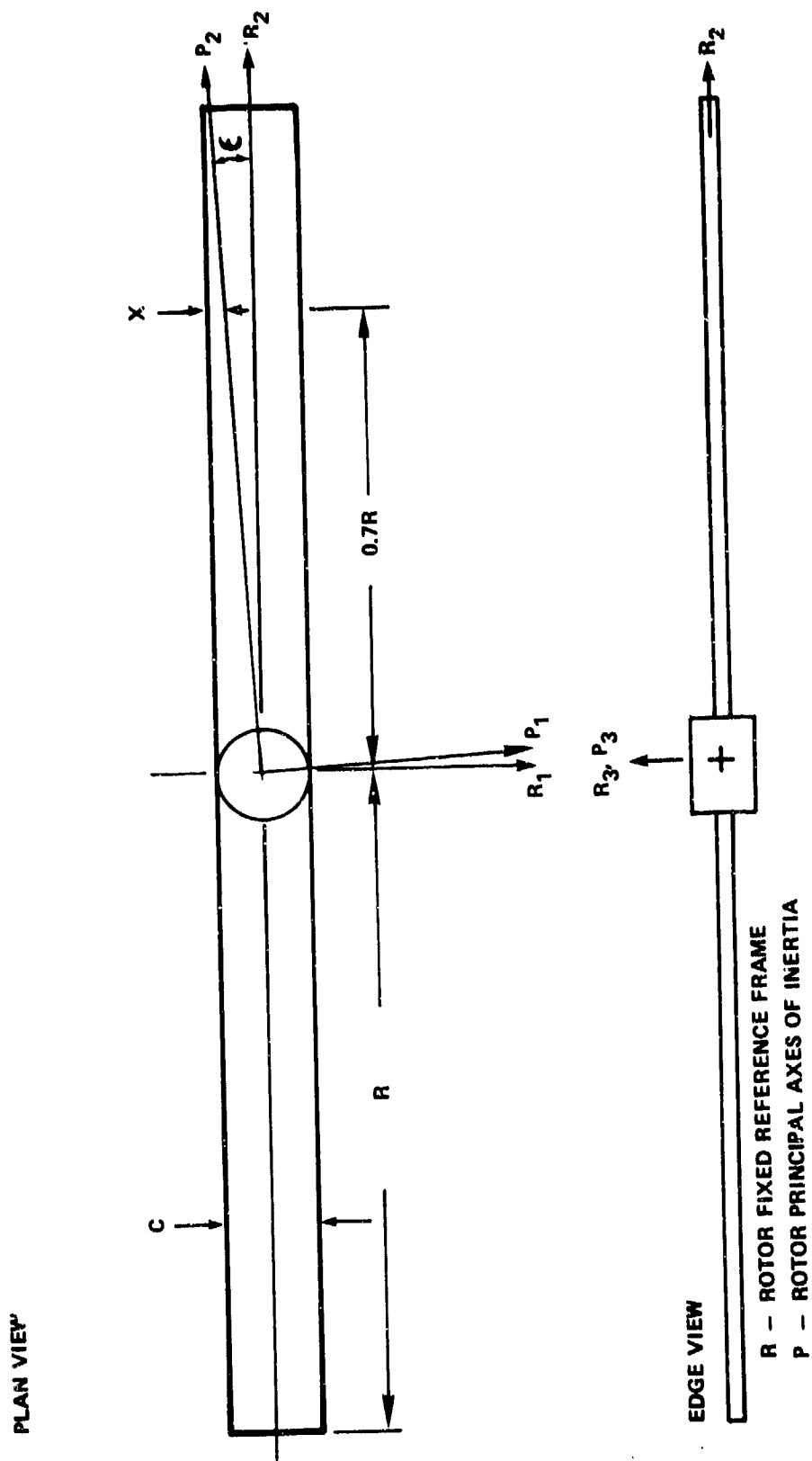


Figure 2 - Rotor Fixed Reference Frame

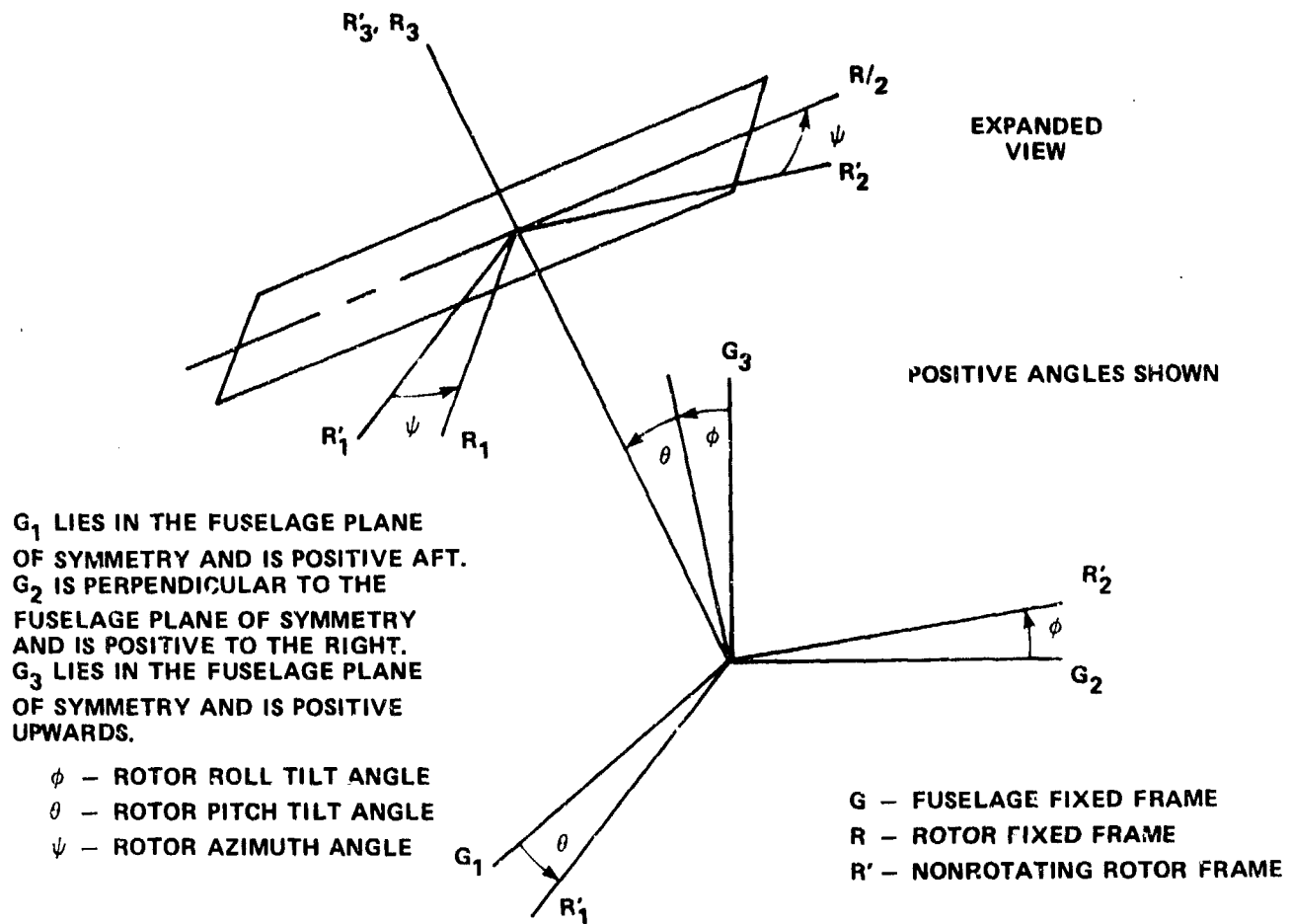


Figure 3 - Euler Angles for Rotor Dynamic Calculations

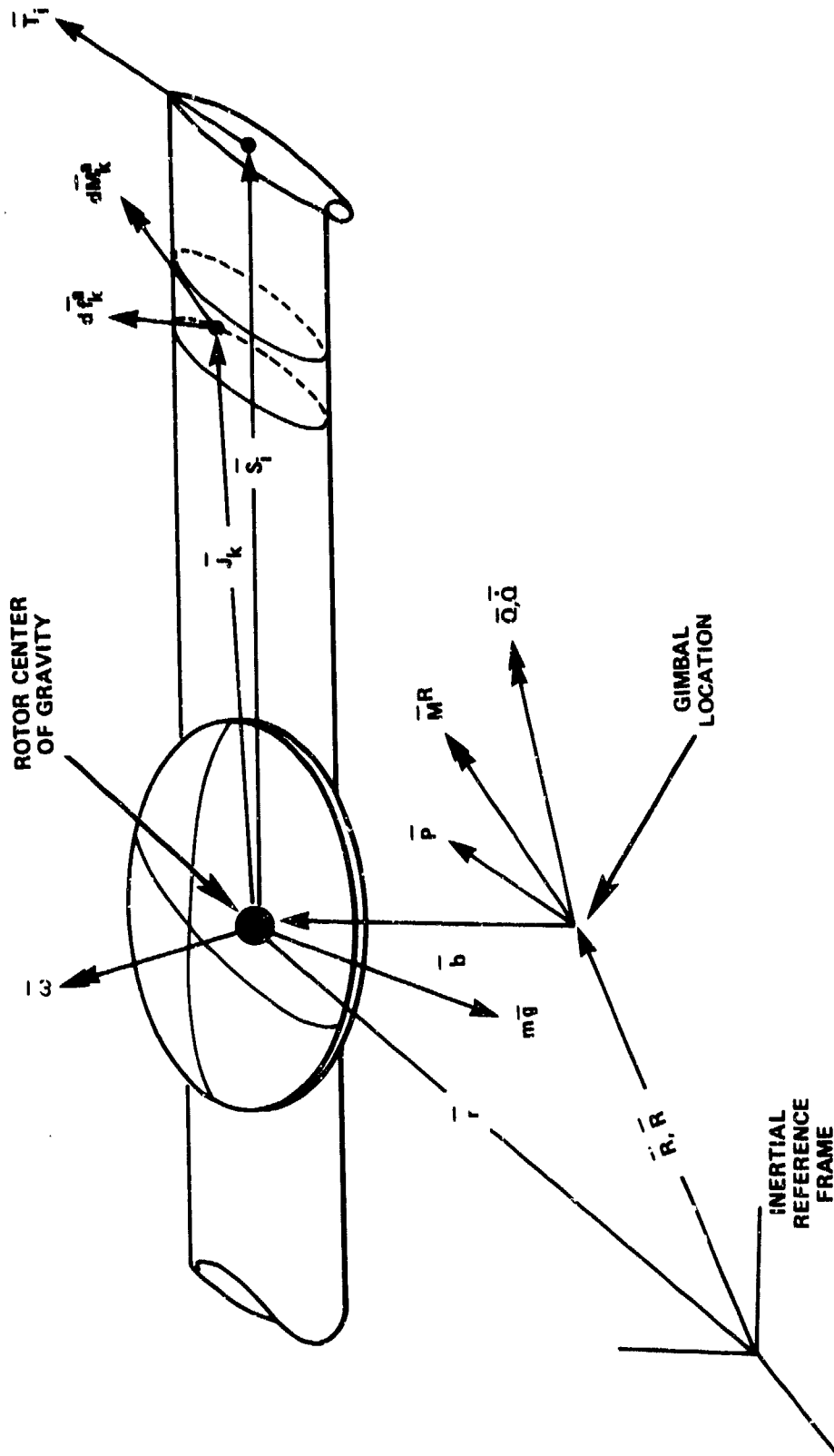


Figure 4 - Rotor Forces and Moments

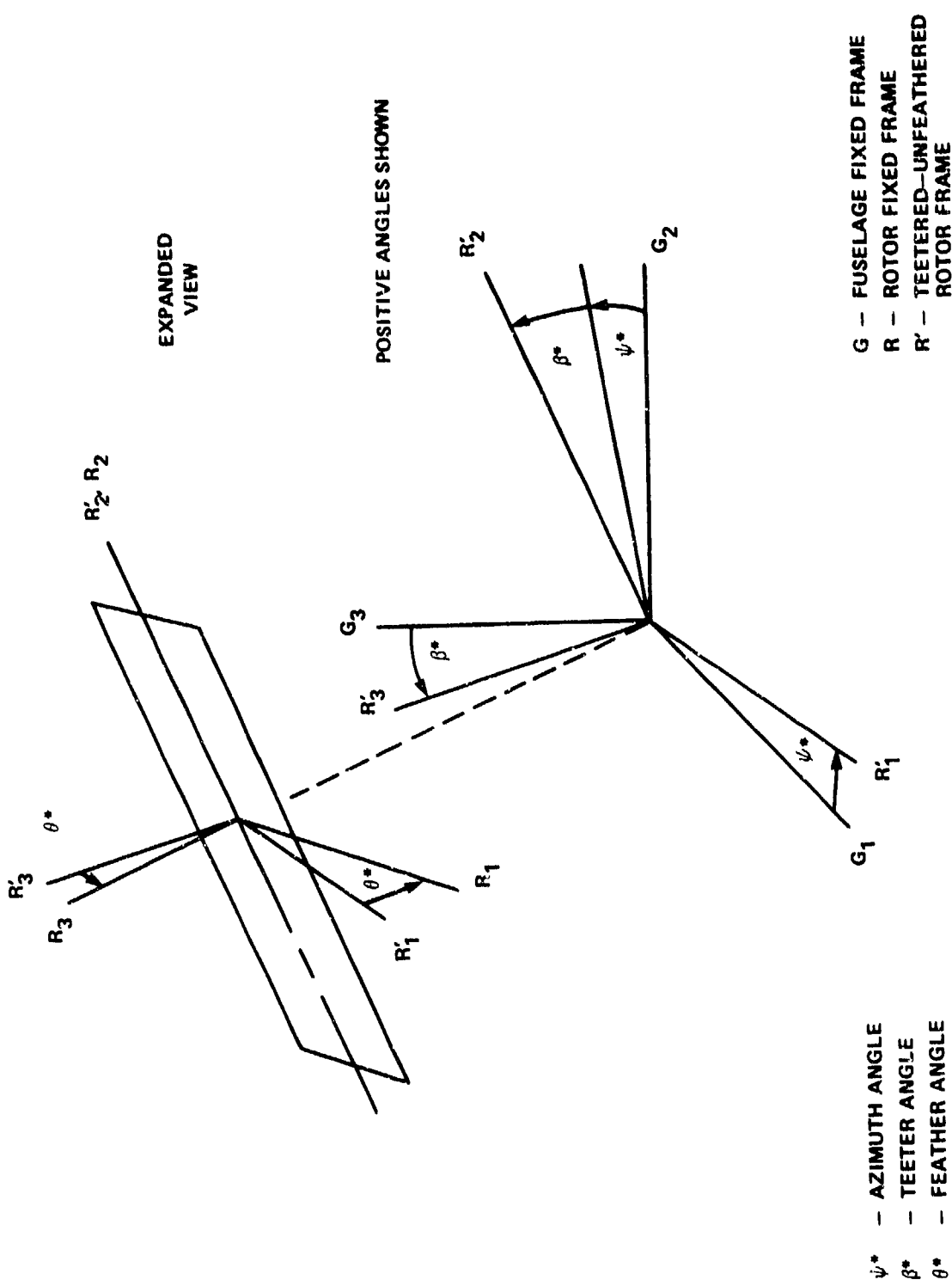


Figure 5 - Euler Angles for Feedback Calculations

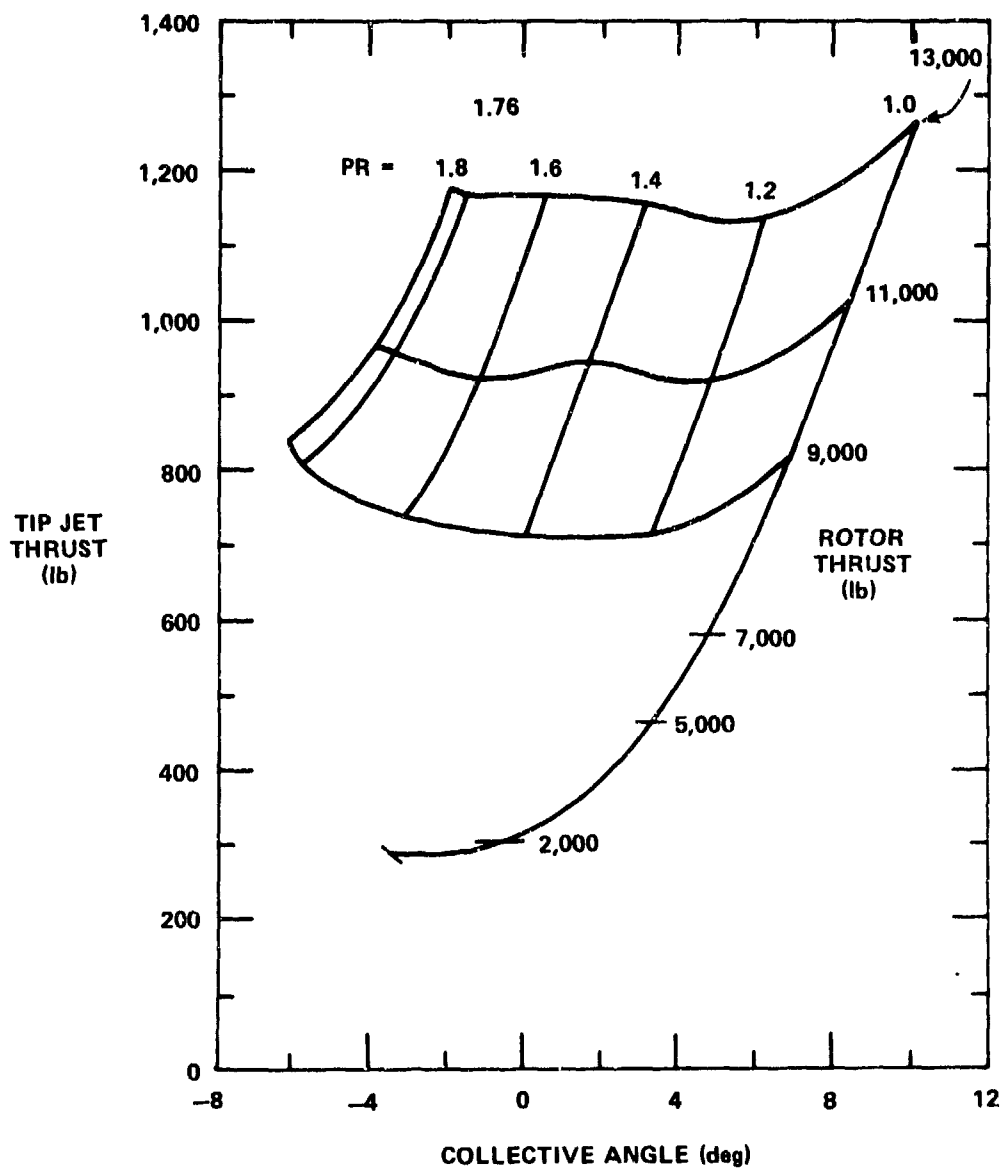


Figure 6 - Rotor Hover Performance Map

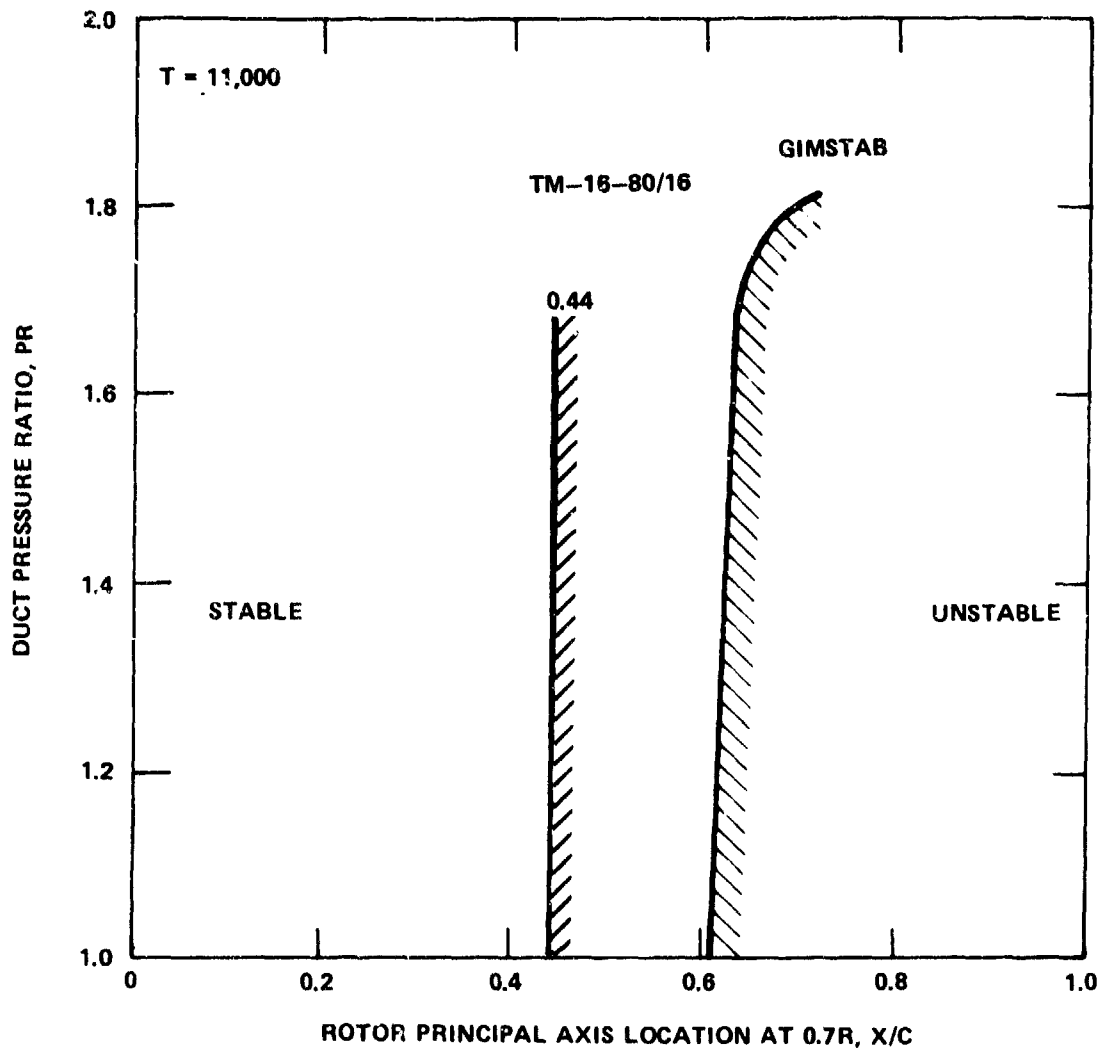


Figure 7 - Rotor Dynamic Equilibrium Boundary in Hover

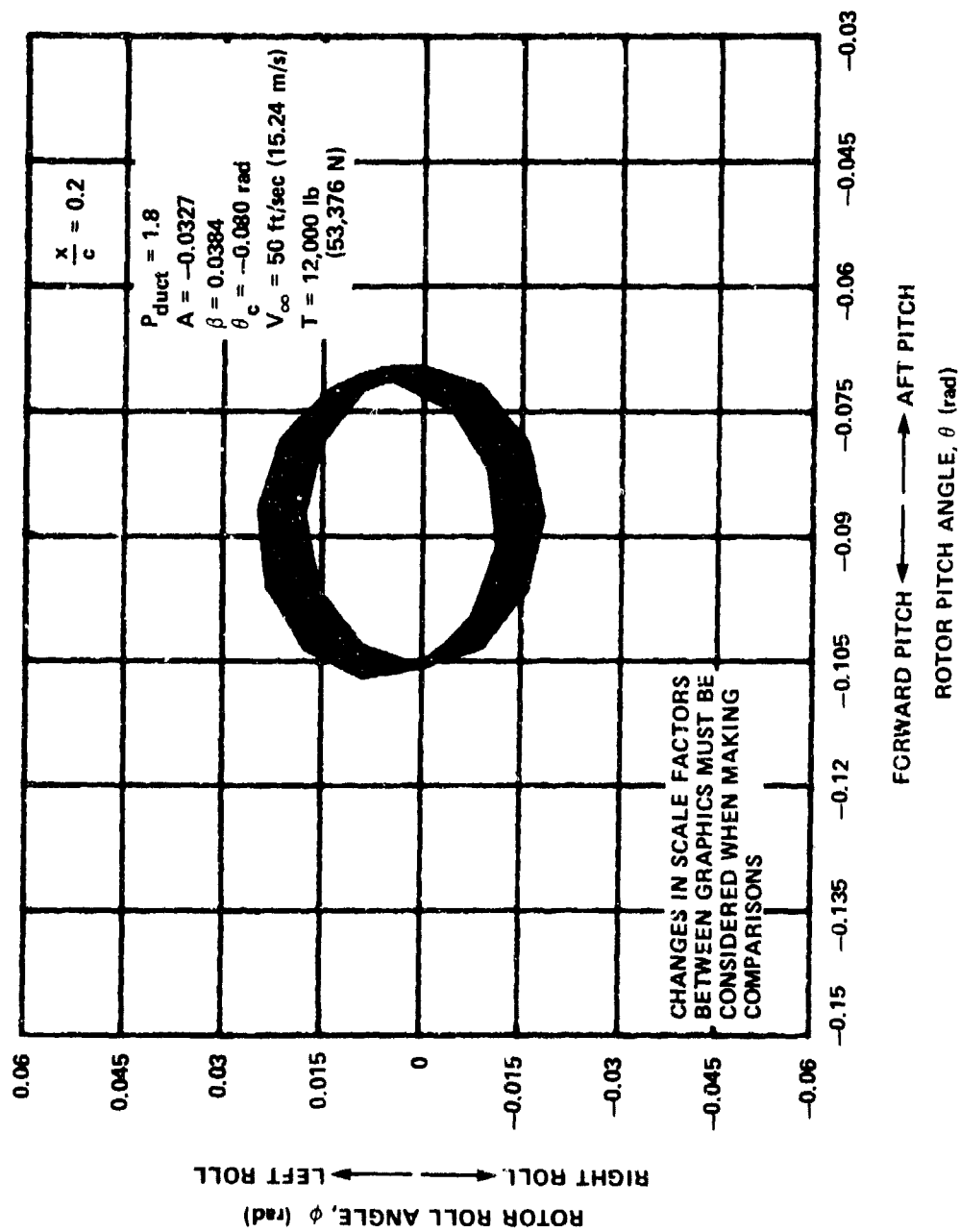


Figure 8 - Equilibrium Dynamics in Forward Flight

Figure 9 - Effect of Principal Axis Location on Rotor Motions for 100-Percent Circulation Control Lift

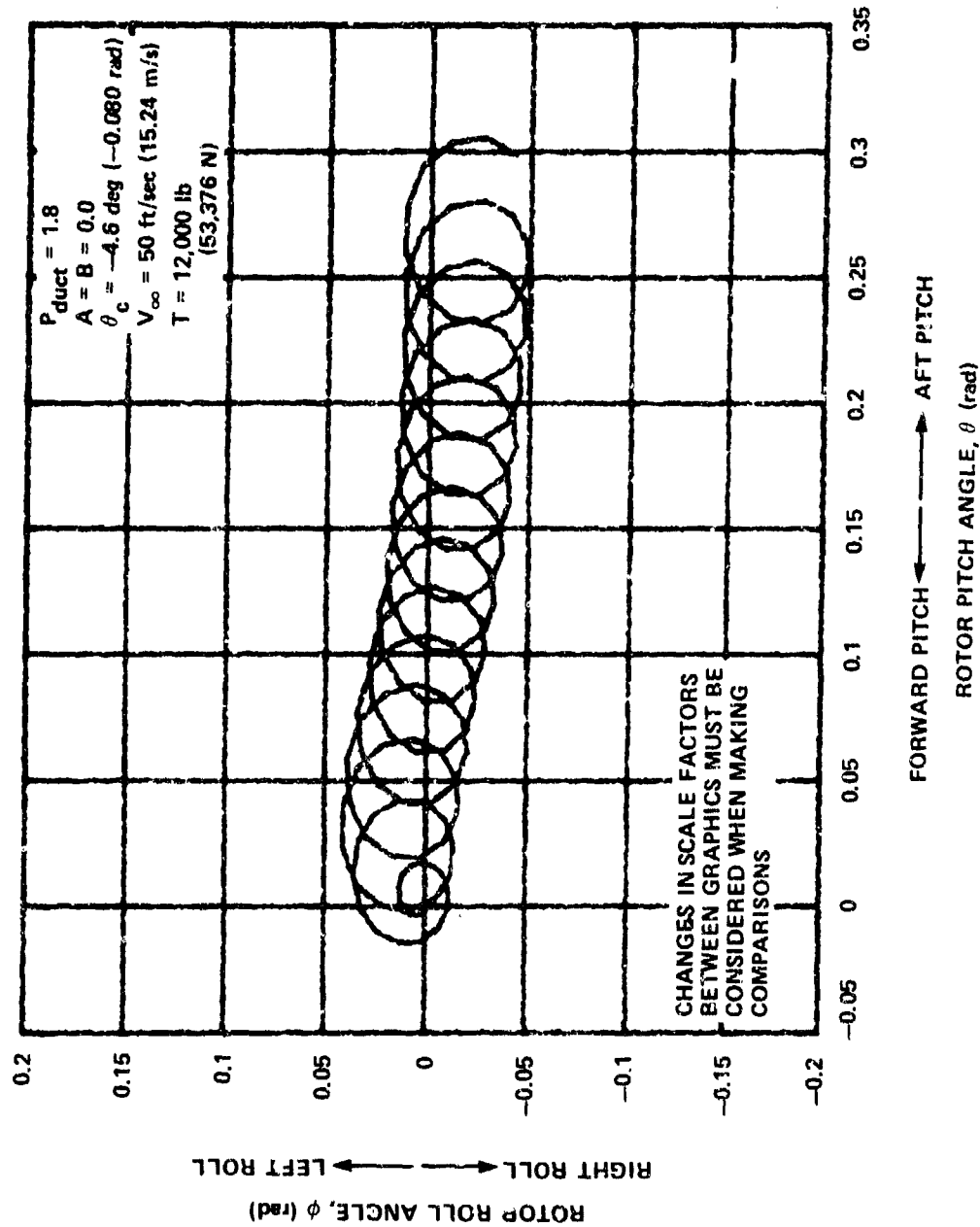


Figure 9a - Principal Axis Located at 20-Percent Chord

Figure 9 (Continued)

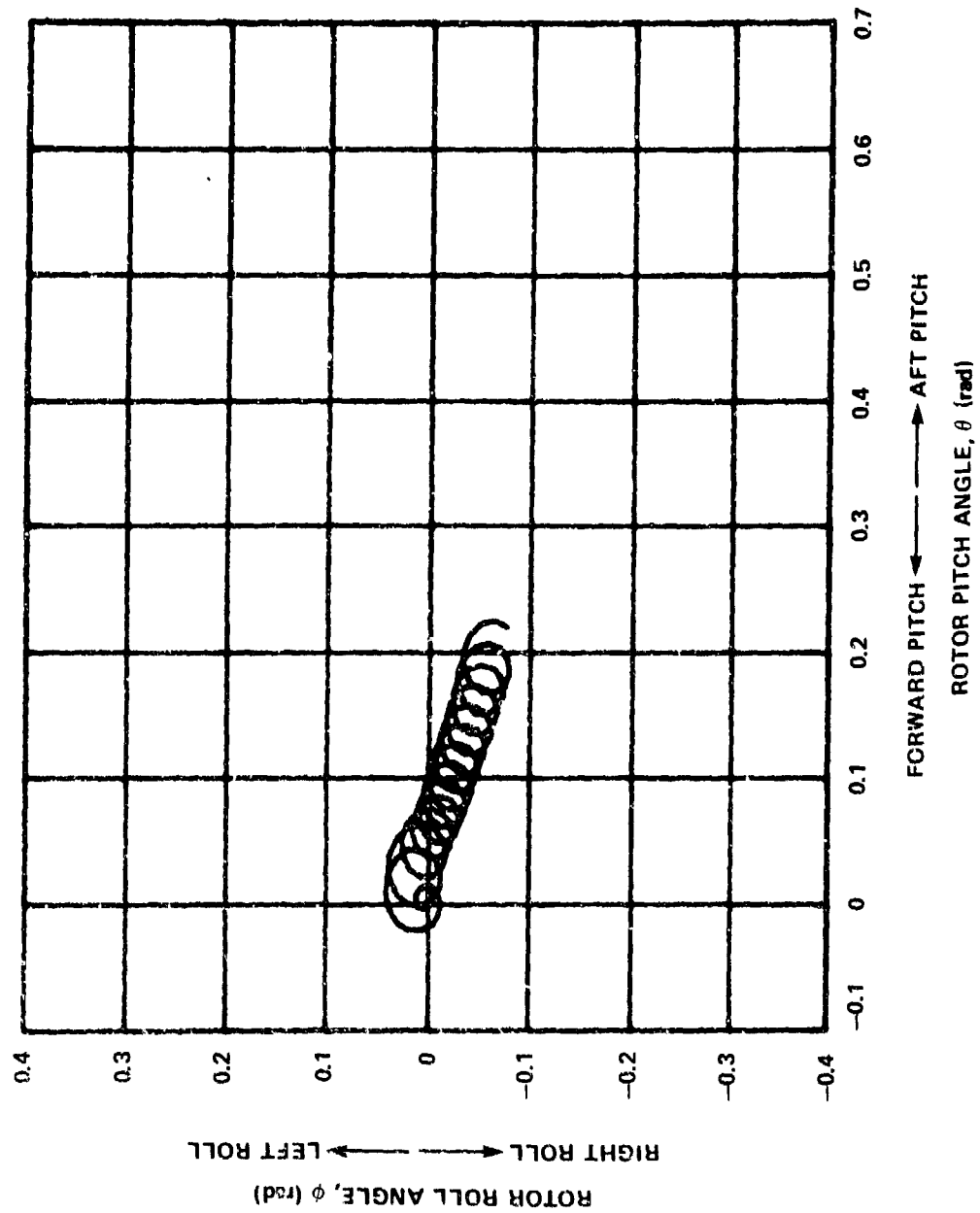


Figure 9b - Principal Axis Located at 25-Percent Chord

Figure 9 (Continued)

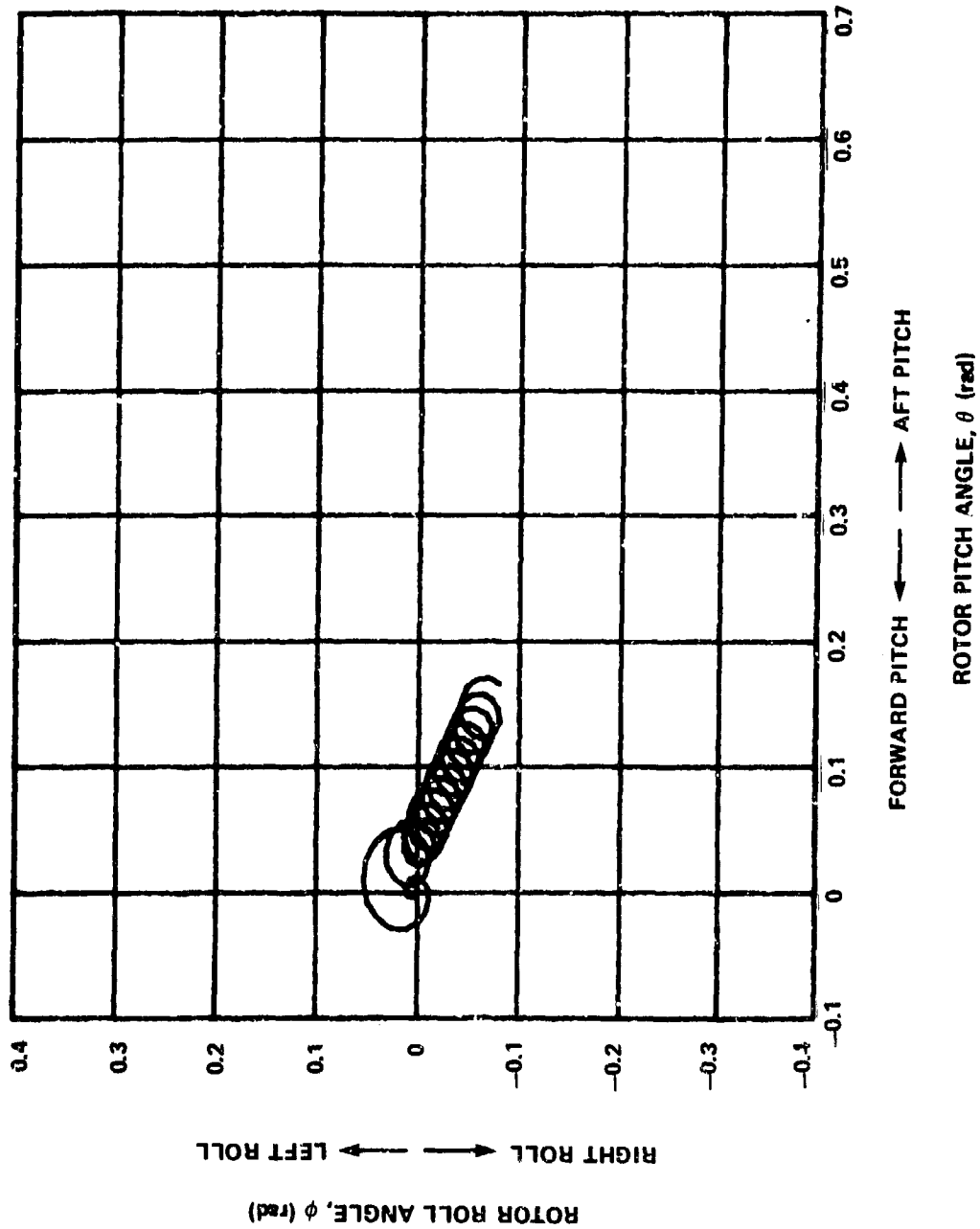


Figure 9c - Principal Axis Located at 30-Percent Chord

Figure 9 (Continued)

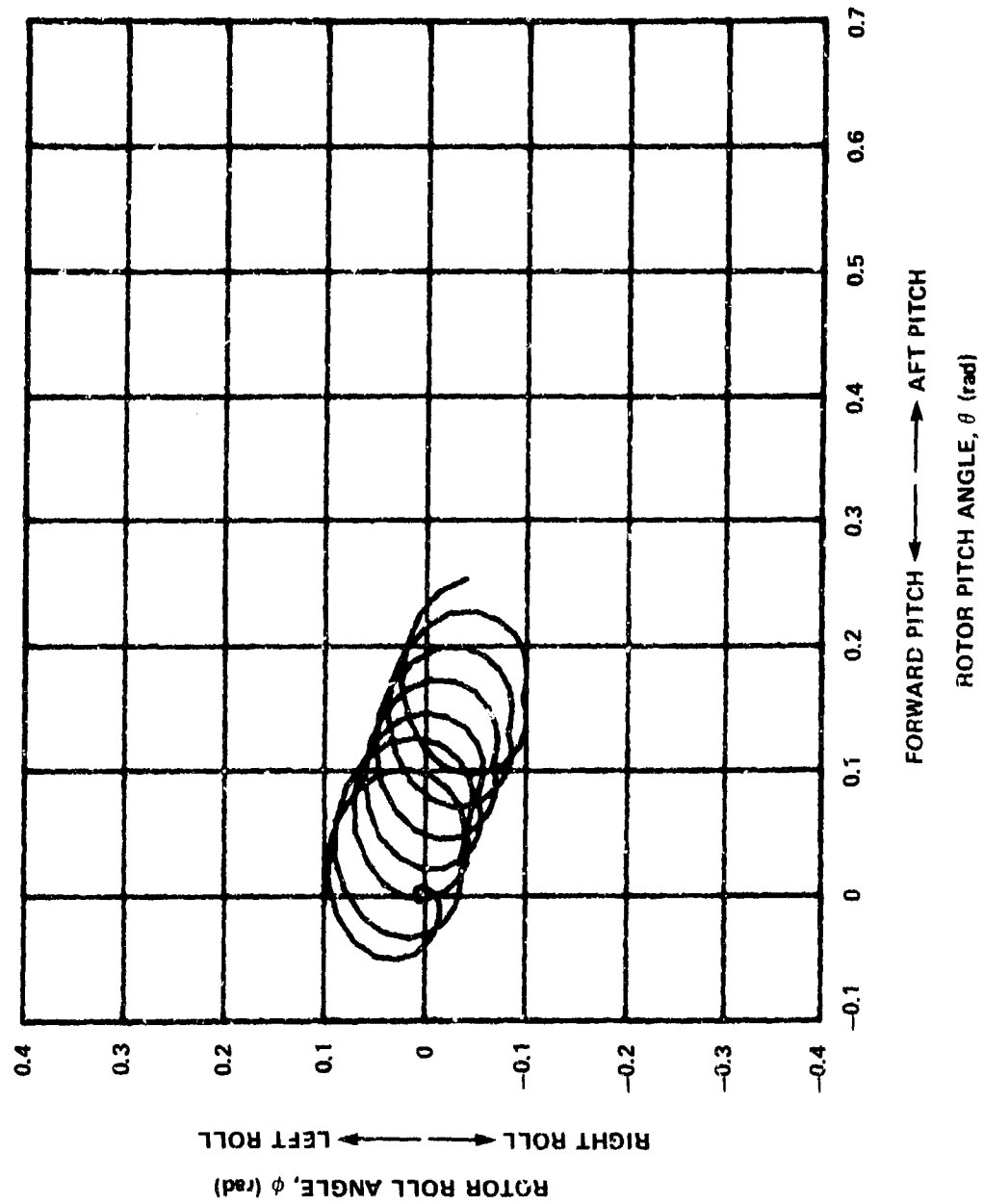


Figure 9d - Principal Axis Located at 40-Percent Chord

Figure 10 - Effect of Principal Axis Location on Rotor Motions for 100-Percent Angle-of-Attack Lift

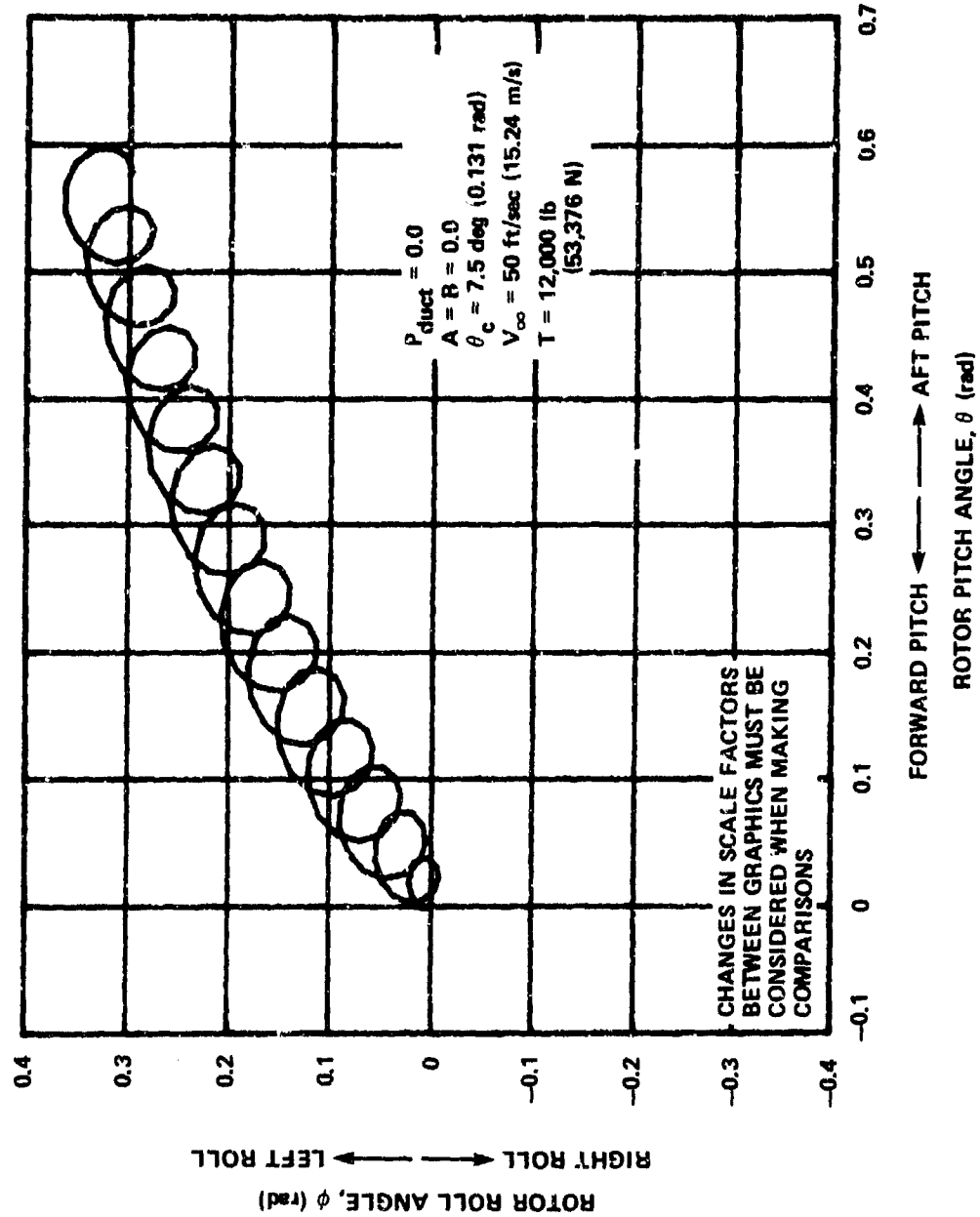


Figure 10a - Principal Axis Located at 20-Percent Chord

Figure 10 (Continued)

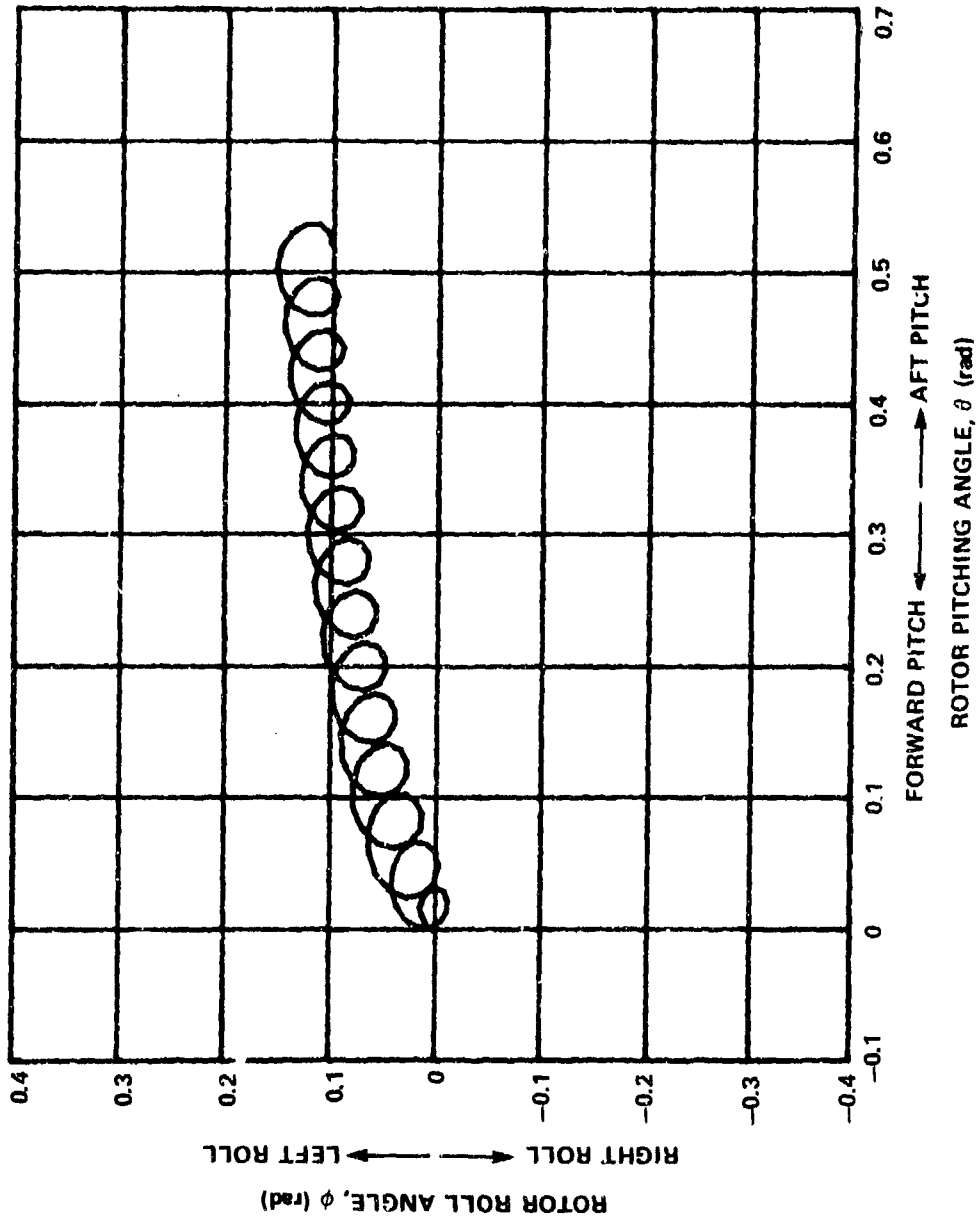


Figure 10b - Principal Axis Located at 25-Percent Chord

Figure 10 (Continued)

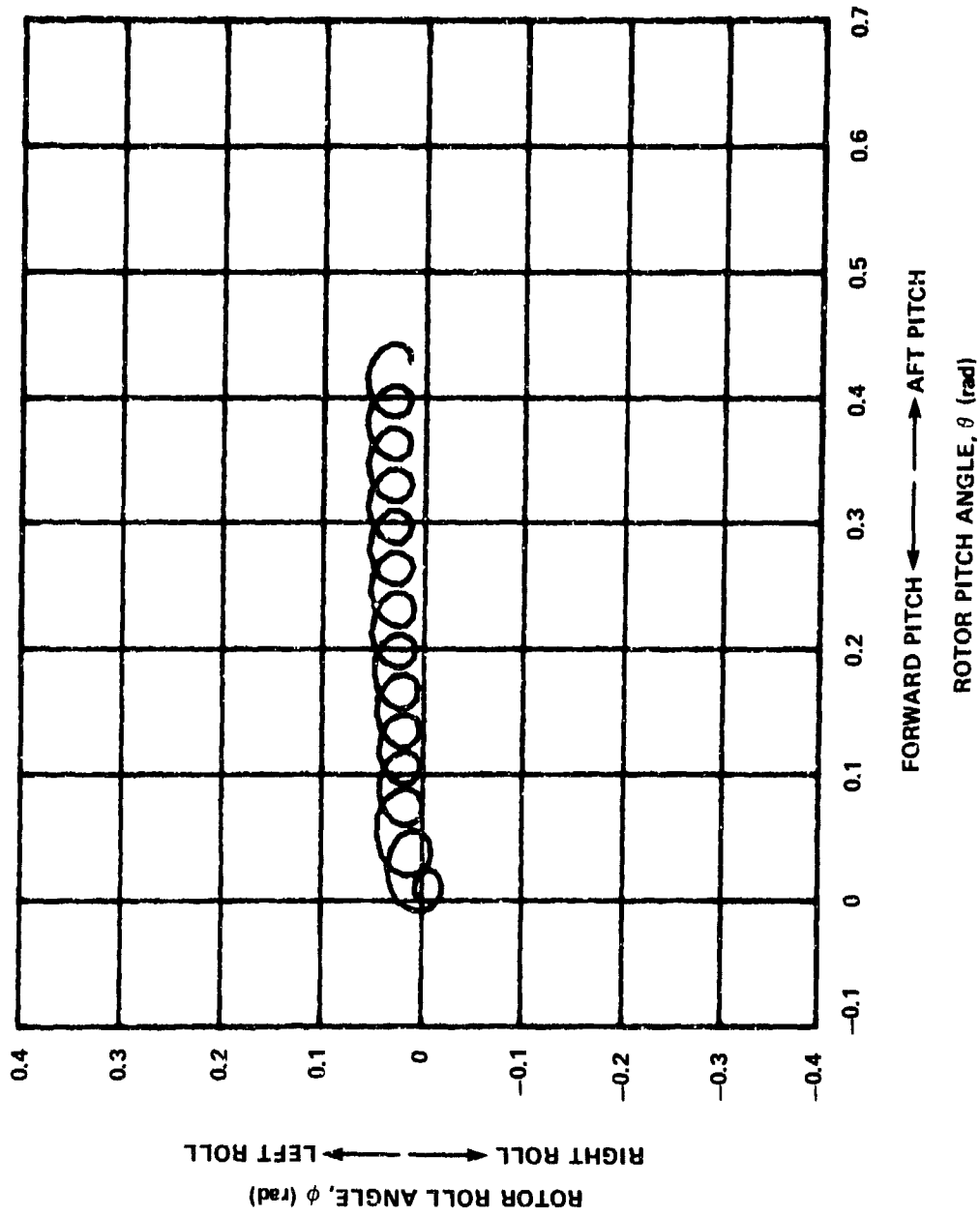


Figure 10c - Principal Axis Located at 30-Percent Chord

Figure 10 (Continued)

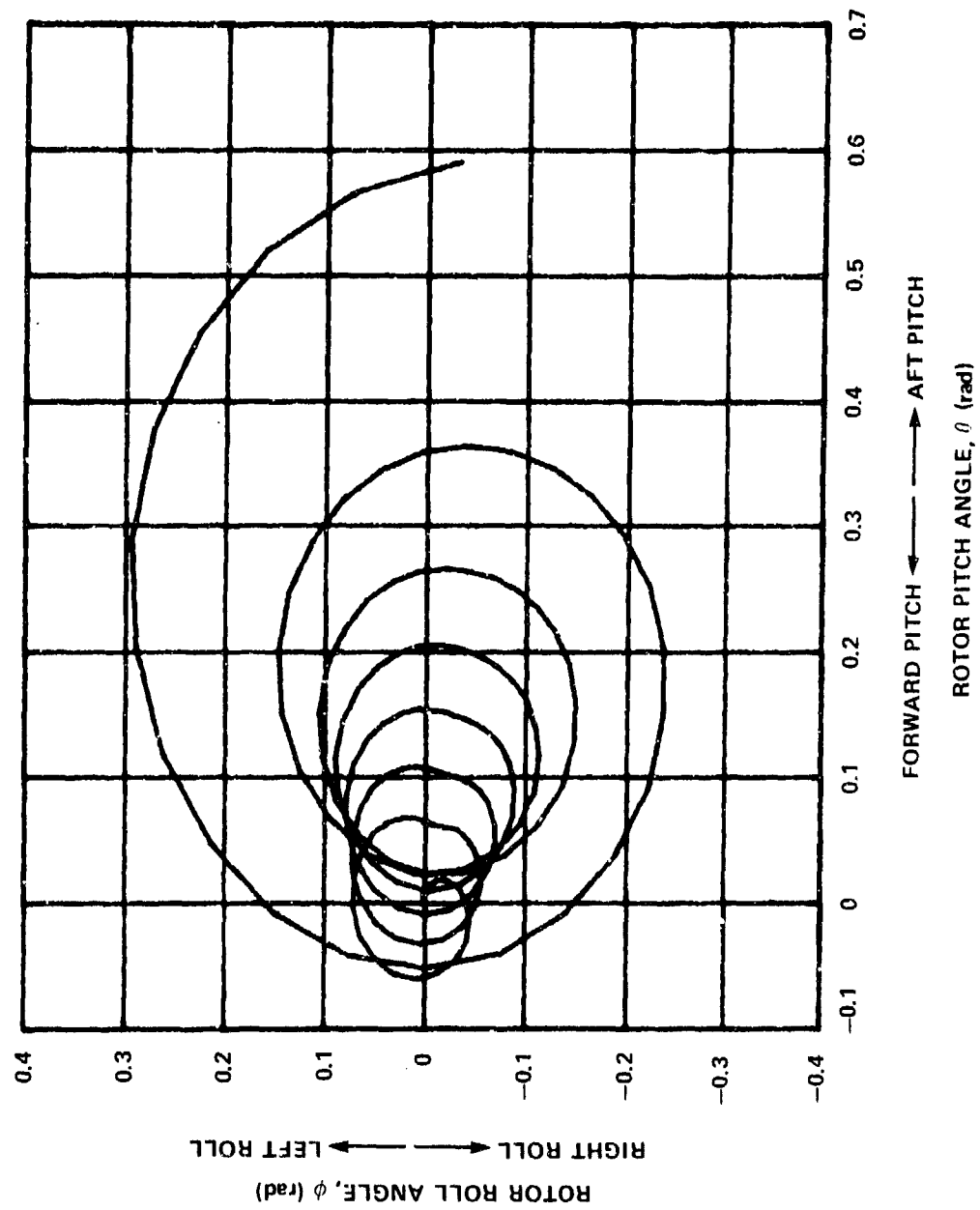


Figure 10d - Principal Axis Located at 40-Percent Chord

Figure 11 - Effect of Principal Axis Location on Rotor Oscillation Frequency

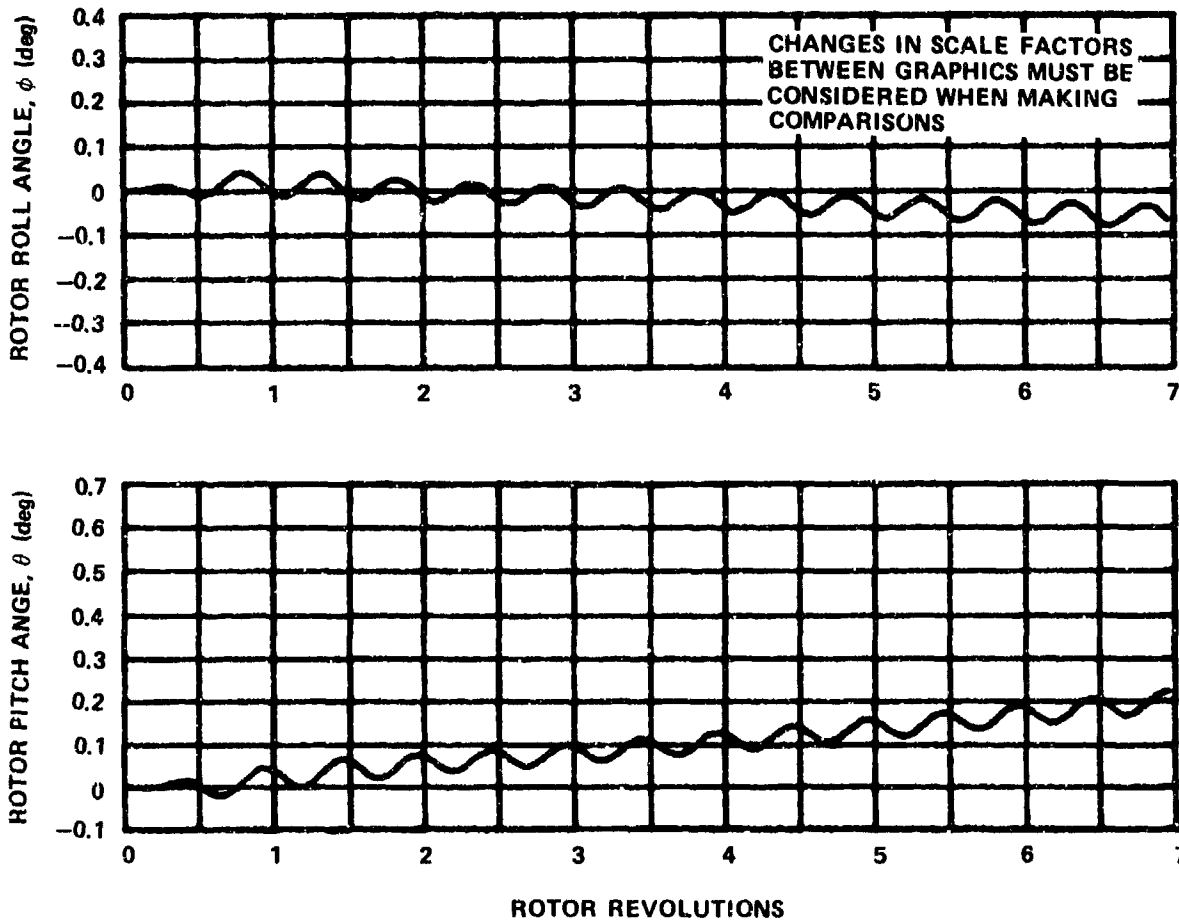


Figure 11a - 100-Percent Circulation Control Lift, Principal Axis Located at 25-Percent Chord

Figure 11 (Continued)

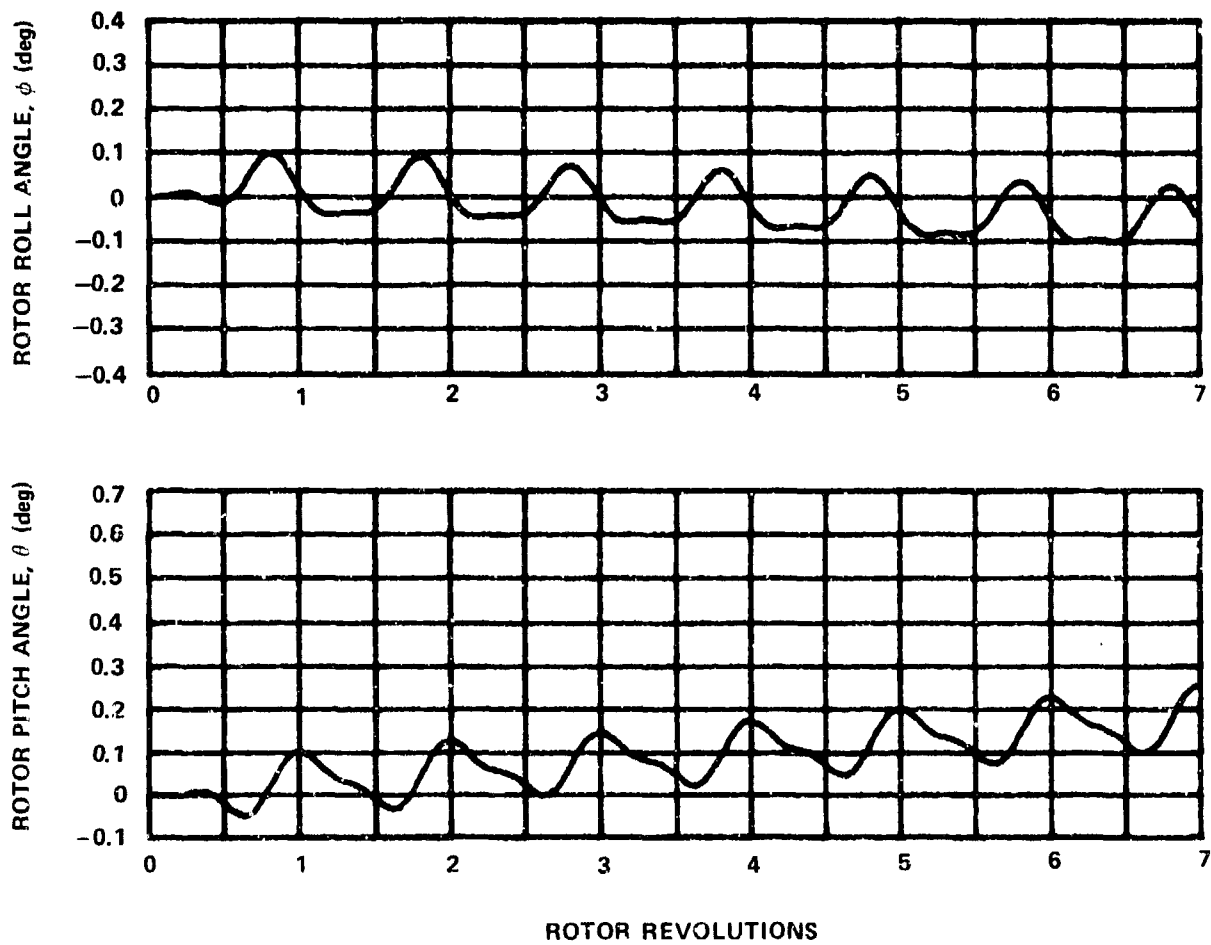


Figure 11b - 100-Percent Circulation Control Lift, Principal Axis Located at 40-Percent Chord

Figure 11 (Continued)

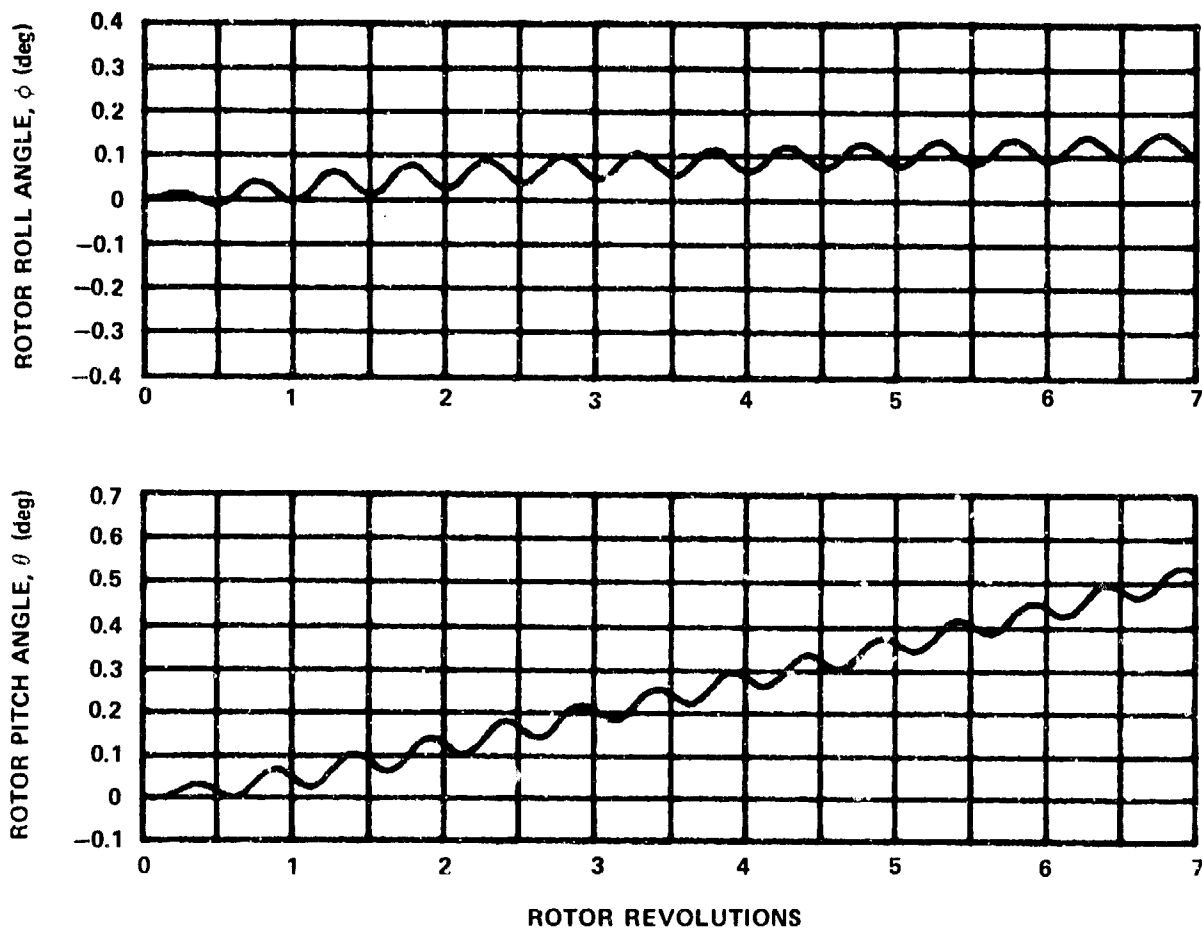


Figure 11c - 100-Percent Angle-of-Attack Lift, Principal Axis
Located at 25-Percent Chord

Figure 11 (Continued)

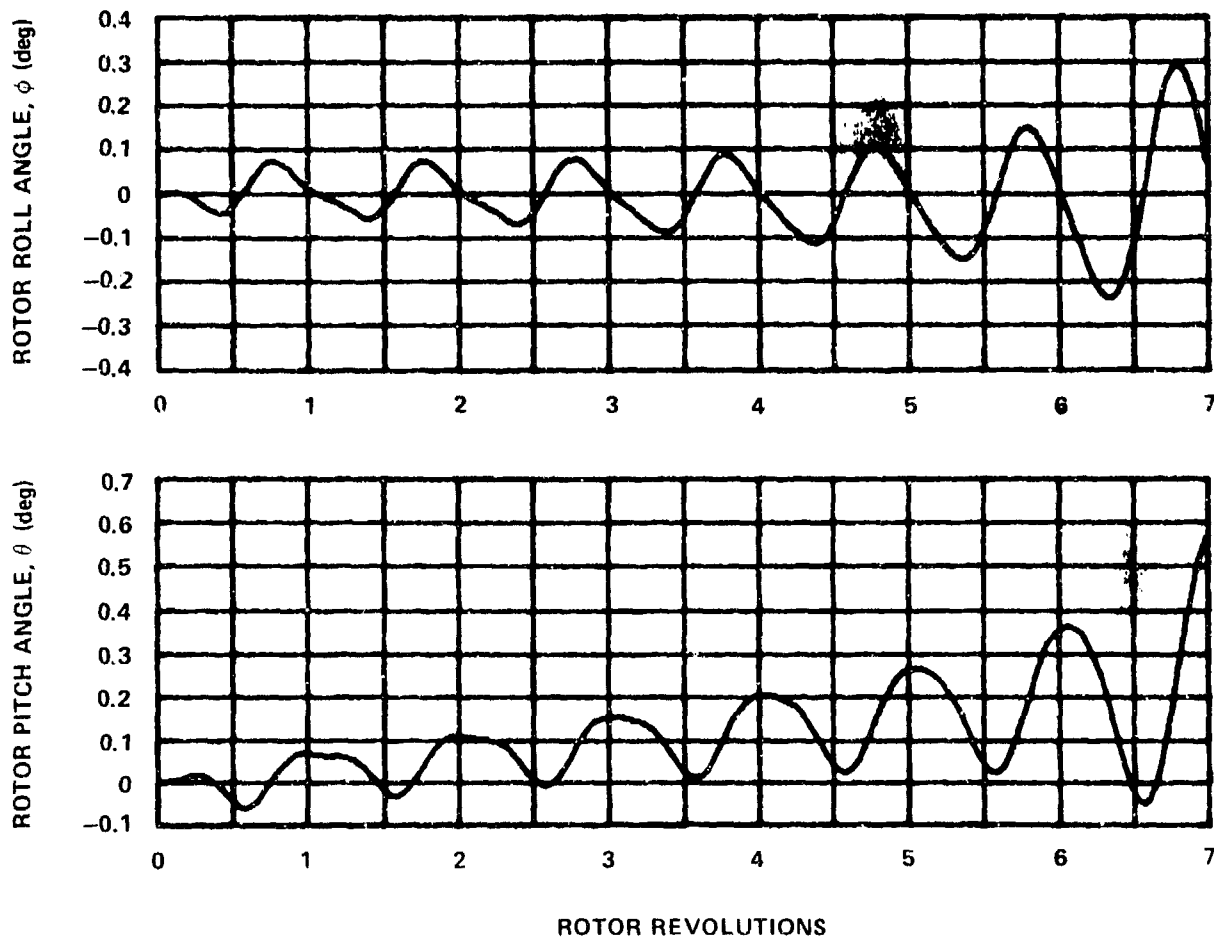


Figure 11d - 100-Percent Angle-of-Attack Lift, Principal Axis Located at 40-Percent Chord

Figure 12 - Effects of Teeter Feedback

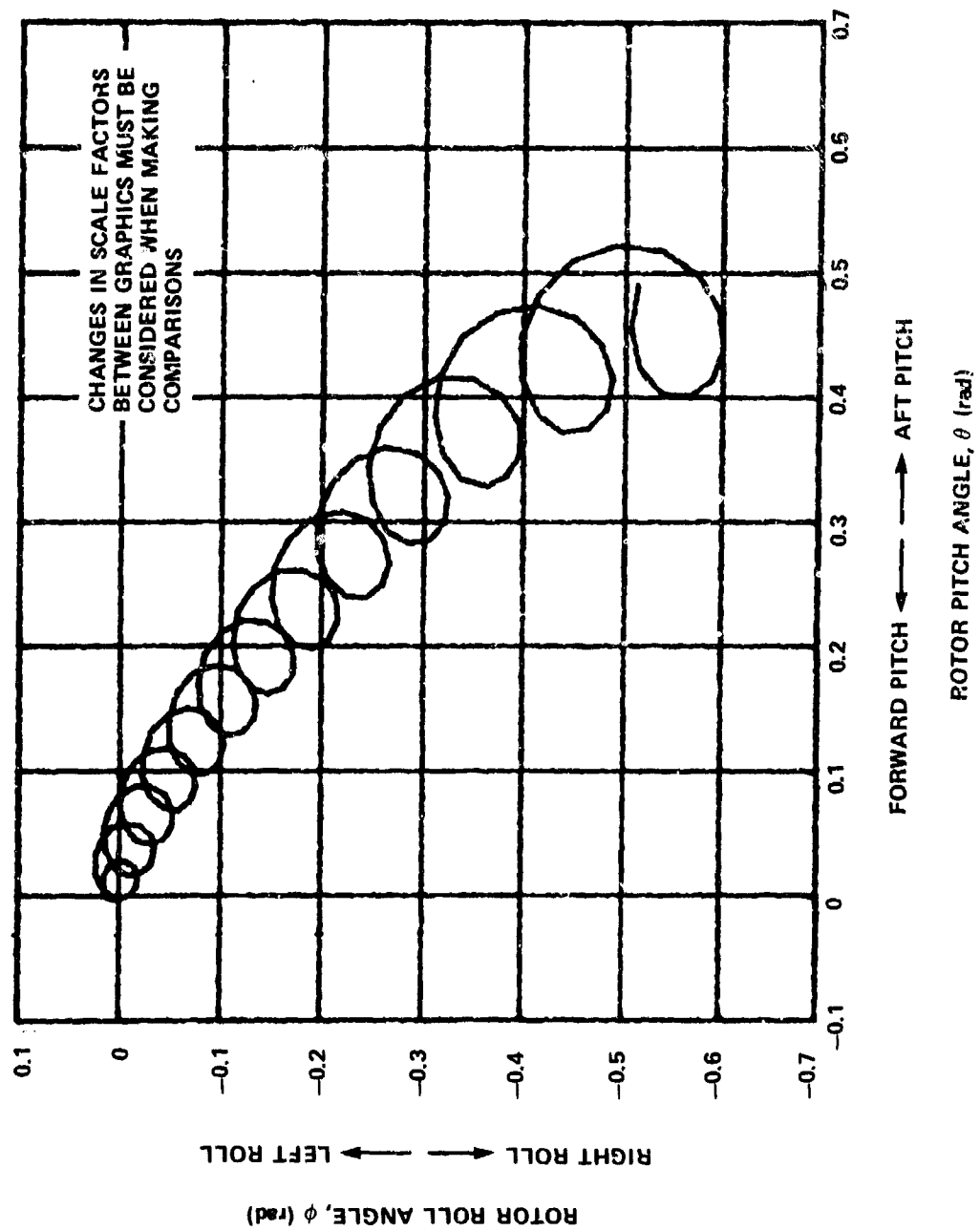


Figure 12a - Teeter Angle Feedback; Gain, $k_g = 1000$

Figure 12 (Continued)

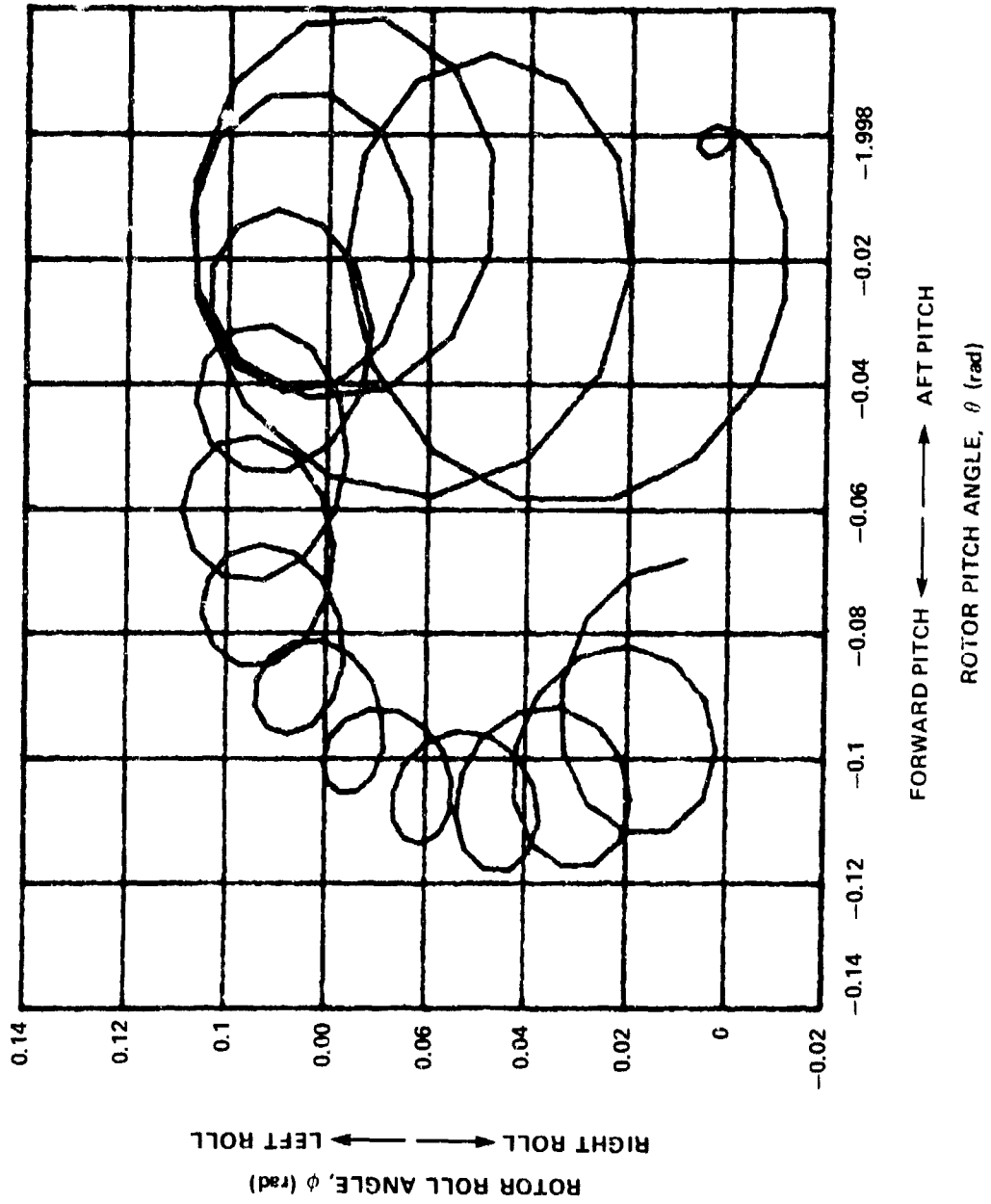


Figure 12b - Teeter Angle Feedback; Gain, $k_g = -3000$

Figure 12 (Continued)

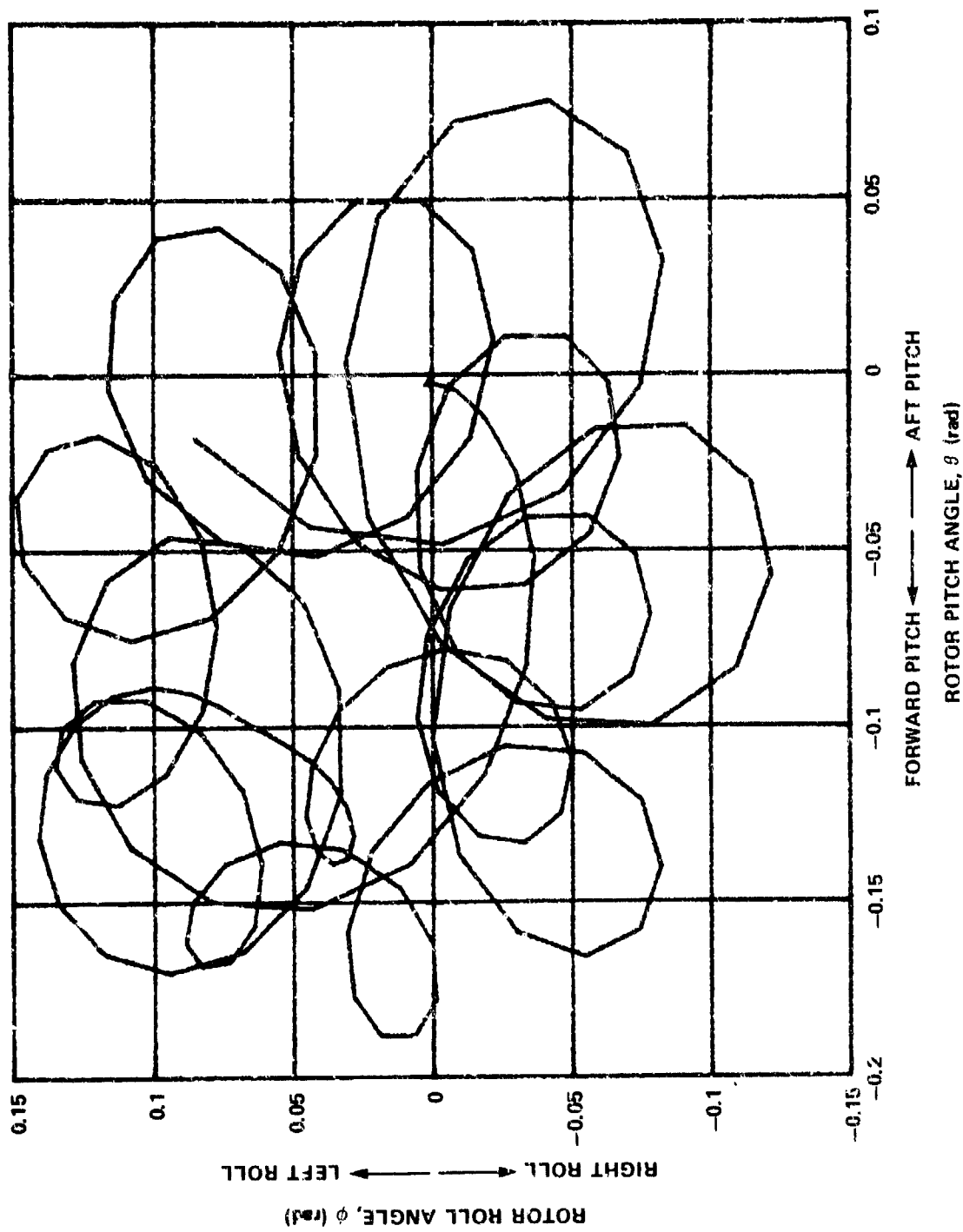


Figure 12c - Teeter Angle Feedback; Gain, $k_2 = -10,000$

Figure 12 (Continued)

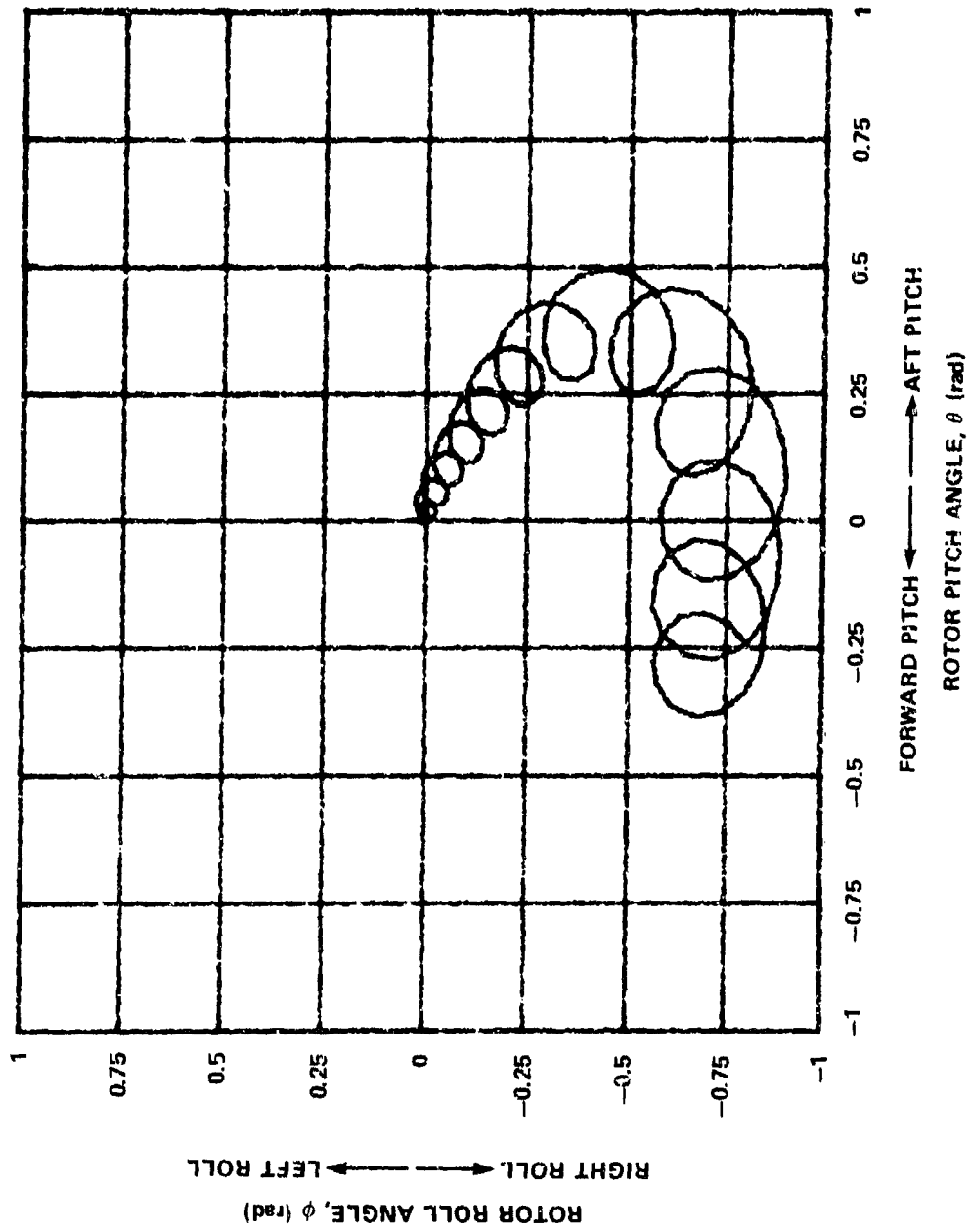


Figure 12d - Teeter Angular Rate Feedback; Gain, $k_g = -50$

Figure 12 (Continued)

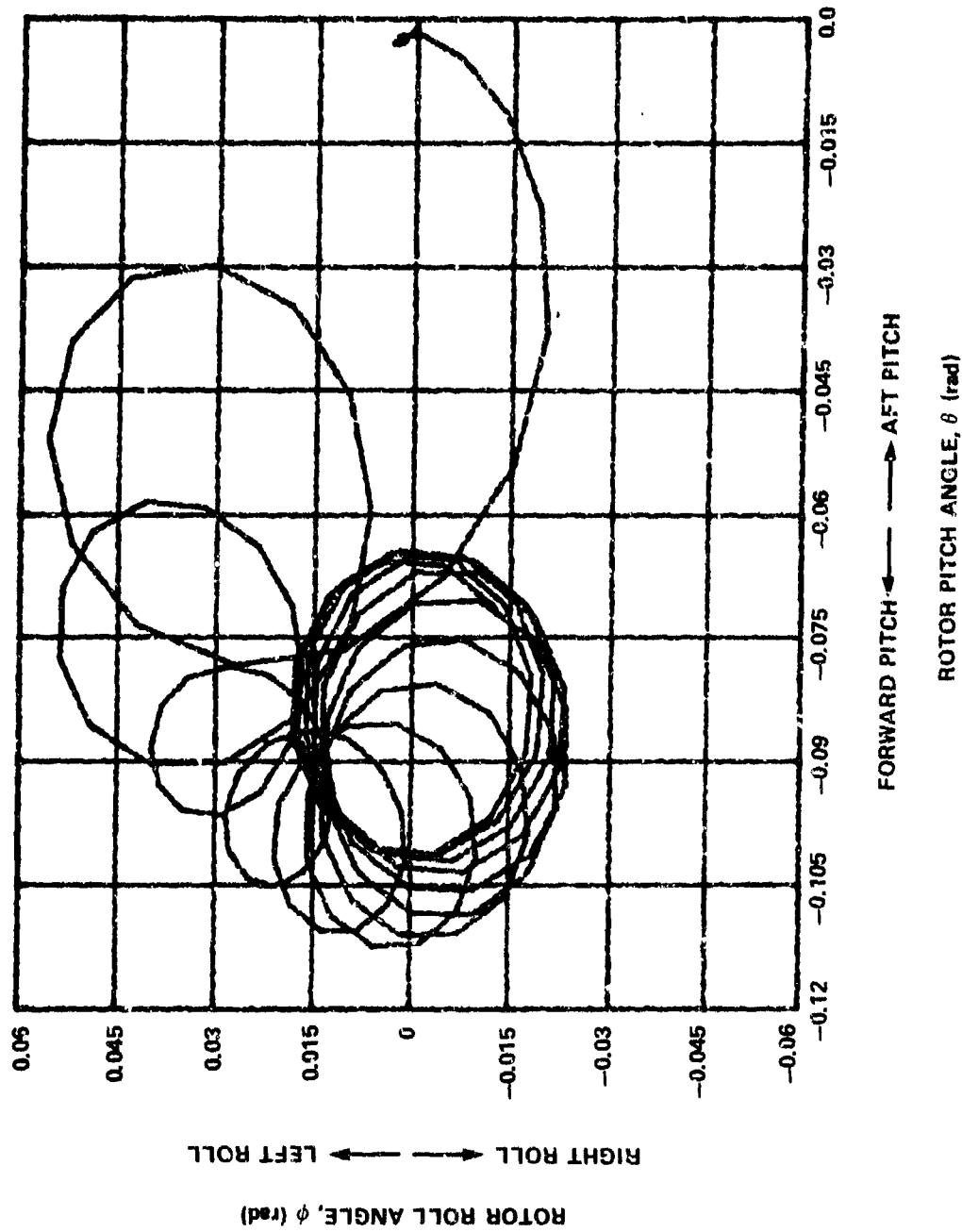


Figure 12e - Teeter Angular Rate Feedback; Gain, $k_{\beta} = 200$

Figure 12 (Continued)

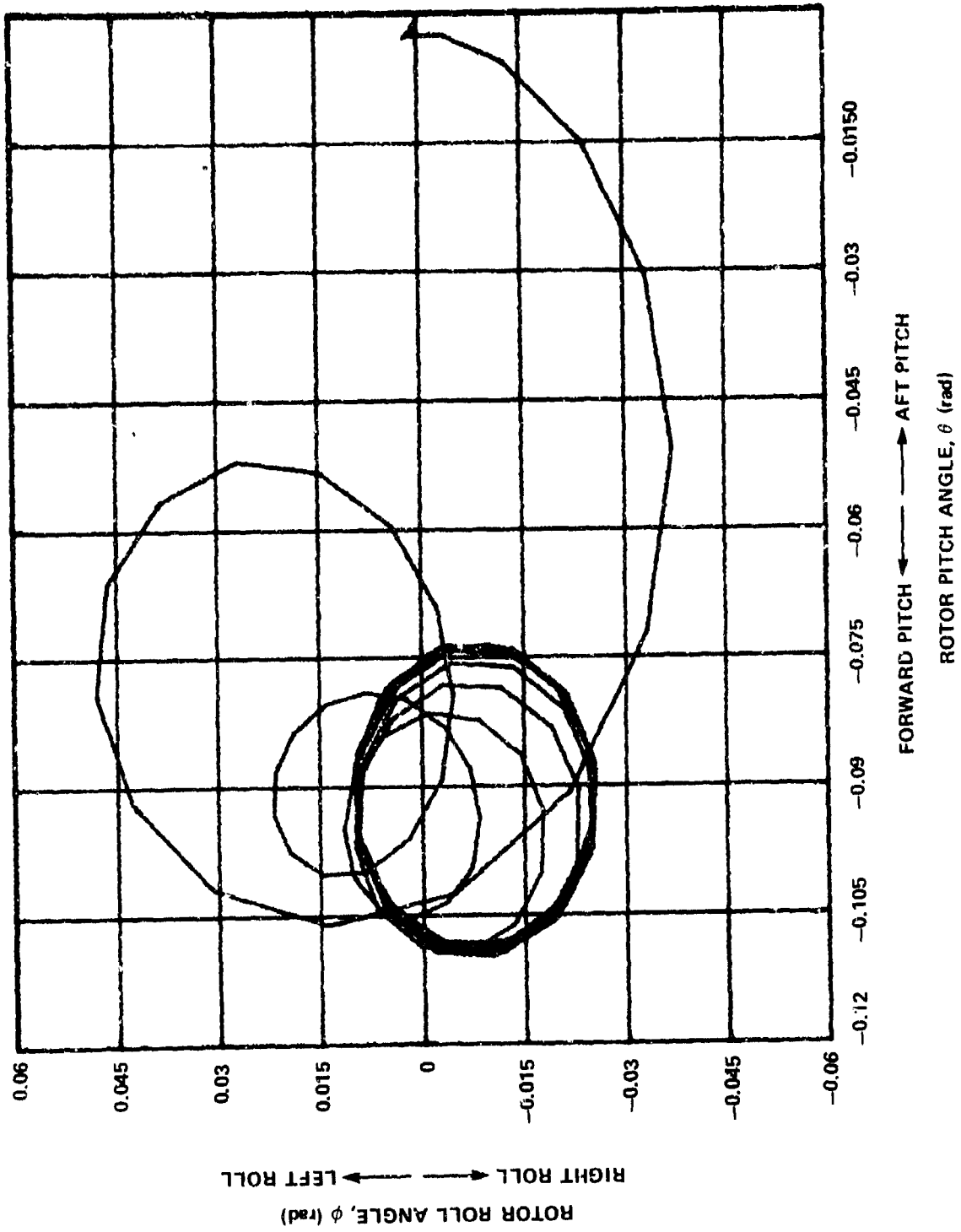


Figure 12f - Teeter Angular Rate Feedback; Gain, $k_2 = 400$

Figure 12 (Continued)

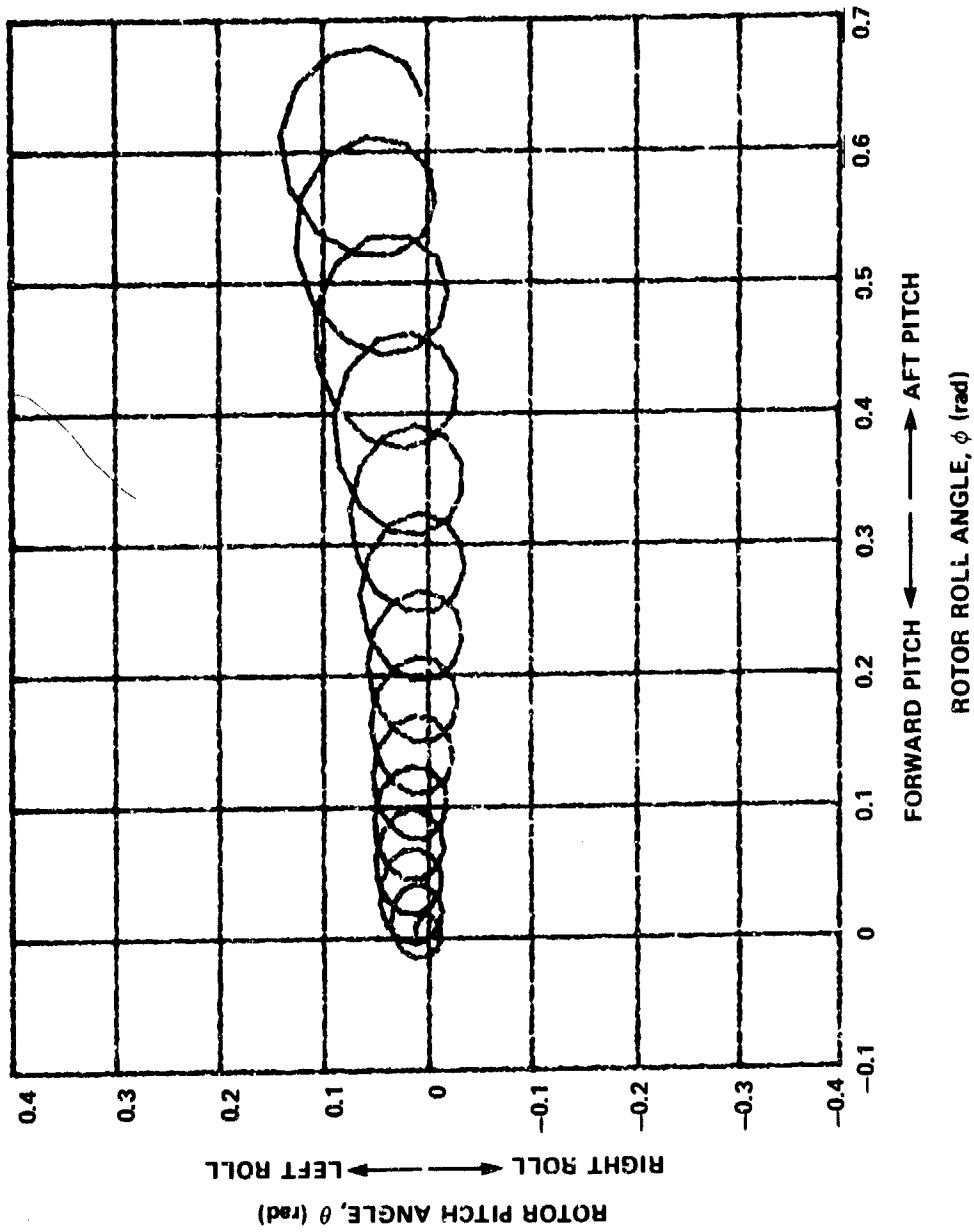


Figure 12g - Teeter Angular Acceleration Feedback; Gain, $k_{\ddot{\theta}} = 1$

Figure 12 (Continued)

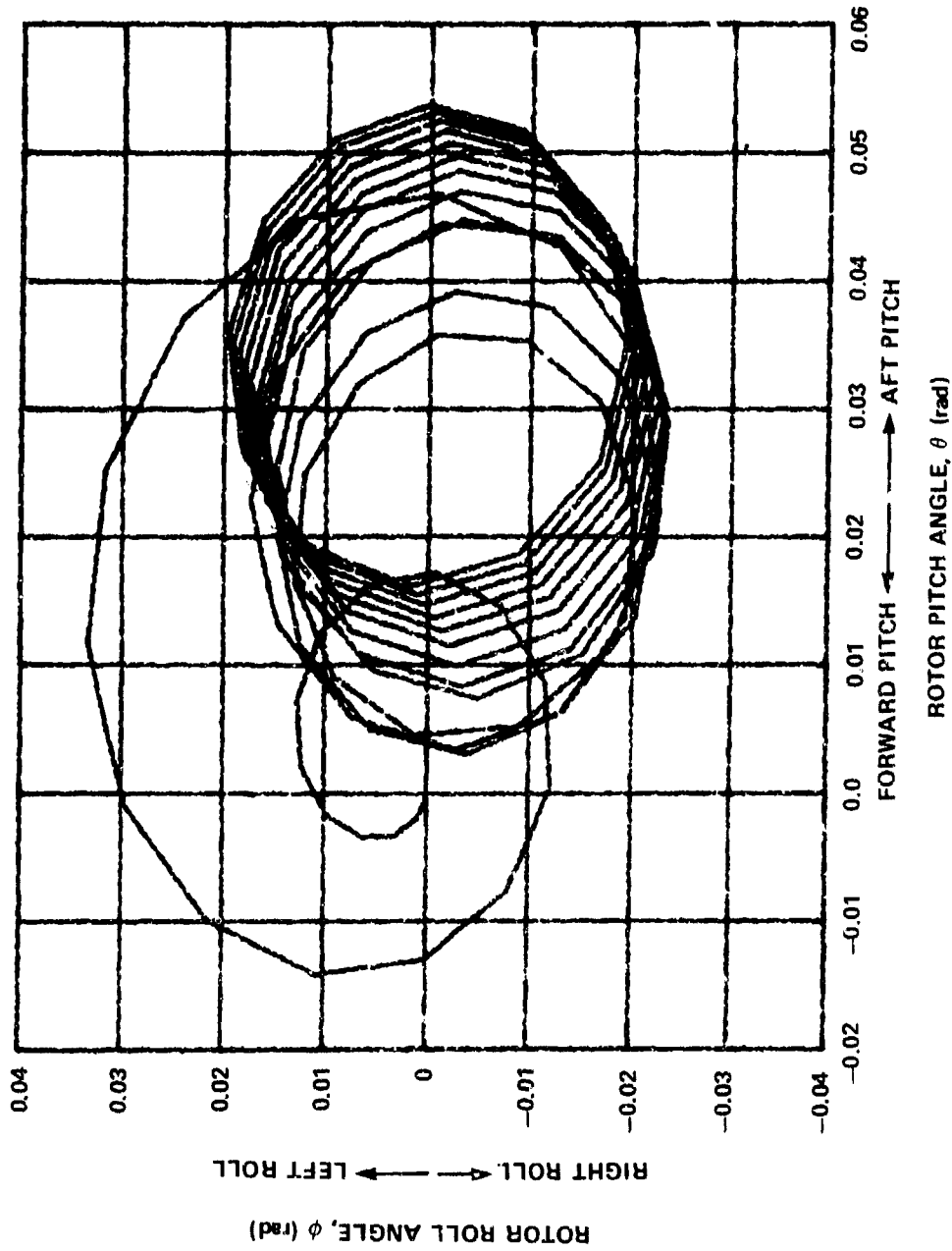


Figure 12h - Teeter Angular Acceleration Feedback; Gain, $k_{\ddot{\theta}} = -5$

Figure 12 (Continued)

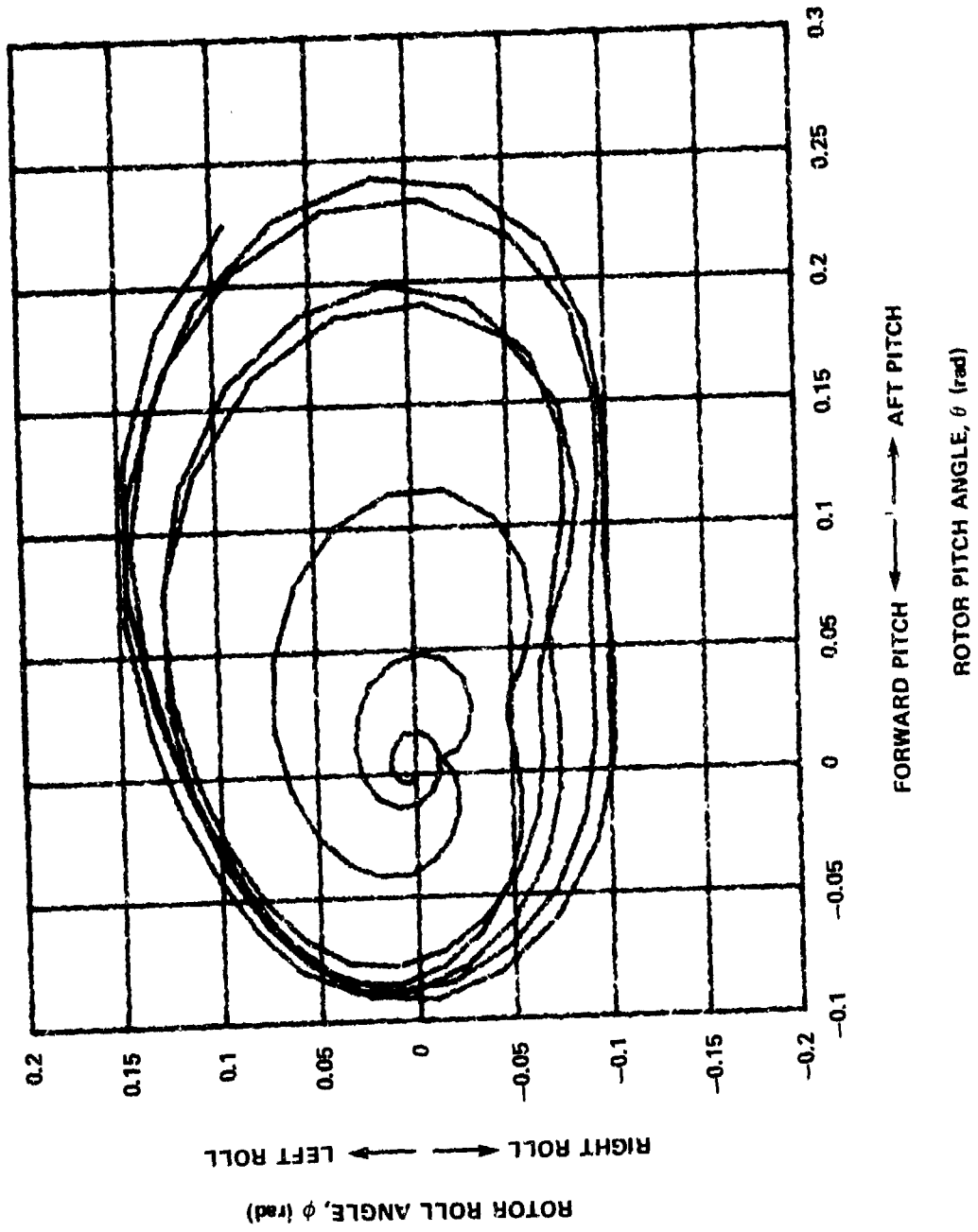


Figure 12i - Teeter Angular Acceleration Feedback; Gain, $k_{\ddot{g}} = -10$

Figure 13 - Effects of Feather Feedback

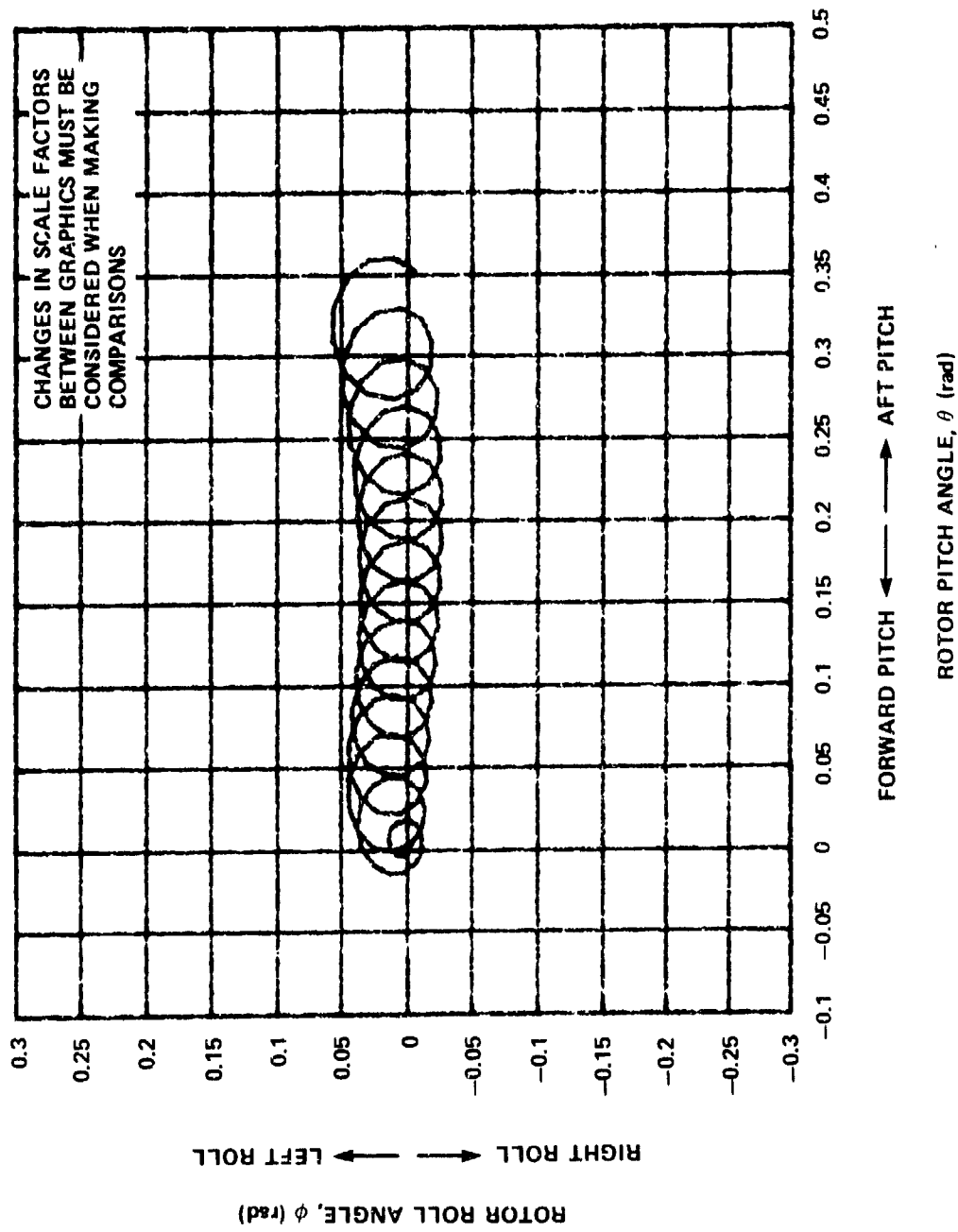


Figure 13a - Feather Angle Feedback; Gain, $k_{\theta} = 100$

Figure 13 (Continued)

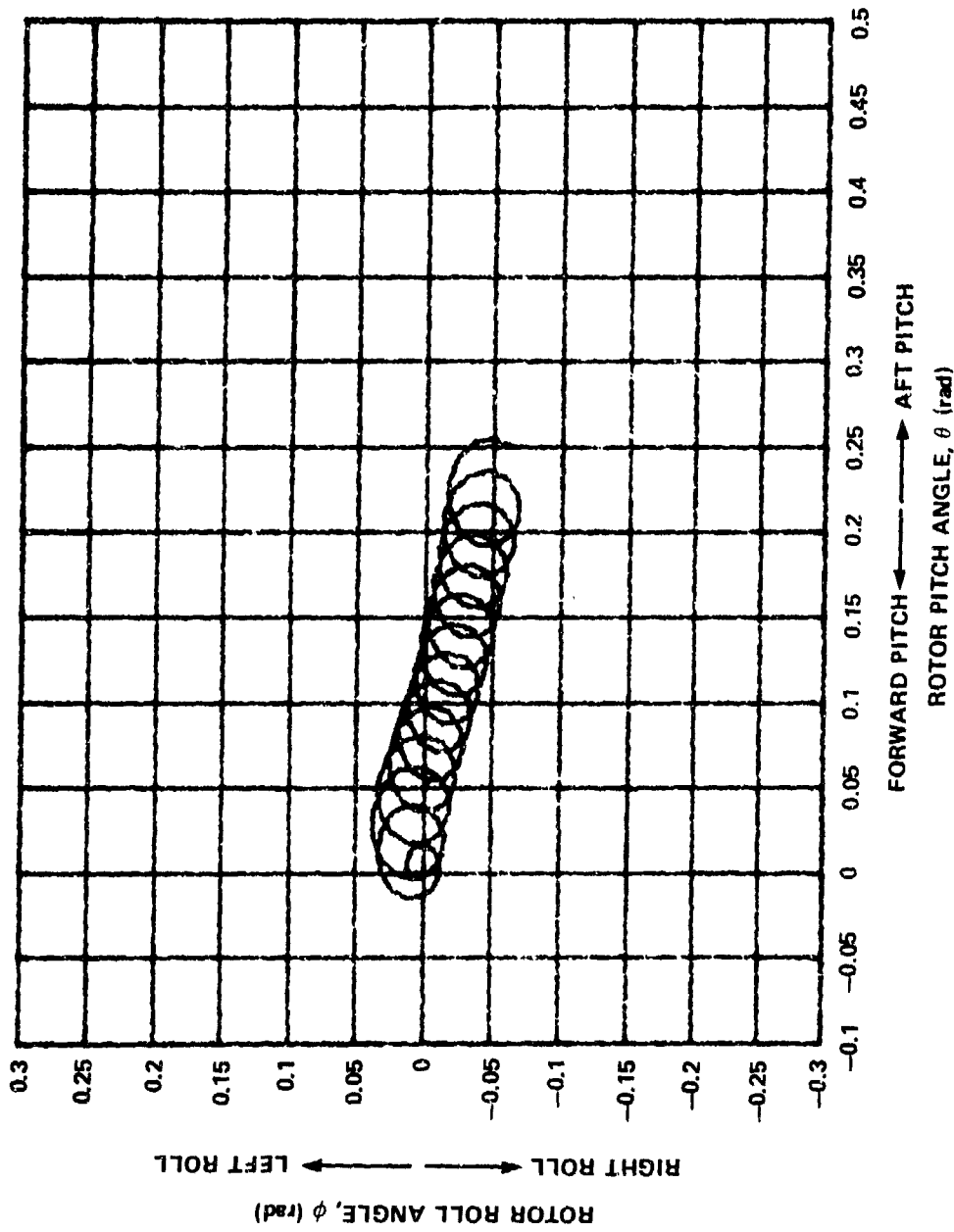


Figure 13b - Feather Angle Feedback; Gain, $k_{\theta} = -100$

Figure 13 (Continued)

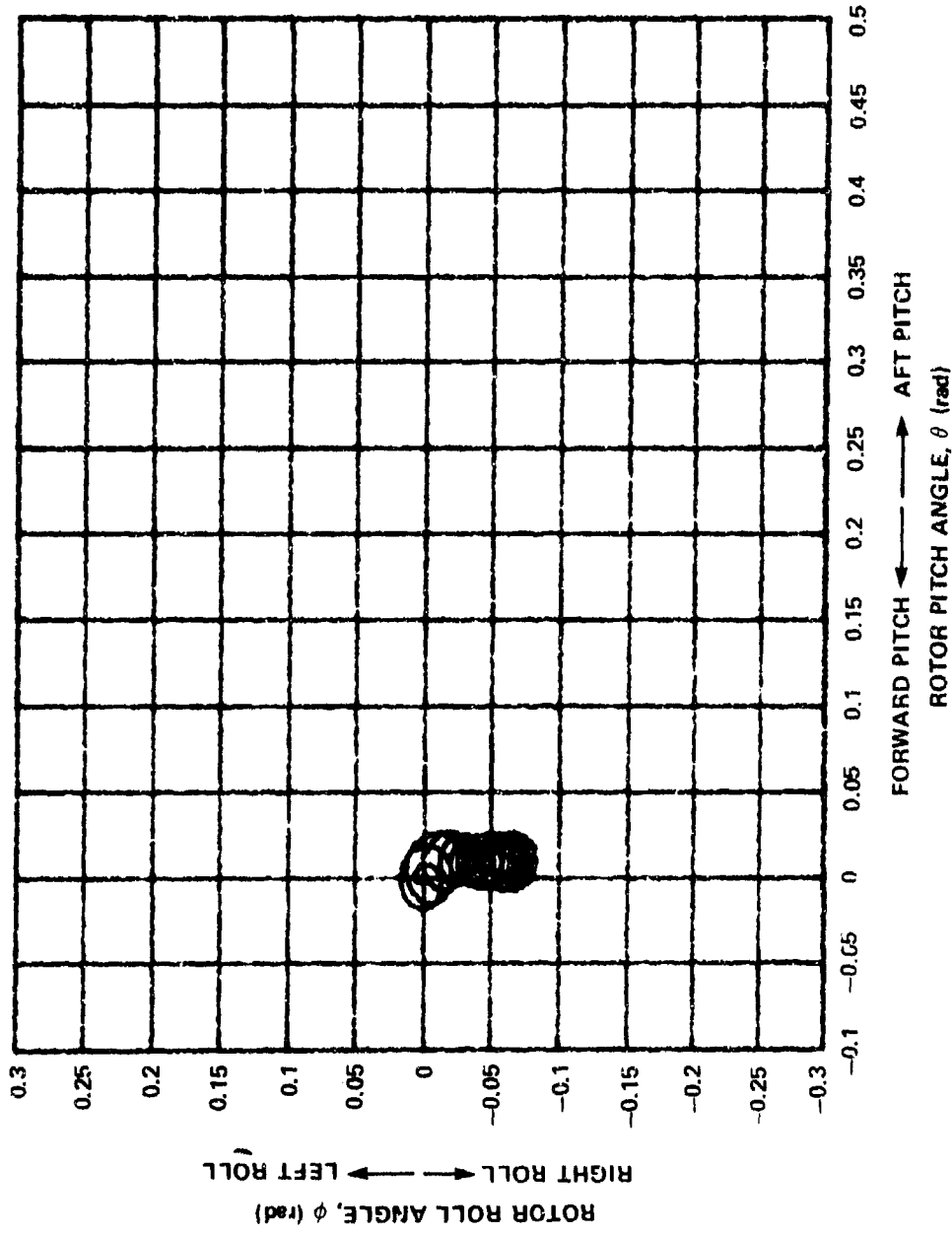


Figure 13c - Feather Angle Feedback; Gain, $k_a = -1000$

Figure 13 (Continued)

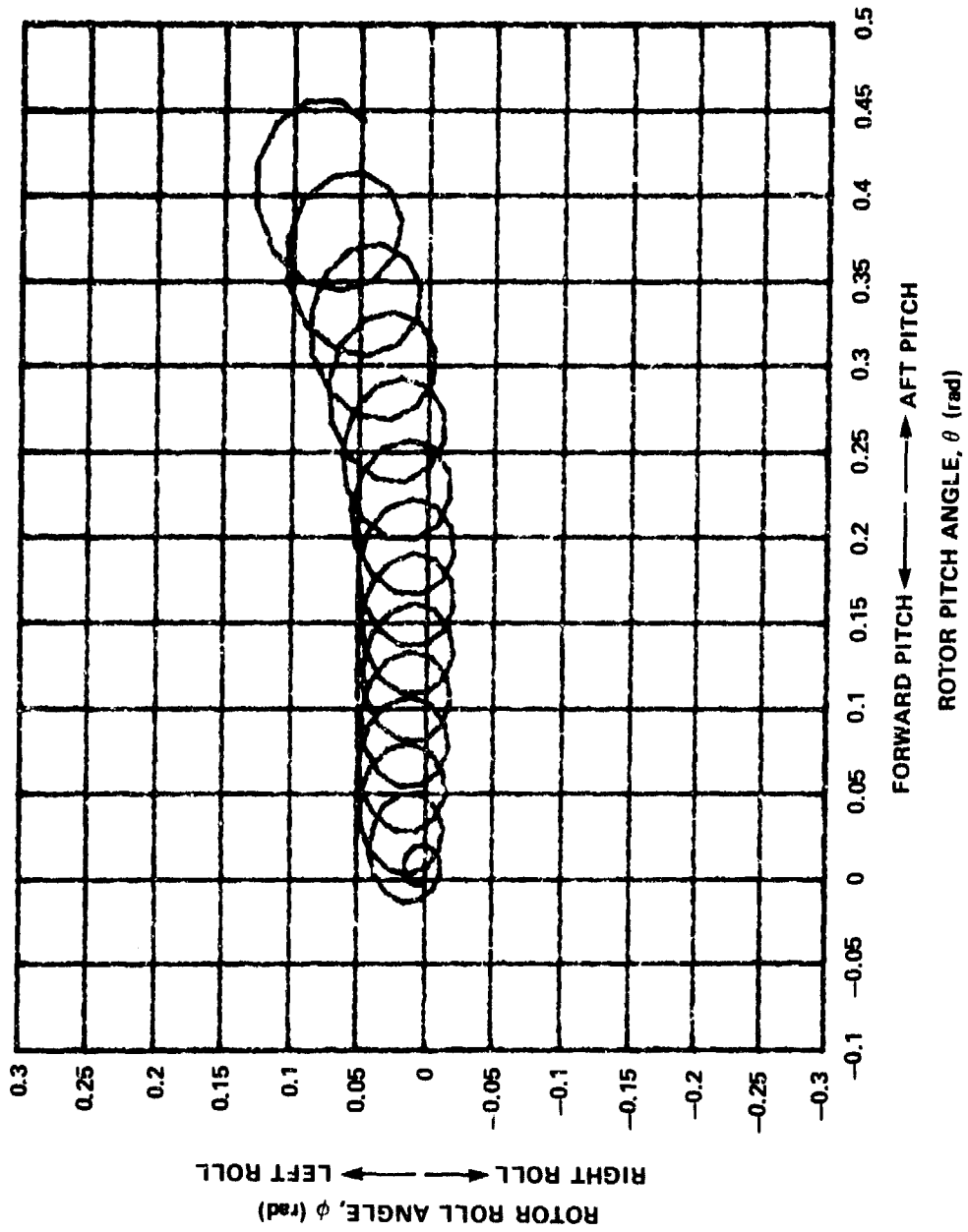


Figure 13d - Feather Angular Rate Feedback; Gain, $k_{\theta}^{\phi} = 10$

Figure 13 (Continued)

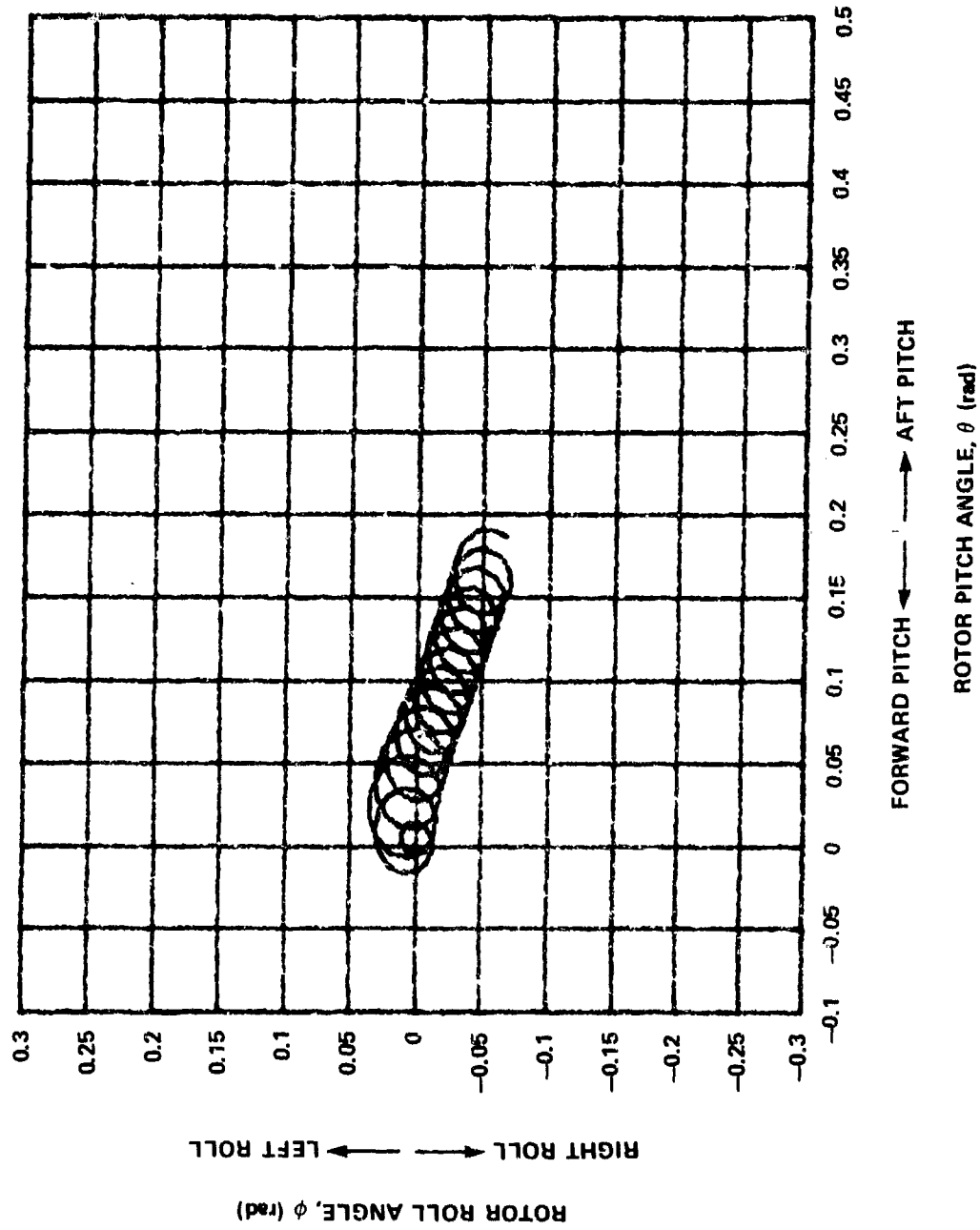


Figure 13e - Feather Angular Rate Feedback; Gain, $k_{\theta} = -10$

Figure 13 (Continued)

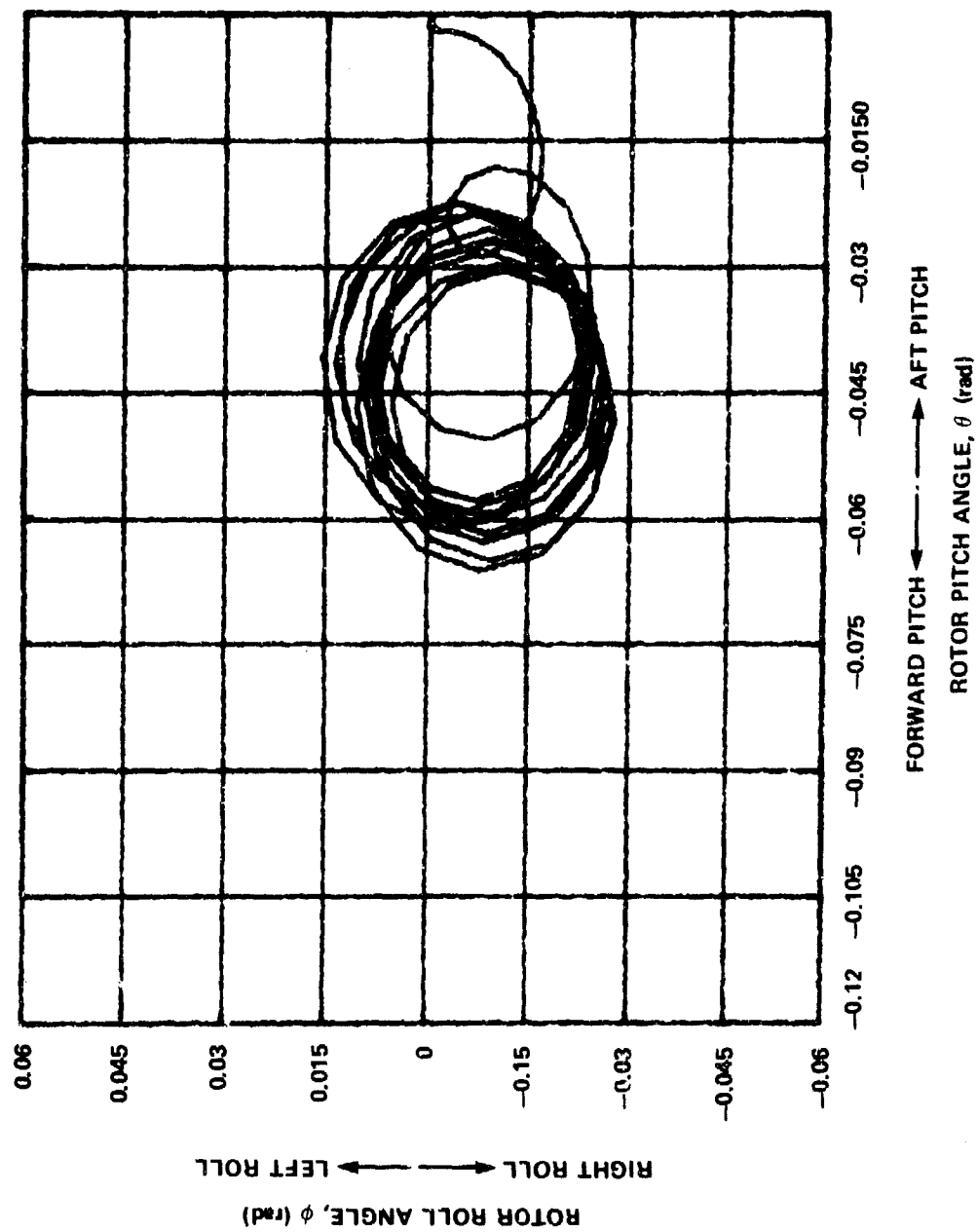


Figure 13f - Feather Angular Rate Feedback; Gain, $k_{\theta} = -100$

Figure 13 (Continued)

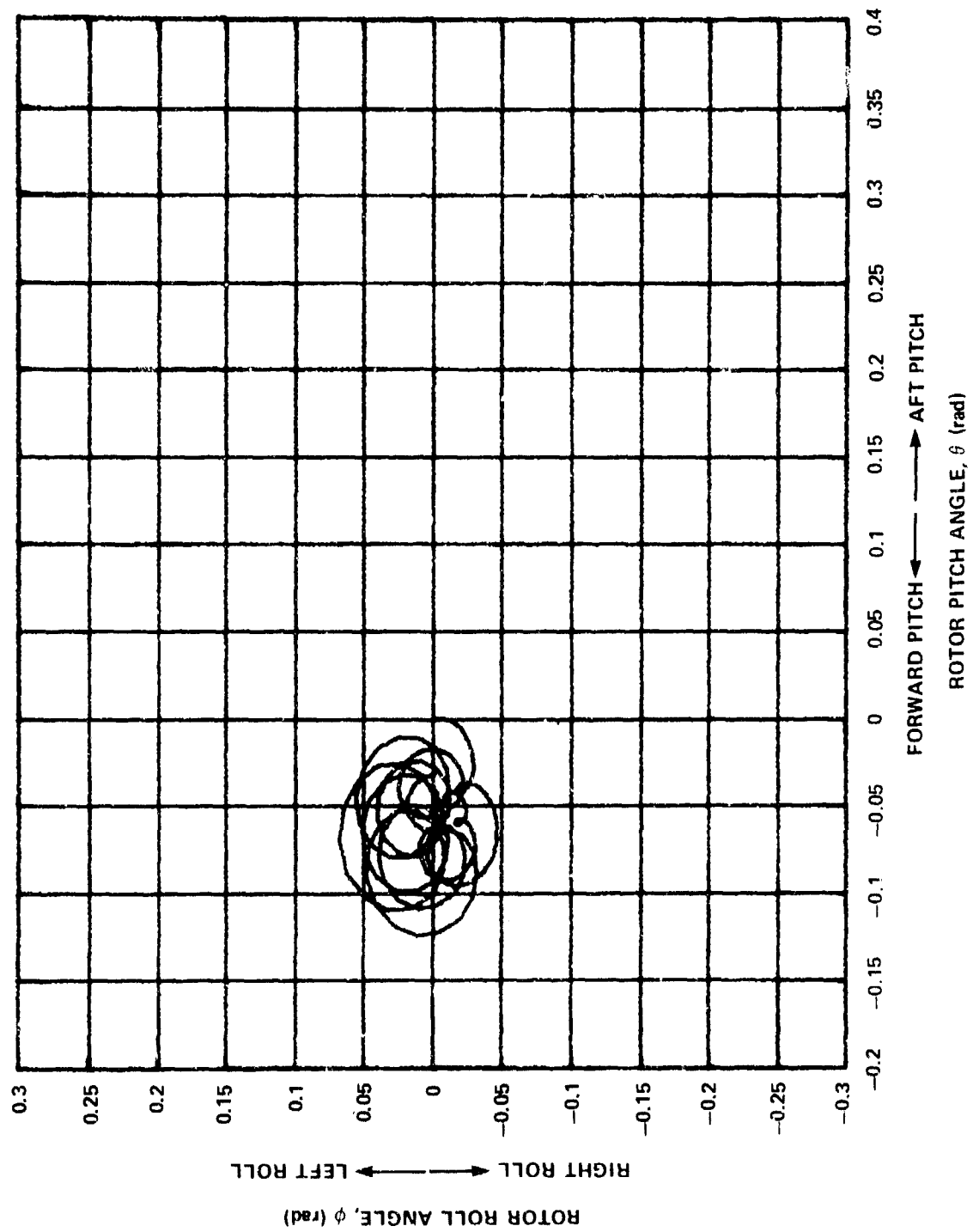


Figure 13g - Feather Angular Rate Feedback; Gain, $k_g = -200$

Figure 13 (Continued)

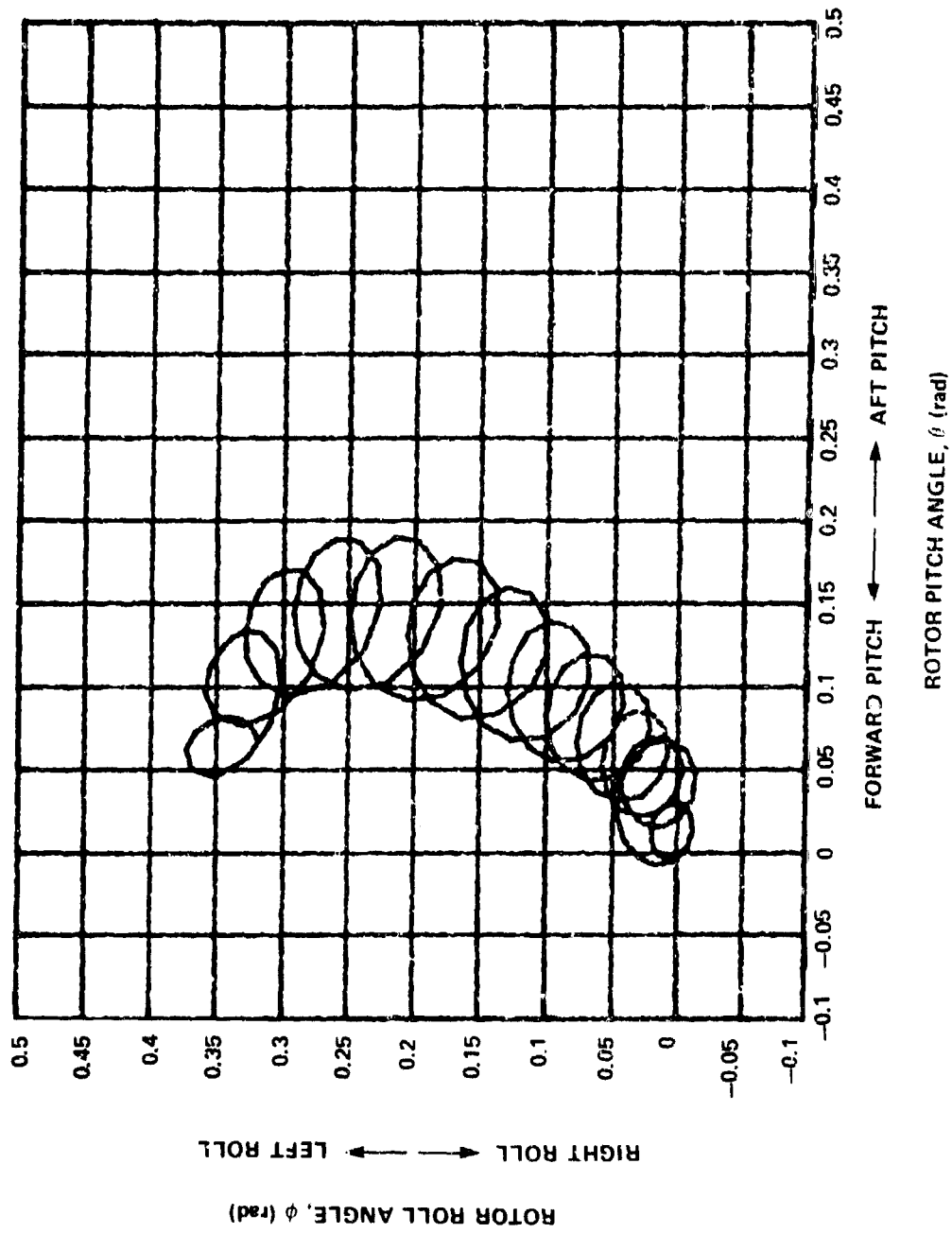


Figure 13h - Feather Angular Acceleration Feedback; Gain, $k_{\phi}^{\ddot{\theta}} = -5$

Figure 13 (Continued)

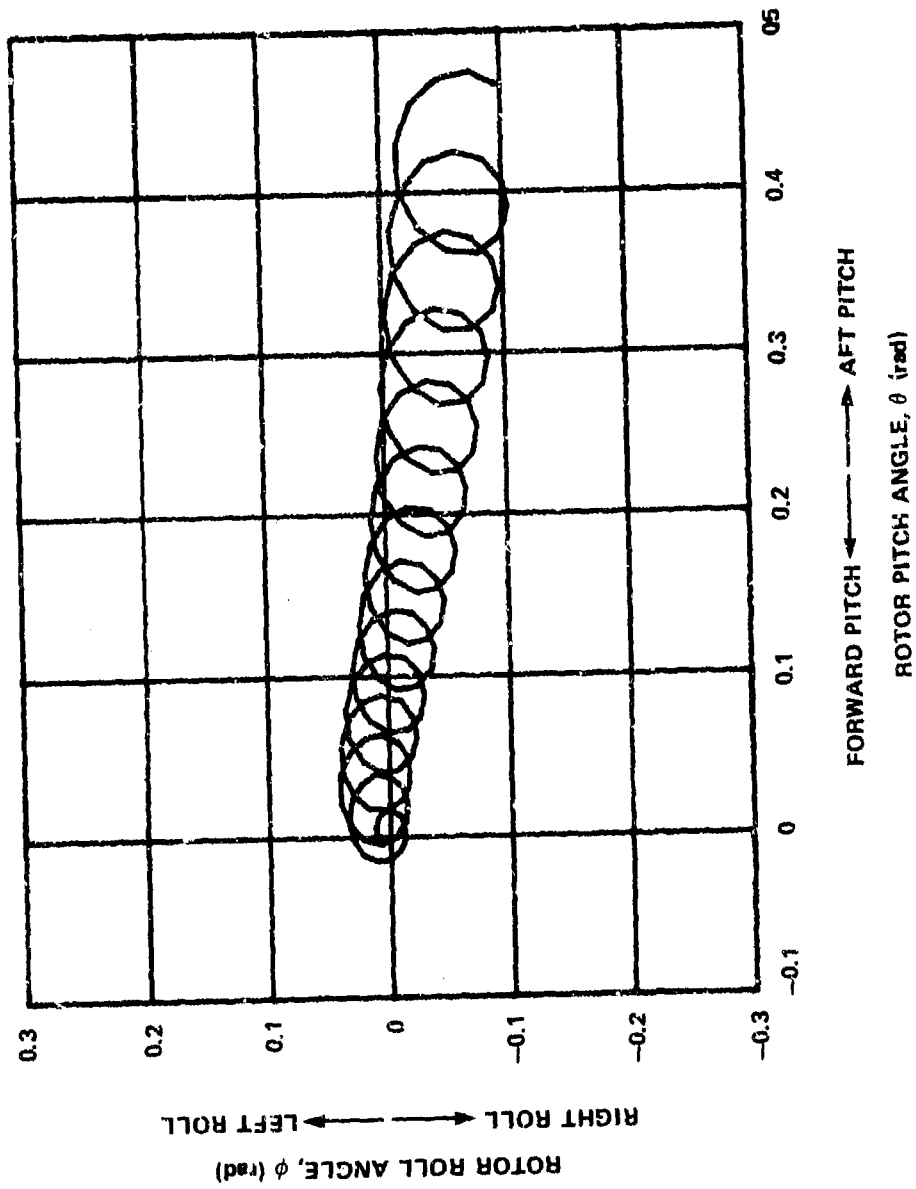


Figure 13i - Feather Angular Acceleration Feedback; Gain, $k_{\theta}'' = +1$

Figure 14 - Effects of Lift Type on Teeter Rate ($k_g = 400$) Feedback

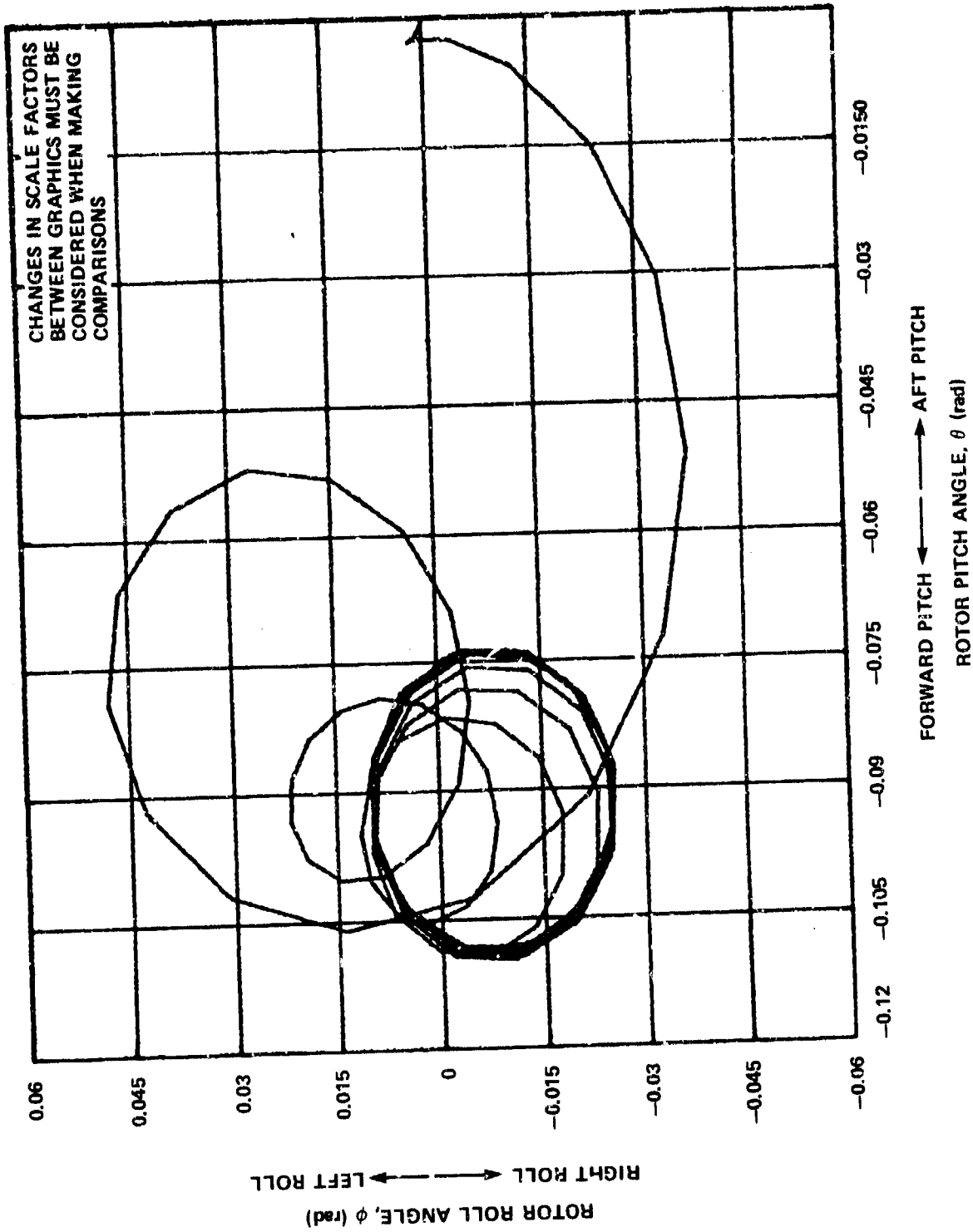


Figure 14a - Duct Pressure Ratio, 1.8; Collective Angle, -4.6 deg (-0.080 rad)

Figure 14 (Continued)

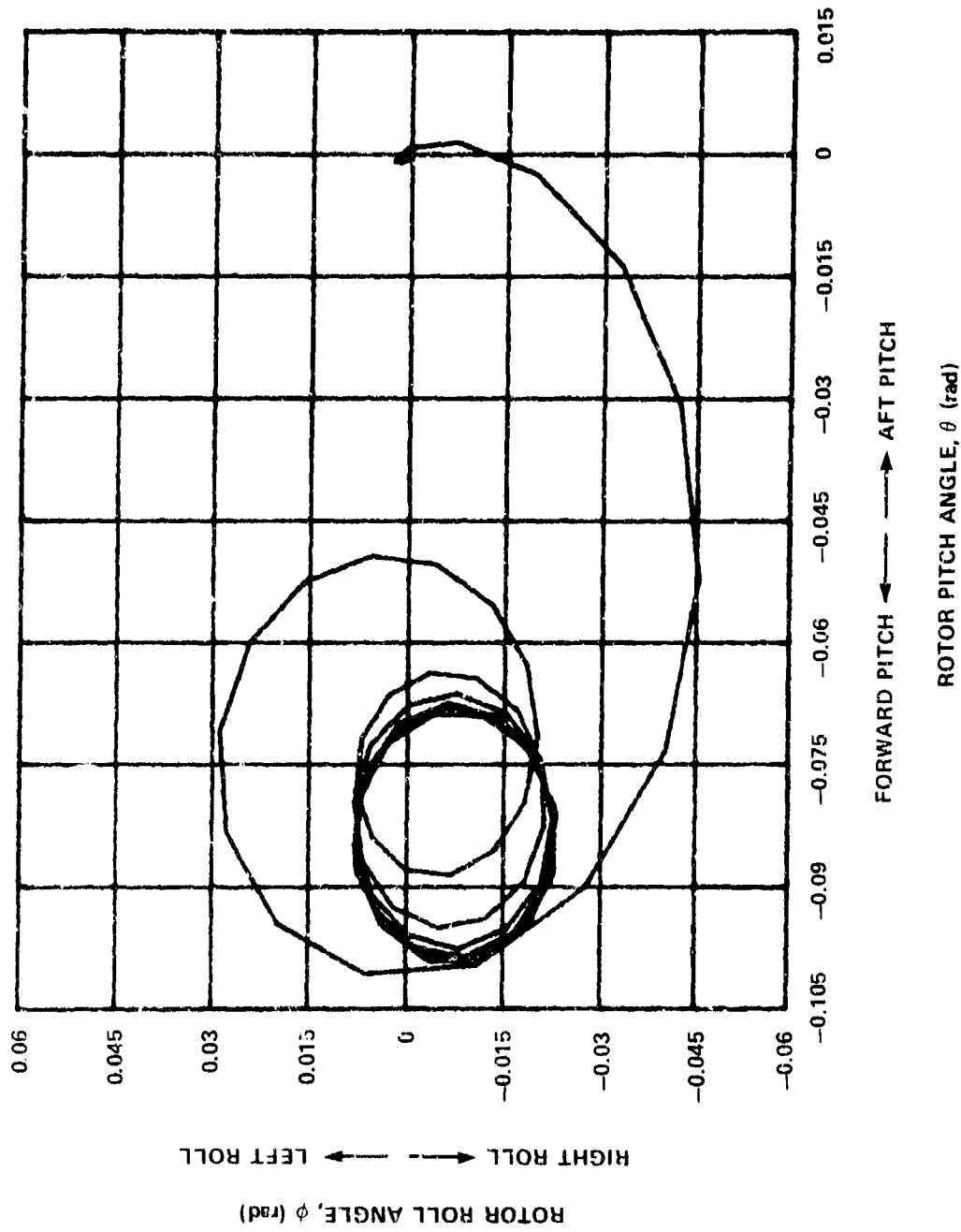


Figure 14b - Duct Pressure Ratio, 1.42; Collective Angle, 1.0 deg (0.017 rad)

Figure 14 (Continued)

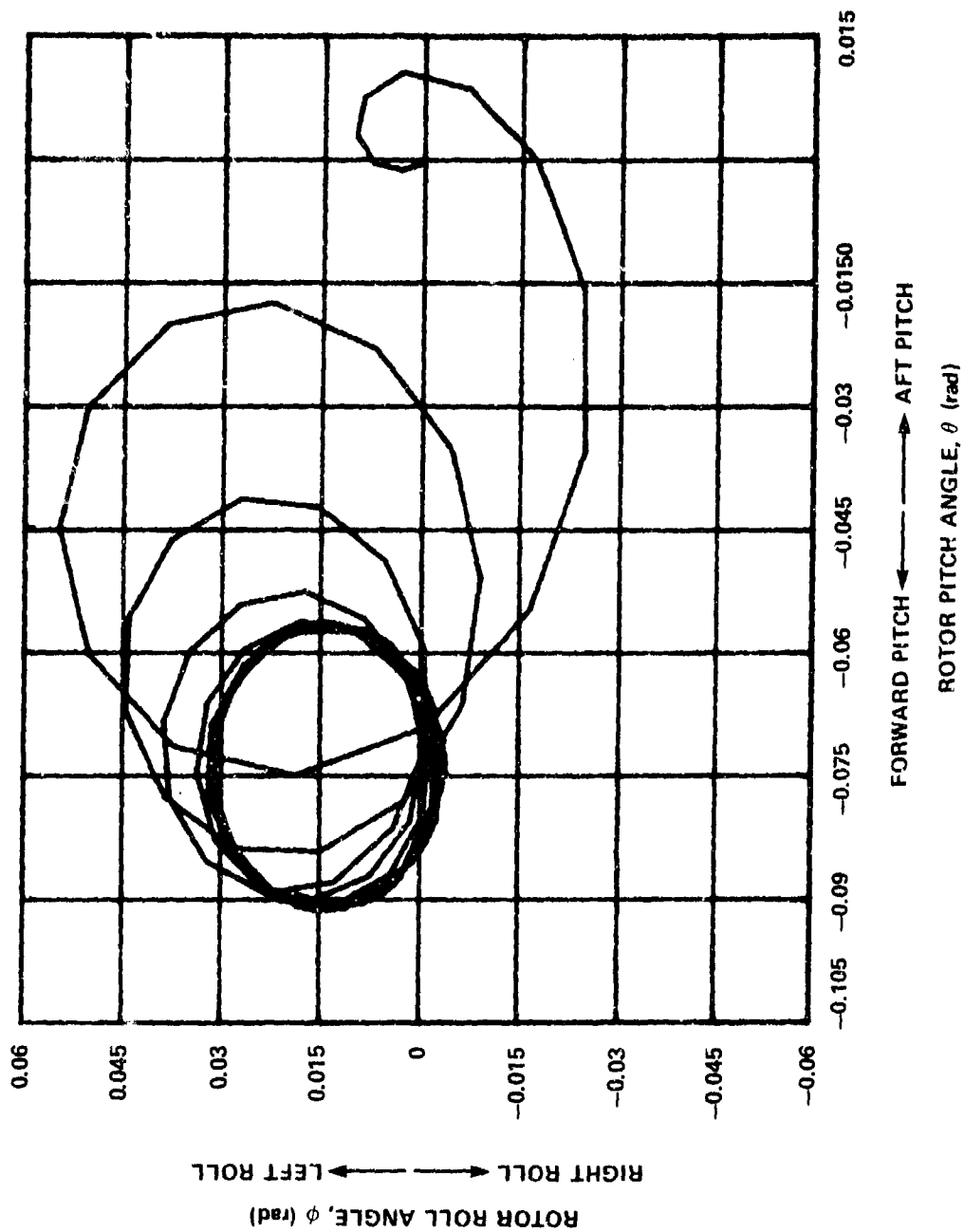


Figure 14d - Duct Pressure Ratio, 1.0; Collective Angle, 7.5 deg (0.131 rad)

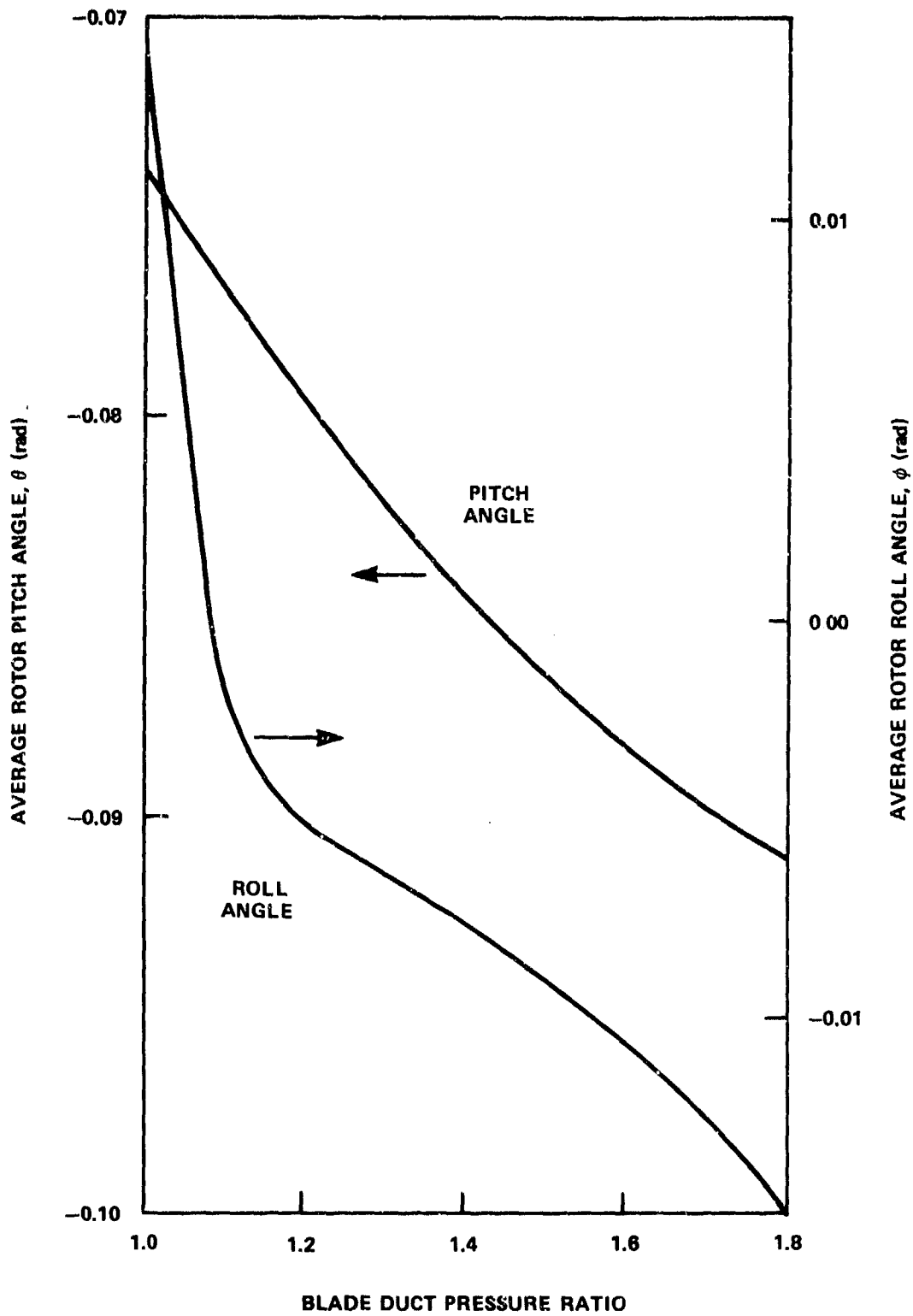


Figure 15 - Effect of Lift Type on the Average Equilibrium Rotor Pitch and Roll Angles with Teeter Rate Feedback

Figure 16 - Effects of Horizontal Gust Disturbances on Open Loop Rotor Dynamics

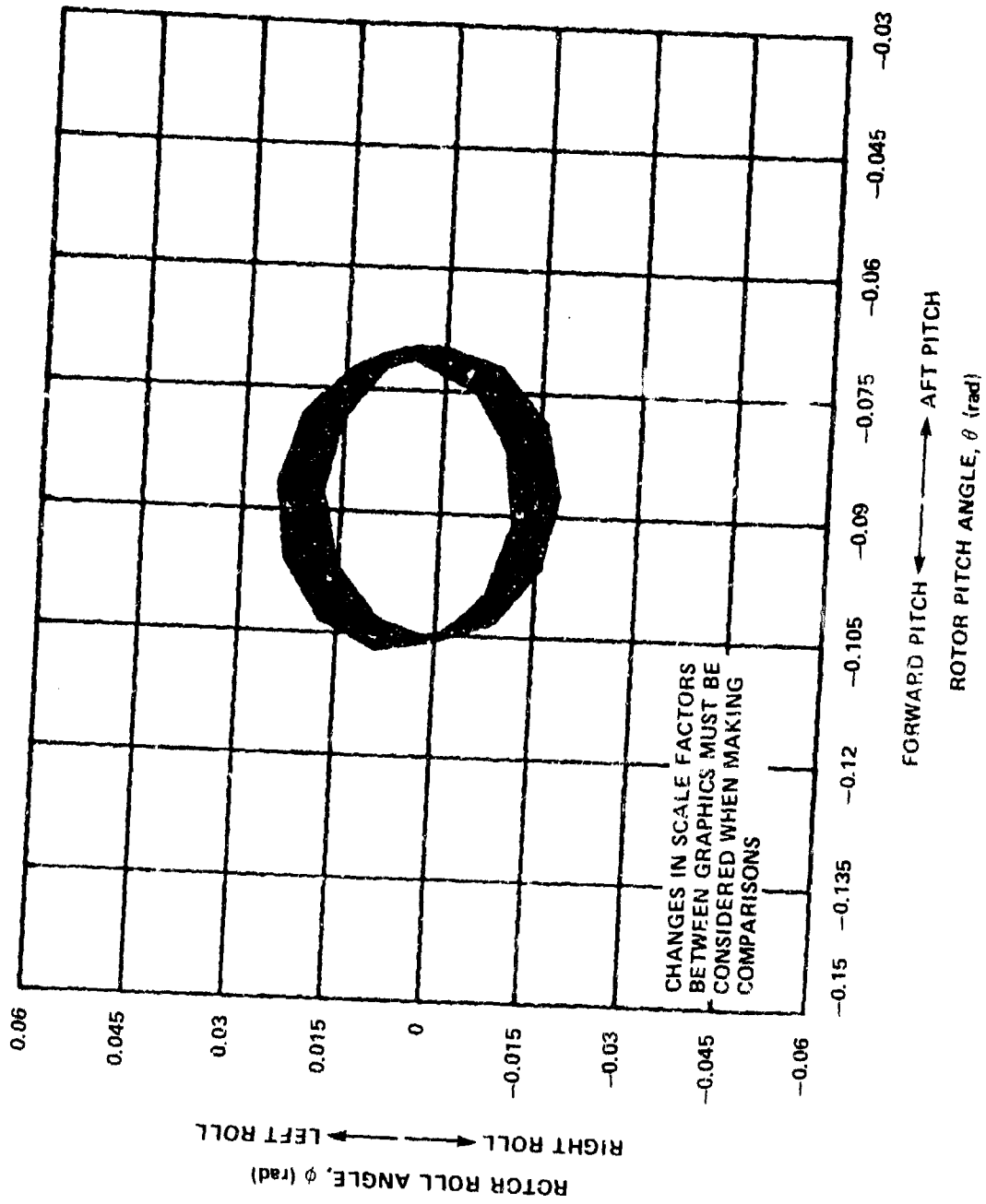


Figure 16a - No Gust Disturbances

Figure 16 (Continued)

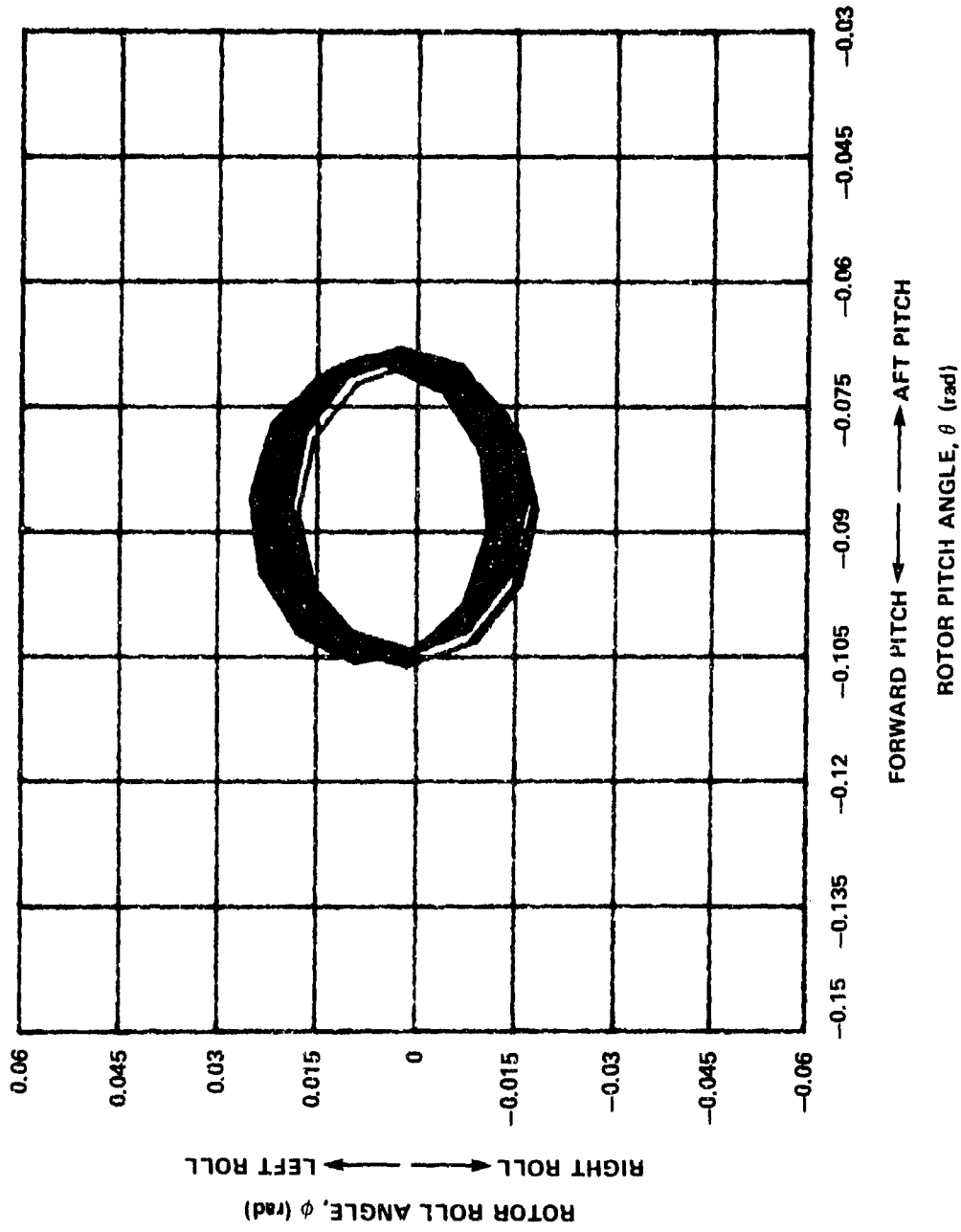


Figure 16b - 10-Percent Pulsed Gust Disturbances

Figure 16 (Continued)

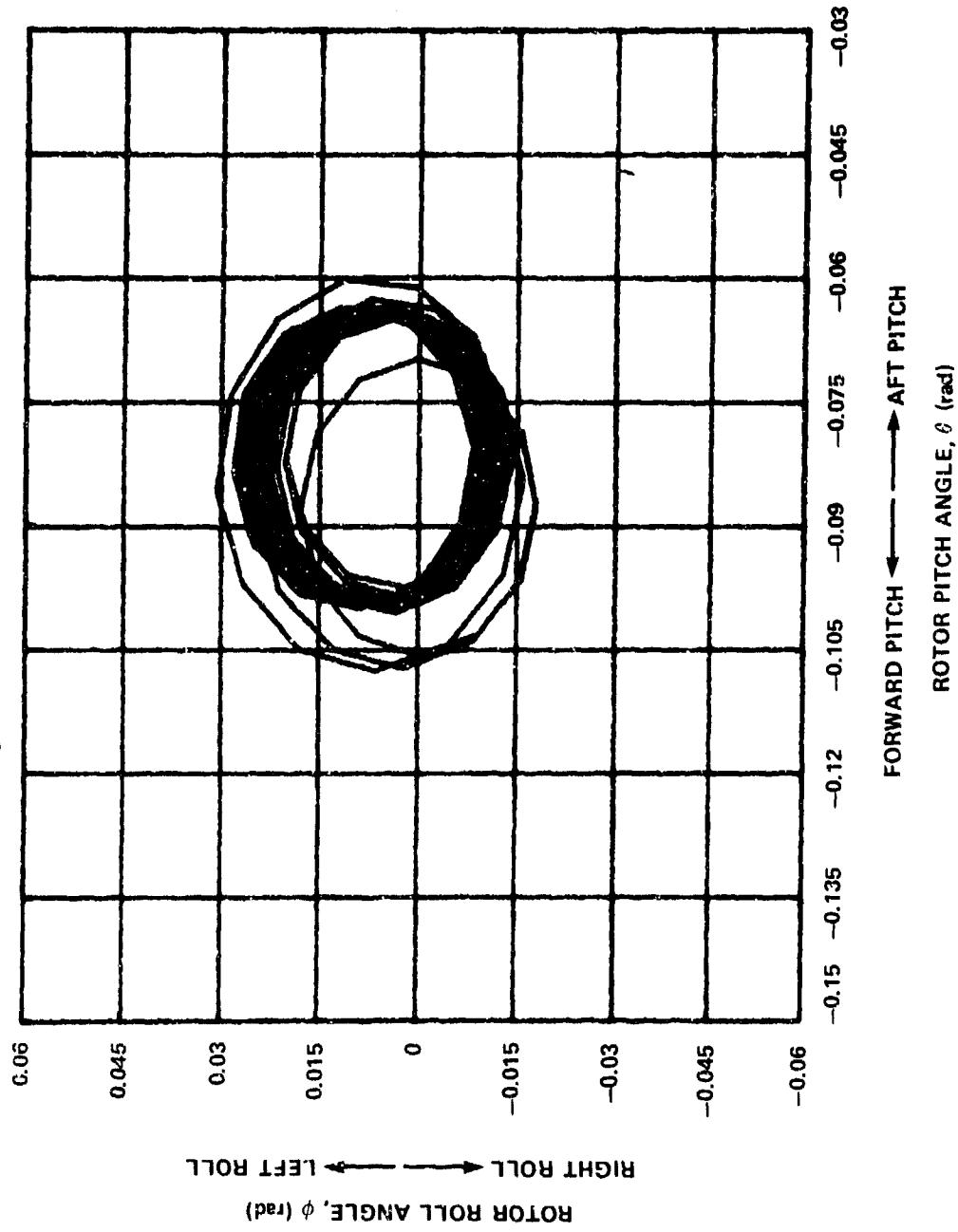


Figure 16c - 50-Percent Pulsed Gust Disturbances

Figure 16 (Continued)

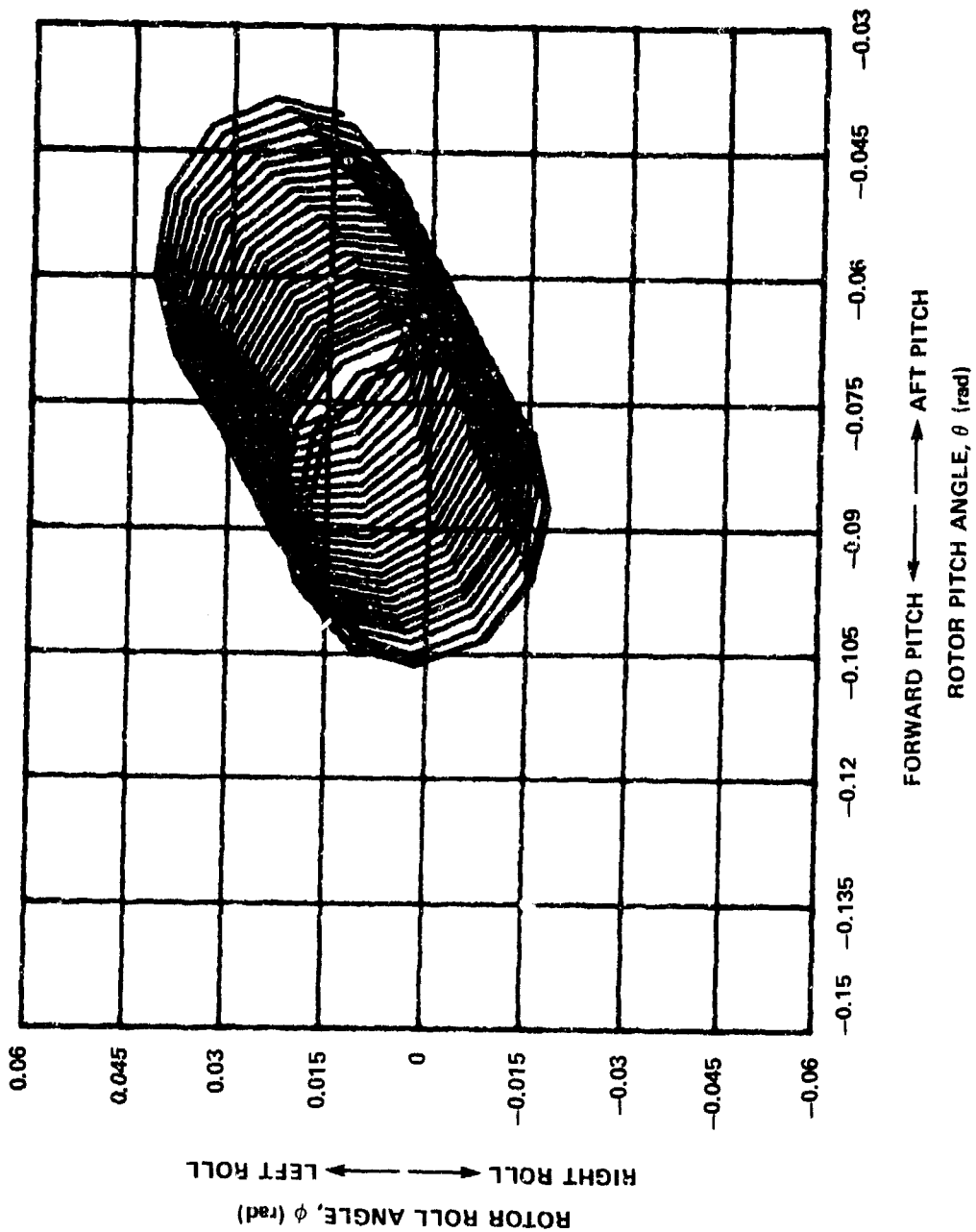


Figure 16d - 10-Percent Step Gust Disturbances

Figure 16 (Continued)

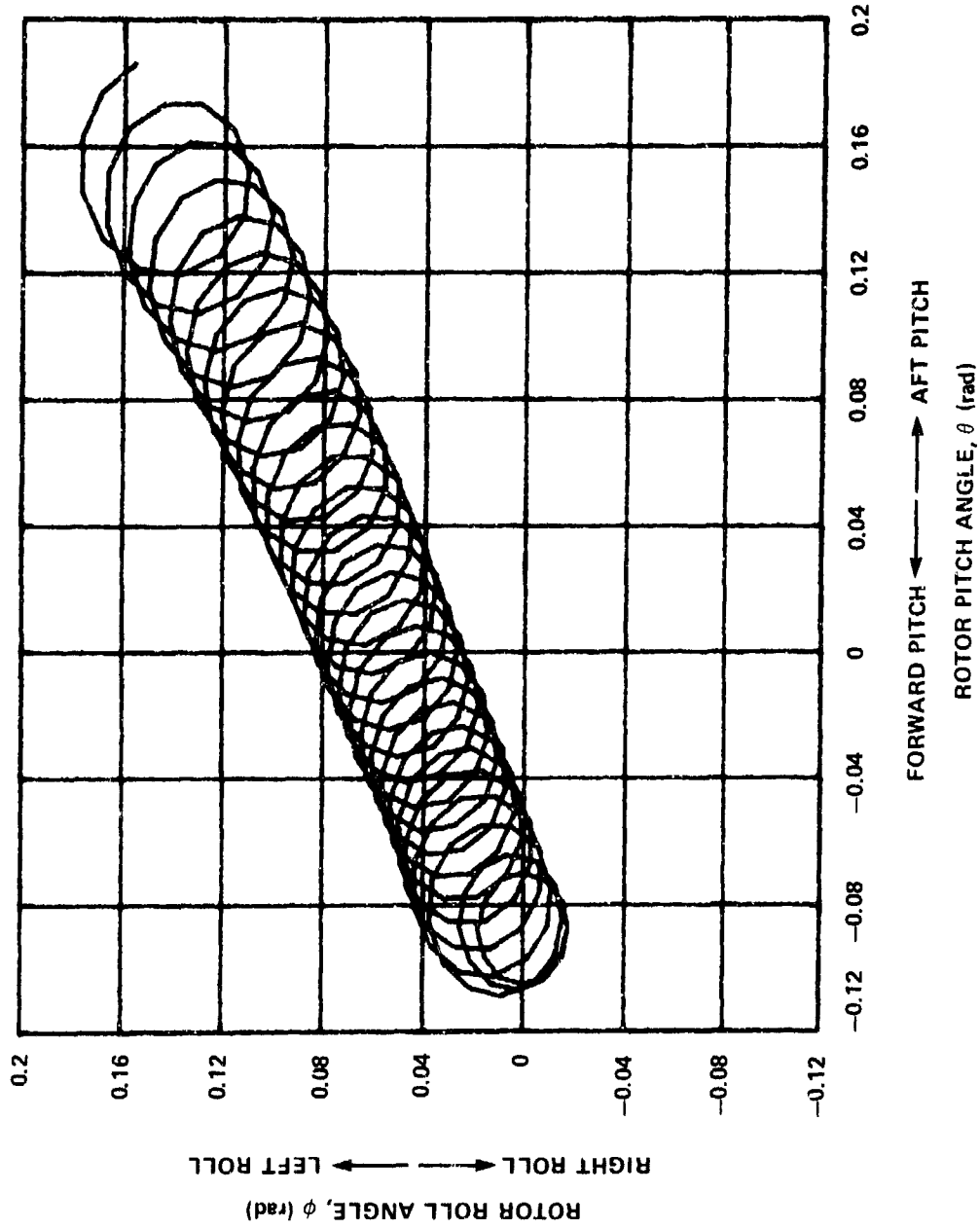


Figure 16e - 50-Percent Step Gust Disturbances

Figure 17 - Effects of Horizontal Gust Disturbances on Closed Loop Rotor Dynamics

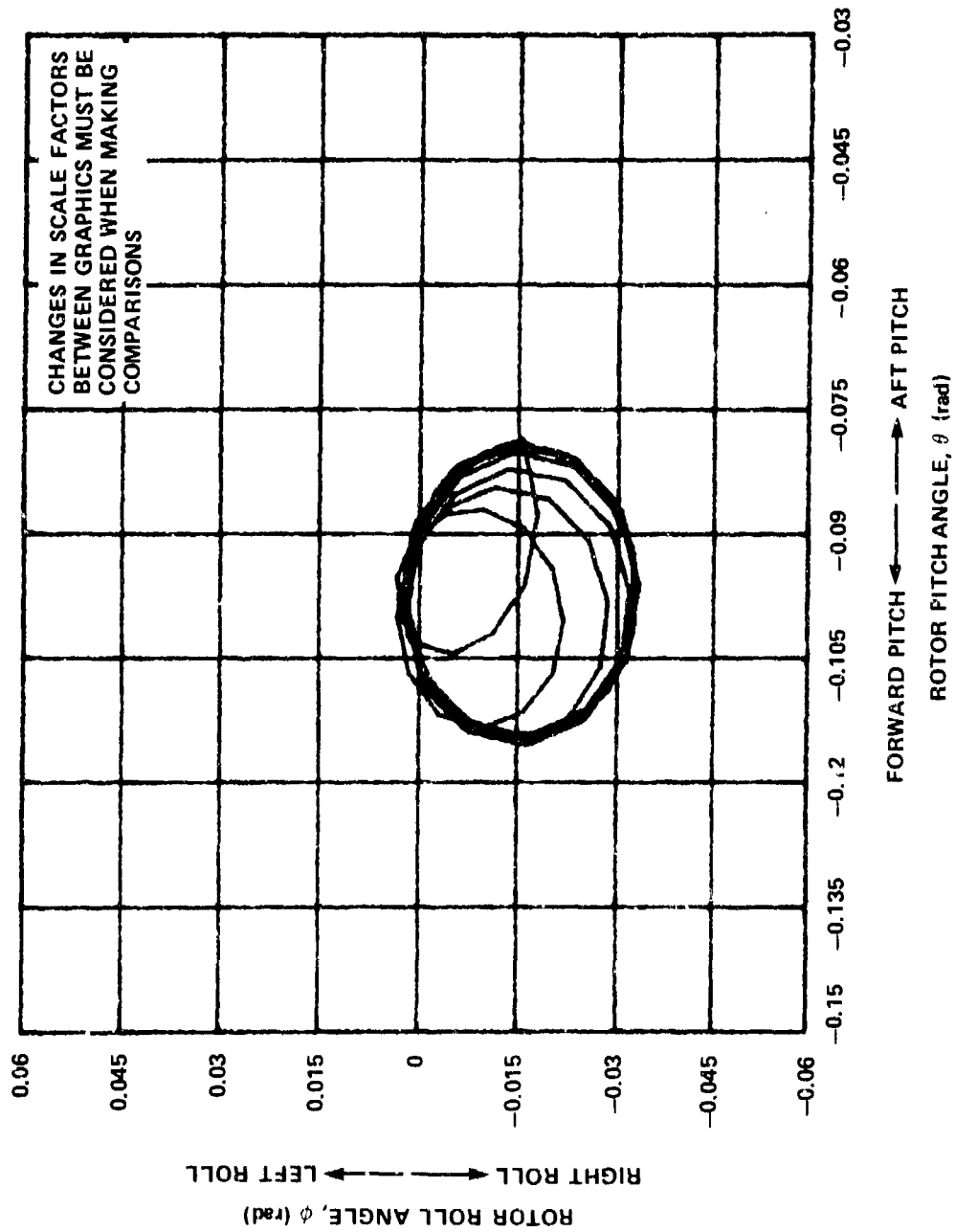


Figure 17a - No Disturbances

Figure 17 (Continued)

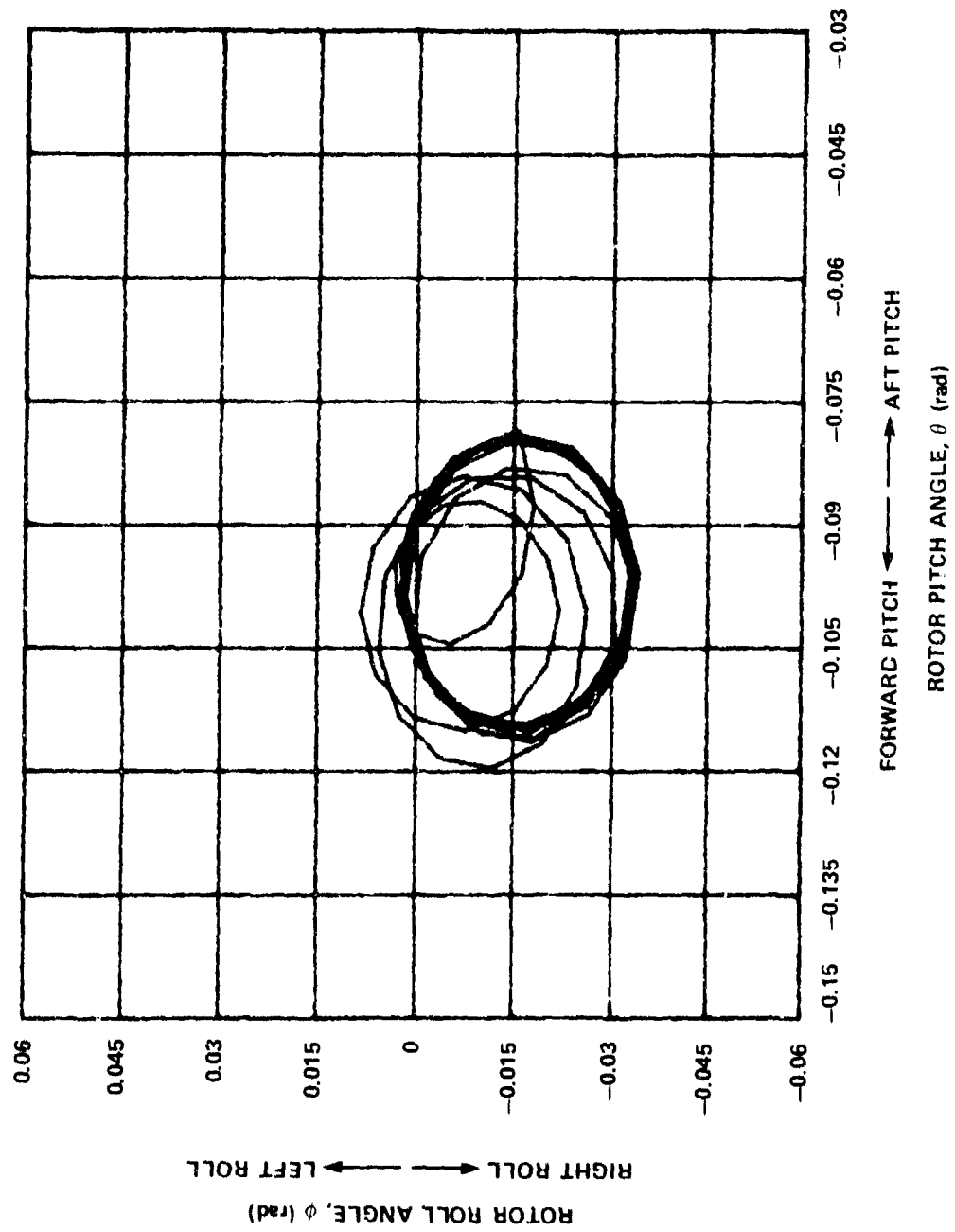


Figure 17b - 50-Percent Pulsed Gust Disturbance

Figure 17 (Continued)

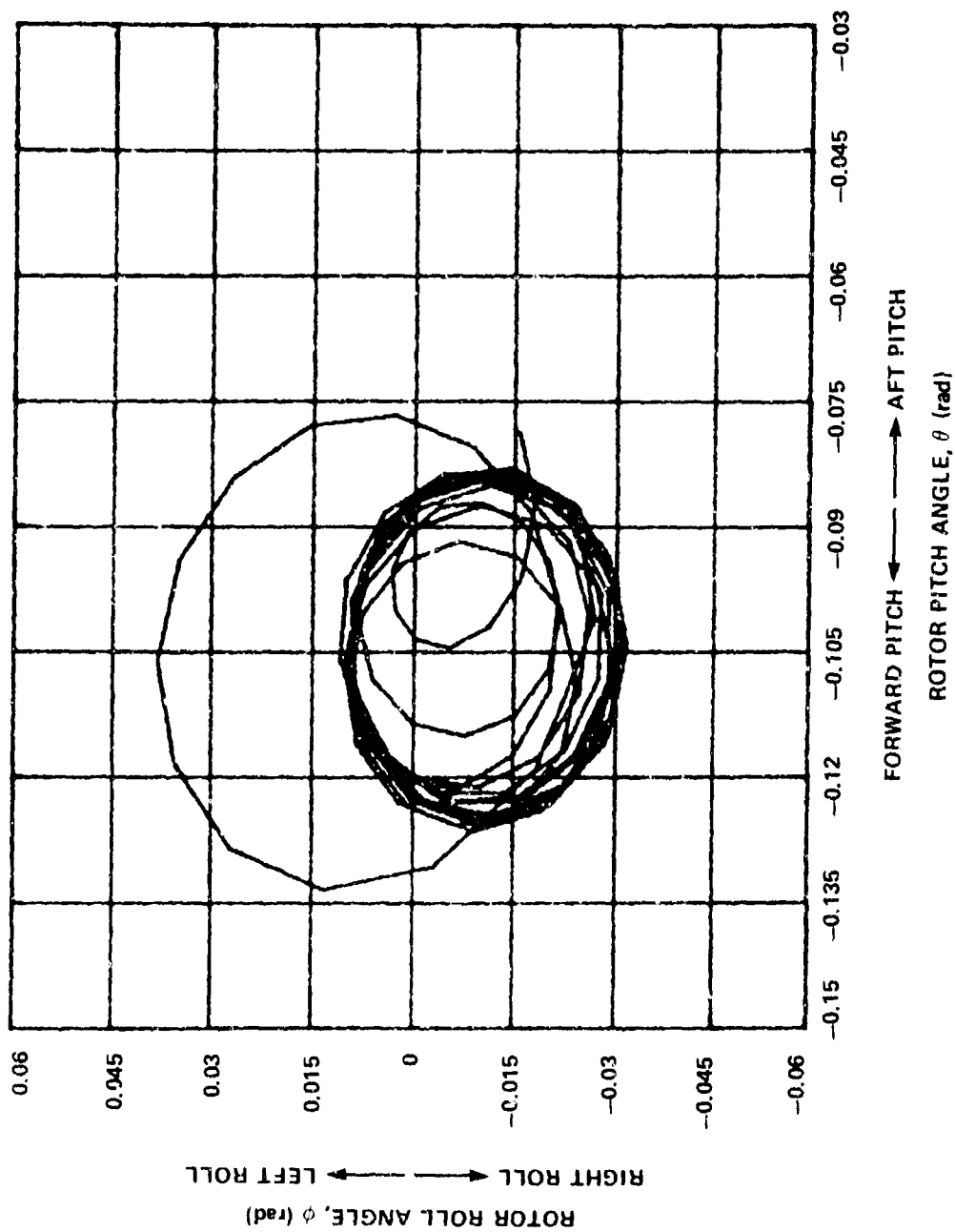


Figure 17c - 50-Percent Step Gust Disturbance

TABLE 1 - ROTOR MODEL CHARACTERISTICS

Rotor Radius	22.0 ft	(6.71 m)
Blade Chord	2.933 ft	(0.894 m)
Airfoil Thickness Ratio		
Root Section	0.231	
Tip Section	0.153	
Airfoil Camber Ratio		
Root Section	0.0625	
Tip Section	0.0100	
Blade Twist*	-8.63 deg	(-0.151 rad)
Rotor Solidity	0.0849	
Rotor Weight**	2,817.3 lb	(12,531.72 N)
Rotor Moments of Inertia***		
I_{p11}	4,750 slug-ft ²	(6,640 kg-m ²)
I_{p22}	95 slug-ft ²	(129 kg-m ²)
I_{p33}	4,815 slug-ft ²	(6,529 kg-m ²)
Rotor Design Tip Speed	615 ft/sec	(187.5 m/s)

*Each blade.

**Includes hub weight.

***Principal moments of inertia. See Table 2 for moments of inertia in the rotor fixed reference frame.

TABLE 2 - VARIATION OF ROTOR INERTIAS WITH PRINCIPAL AXIS LOCATION

Principal Axis Location (x/c)	Rotor Inertias - slug-ft ² (kg-m ²)		
	I ₁₁	I ₂₂	I ₁₂
0.20	4734.85 (6419.92)	110.15 (149.35)	-265.13 (-359.49)
0.25	4739.47 (6426.18)	105.53 (143.09)	-221.17 (-299.88)
0.30	4743.25 (6431.31)	101.75 (137.96)	-177.08 (-240.10)
0.40	4748.31 (6438.17)	96.69 (131.10)	- 88.63 (-120.17)
0.50	4750.00 (6440.46)	95.00 (128.81)	0.0 (0.00)

Notes:

1. The remaining moments and products of inertia were constants as follows: $I_{33} = I_{p33} = 4815 \text{ slug-ft}^2 (6529 \text{ kg-m}^2)$; $I_{23} = 0$; and $I_{13} = 0$.

2. Refer to Figure 2 for the relationship of rotor principal axis location to the rotor fixed reference frame.

INITIAL DISTRIBUTION

Copies		Copies	
1	AASC/Library	14	NAVAIRSYSCOM (Continued)
2	HQ USARTL (AVRADCOM)		1 AIR-03B (H. Andrews)
	1 DAVDL-D (R.M. Carlson)		1 AIR-310 (T.S. Momiyama)
	1 DAVDL-AS (A.W. Kerr)		1 AIR-310C (D.E. Hutchins)
2	ATL, USARTL (AVRADCOM)		1 AIR-310D (D.G. Kirkpatrick)
	1 Tech Library		1 AIR-5284 (F.J. O'Brinski)
	1 G. Hammond/ATA		1 AIR-530 (A.R. Somoroff)
4	AML, USARTL (AVRADCOM)		1 AIR-5301 (R.J. Tracy)
	1 Tech Dir/I.C. Statler		1 AIR-5302
	1 D.L. Key		1 AIR-5302E
	1 H.A. Morse		1 AIR-PMA 261
	1 F.H. Schmitz		1 AIR-PMA 2614 (H.R. Burden)
1	CMC/Science Advisor	1	NWC/Tech Library
	A.L. Slafkosky		
1	MCDEC/Tech Advisor	12	DTIC
2	DARPA	2	ASD/W-P AFB
	1 Library		1 FDL/FIMS, Flight Vehicle Br
	1 R.M. Williams		1 XRH, Design Analysis
1	CHONR	1	AFOSR/Mechanics Div
	R.E. Whitehead (Code 432)		
1	NRL/Tech Library (Code 2620)	2	NASA HQ/RJL
1	NAVPSCOL/J. Miller		1 J. Ward
4	NAVAIRDEVCCEN		1 D. Maiden
	1 Tech Library	8	NASA Ames Res Center
	1 Tech Director		1 S.B. Anderson (210-10)
	1 R. McGiboney		1 W.H. Deckert (237-2)
	1 G. Woods		1 L.A. Haslim (237-3)
1	USNA/Tech Library		1 R.M. Hicks (227-8)
2	NAVAIRTFSTCEN		1 W.R. Johnson (247-1)
	1 Director, TPS		1 W.J. Snyder (237-3)
	1 N. Jubeck		1 R.N. Stroub (247-1)
14	NAVAIRSYSCOM	2	NASA Langley Res Center
	1 AIR-00DR (Tech Library)		1 Tech Library
	1 AIR-03 (R.D. Friichtenicht)		1 R.J. Huston
	1 AIR-03A (E.D. Cooper)	1	Rensselaer Polytech Inst
			K.G. Loewy
		2	University of Maryland
			1 A. Geasow
			1 I. Chopra

Copies

1 University of Tennessee
Space Inst/M. Wright

1 VA Polytechnic Inst
Engr and Mech Library

1 West VA U/Aero Engr Lib

1 Analytical Methods, Inc.
F.A. Dvorak

1 ARO/Engr Sciences Div
S. Kumar, Asso Dir

1 Bell Helicopter Textron

2 Boeing Vertol Co.
1 Tech Library
1 D.A. Richardsen

1 Global Analytics, Inc.
P.H. Kesling

4 Hughes Helicopter, Inc.
1 Tech Library
1 D.C. Borgman
1 R. Head
1 A.H. Logan

3 Kaman Aerospace Corp.
1 Tech Library
1 D.R. Barnes
1 A.Z. Lemnios

3 Lockheed California Co.
1 Tech Library
1 W.D. Anderson
1 A.J. Potthast

1 Paragon Pacific, Inc.
J.H. Hoffman

1 P. asecki Aircraft Co.

4 Sikorsky Aircraft
1 Library
1 E.A. Fradenburgh
1 L. Kingston
1 P.C. Ogle

Copies

1 Systems Res Labs/R.P. White

2 United Tech Res Ctr/E. Hartford
1 Tech Library
1 A.J. Landgrebe

CENTER DISTRIBUTION

Copies	Code	Name
1	012	Director of Technology
1	012.3	Research Coordinator
20	169	P. Montana
1	1606	
2	1606	Aerodynamics Collection
10	5211.1	Reports Distribution
1	522.1	Unclassified Lib (C)
1	522.2	Unclassified Lib (A)
1	93	Patent Counsel